Dynamical structures and manifold detection in 2D and 3D chaotic flows

---

DISSERTATION

ZUR ERLANGUNG DES AKADEMISCHEN GRADES

DOKTOR DER NATURWISSENSCHAFTEN (DR. RER. NAT.)

IN DER WISSENSCHAFTSDISZIPLIN THEORETISCHE PHYSIK

JUDITH SCHNEIDER

INSTITUT FÜR PHYSIK

FAKULTÄT MATHEMATIK UND NATURWISSENSCHAFTEN

UNIVERSITÄT POTSDAM

Mai 2004

תְּהוֹם	עַל־פְּנֵי	וְחֹשֶׁךְ	וּבֹהוּ	תֹּהוּ	הָיְתָה	וְהָאָרֶץ
Tehoum	Al Phani	Ve Hhoshekh	Ve Bohu	Ha Tohu	Ha Ita	Ve Ha Eretz
abyss	on the face	and darkness	and waste	desolation	being	and the earth

Genesis 1:1-2

In the beginning God created the heaven and the earth.

And the earth was (hayah = became) without form (tohu), and void (bohu); and darkness was upon the face of the deep.

"The earth was Chaos (Tohu) and Desolation (Bohu). What is the meaning of the word "was" in this verse? This indicates that the Chaos existed previously [and already was]. What is Chaos (Tohu)? Something that confounds (Taha) people.

Aryeh Kaplan, The Bahir, Weiser, 1989, section 2 p.1.

Contents

I. Introduction VII

II. Basics of Chaos XII

III. The leaking method XXI

A. Background XXI

B. Introducing Leaking in 2d flows XXVII

1. Numerical procedure XXIX
2. The Baker map XXX
3. The Sine map XXXIII
4. The random sine map XXXVI
5. Conclusions XXXVIII

C. Fractal structures due to leaking in 3d non-Hamiltonian systems XLII

IV. Applications in environmental flows XLIX

A. Background Oceanography XLIX

B. Oceanography - The Gulf Stream LII

1. Time-periodic kinematic model LIII
2. A chaotically time dependent flow LVIII
3. A dynamically consistent model with barriers LX
4. Discussion LXI

C. Oceanography - The Mediterranean LXIV

1. introduction LXIV
2. Mediterranean sea surface circulation LXV
3. The ocean circulation model LXVI
4. Lagrangian diagnostic - Extended Leaking method LXVI
5. Results without diffusion LXVIII
6. Horizontal exchange between sub-basins in the Mediterranean Sea LXVIII
7. stable and unstable manifolds LXX
8. Conclusion LXXV

D. Geology LXXVII

1. Introduction LXXVII
2. Chaotic advection and mixing LXXVIII
3. Models and results LXXIX
4. Discussion LXXXV

V. Summary LXXXVII

VI. Bibliography XCI

References XCI

Acknowledgments XCVII

I. INTRODUCTION

The world around us is filled with uncertainty and unpredictability. If the evolution of things takes an unexpected way, other than we might have predicted or if things look very complicated, or sometimes just disordered, as e.g. manuscripts laying crowdedly on an office-table, we often speak of chaos. But what does it really mean, in the physical context, being chaotic?

Chaos is in a certain sense unpredictability. Imagine the situation of balancing a pen on its tip. Before releasing it, it is impossible to say on which side it will fall. It will depend on small perturbations like a slight air-stream. But this problem of balancing a pen illustrates only an unstable situation, not a chaotic one. For getting chaotic motion, the situation of balancing (and falling) of the pen would be repeated again and again and the pen would never come to a stable (resting) position. This simply example already shows the essence of chaos which is the large sensitivity to perturbations, or to slight variations of initial conditions.

This enormous sensitivity, the so-called 'Butterfly effect' was first discovered by the meteorologist Edward Lorenz in 1963 at the MIT: carrying out numerical experiments about weather patterns, he wanted to re-run one of his simulations. When typing in the initial parameters, but skipping some of the last digits, the simulated values began to diverge and to his surprise he got completely other temporal patterns than before. Due to the slight change of the starting conditions in his simulation and the unexpected outcome, Lorenz incidently opened the door to a new field of physics: chaos theory was born. Spreading his new insights, many physisists and meteorologists were really astonished about the large impact of a tiny perturbation on the outcome of physical- and also real-life experiments. It resulted in one of the following sentences of Lorenz: 'One meteorologist remarked that if theory were correct, one flap of a seagulls wing would be enough to alter the course of the weather forever.' Later on, the seagull became the famous butterfly which flaps in Asia and disturbs our weather in Europe, and this impression about chaos made its way around the world.

In this thesis, the central object is chaos theory, namely chaotic advection in closed flows and, using a new method, in opened up flows.

Chaotic advection attracted interest since the late 1980's [91] and big effort has been made to approach the basic understanding, characterizing and modelling of the features of chaotic advection, especially in environmental flows.

Basically, chaotic advection is referred to as the transport of particles in flows in a chaotic way.

In most of the approaches, the flows were considered to be incompressible and the transported particles or substances were considered as *passive particles* that do not modify the flow structures themself. Such particles take on instantaneously the velocity of the surrounding fluid: $\dot{r} = v(r,t)$. Examples of such passive tracers are simple biological organisms such as plankton which can't move (swim) independently, or pollutants such as oil. For simplicity, in theoretical experiments, these impurities are defined to be pointlike and to have the same density as the surrounding fluid. Monitoring the motion of these particles gives then informations about the local dynamics of the underlying flow: for two-dimensional time-independent systems, the tracers follow exactly the streamlines of the flow. Their motion in space and time is simple and can be forecasted easily. But this picture changes drastically when the flow becomes time-dependent: then the trajectories of the tracer particles do not coincide any more with the flow's streamlines, and cannot be forecasted so easily. Typically, their motion is then chaotic and concepts from dynamical systems theory have been developed to describe successfully this situation [68].

More generally speaking, for obtaining chaotic behavior, (time-continuous) systems with at least three phase-space dimensions are needed. Thus, for one degree of freedom Hamiltonian systems (such as spatially one-dimensional systems), we need to have some time-dependence to create chaos, whereas in higher dimensional systems chaotic motion can appear even without any time-dependence.

As already mentioned, the essence of chaotic motion is large sensitivity to initial conditions and perturbations and the resulting inpredictability. How strong this sensitivity is, is given by the Lyapunov exponents which measure the exponential rate of divergence of two initially nearby particles (or in other words, its a measure how quickly errors/uncertainties grow). Lyapunov exponents and the related quantities (escape rates or residence times, fractal dimensions,...) are used to characterize mixing strength.

Motion of particles displays the chaoticity of the system and also shows the main directions of transport and mixing in the fluid. To give an example, in environmental measurements such as in oceans, oceanographers launch floats or drifters (former ones: stay at a certain depths at the ocean, following gradients; latter ones: stay at the surface of the ocean; hereafter both are referred to as drifters) and keep track of their motion (recording trajectories). This way they can identify vortices and major currents such as the Gulf Stream, or get a first idea about transport routes. However, the resulting pictures of the trajectories (so-called Spaghetti diagrams, see Fig. 1) are usually rather messy due to the highly intertwined trajectories . I will show a possibility of extracting useful

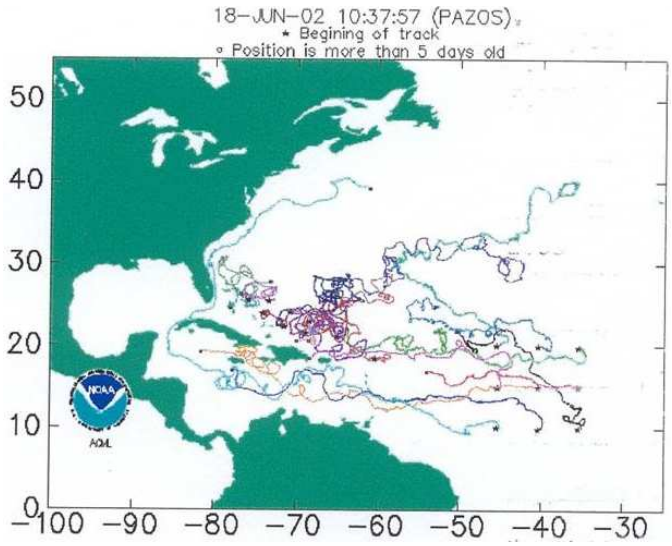

FIG. 1: Spaghetti diagram, showing the trajectories of drifters east of America. Releasing points are marked with a star (picture taken from the www).

information about the underlying dynamics out of these plots (see Chapter III).

One may think that treating drifters, which might be even larger than an average human is, as pointlike particles in theoretical simulations is a too large simplification. This is true at a first view only, since it is a matter of scales: keep in mind that compared to the system size - the ocean - the drifter's size is diminishable. Thus, regarding them as to be pointlike is a good approximation. Whereas, in contrary, going to smaller systems like rivers, it is of importance to take into account the size of the advected particles. Then, moreover, the density of the tracer compared to the one of the surrounding fluid is also crucial (for the effect of finite size particles see [45]).

It has been shown, both theoretically and experimentally, that the displayed motion of tracers corresponds to a movement along the system's unstable foliation: for a chaotic system, particles are moving along the stable manifold towards the corresponding hyperbolic point, then leaving it on its unstable manifold. This means, that after a certain transient time, all particles are located on the unstable manifold. In other words, motion of particles displays us the geometry of the system's unstable manifold and with it the underlying dynamical structures of the system. Recently, Voth, Gollub and Haller showed a nice experimental evidence, comparing the experimental unstable manifold with the theoretical one [87].

The often lamellar structures of the unstable manifold, resulting from continuous squeezing with the negative Lyapunov exponent along the stable manifold and stretching with the positive

Lyapunov exponent along the unstable manifold, are ubiquious not only in laboratory experiments but also in real-world such as on satellite images of ocean temperature gradients, for example [Fig. I]. The study of these geometrical structures (attractors, saddles, manifolds,...) is important both

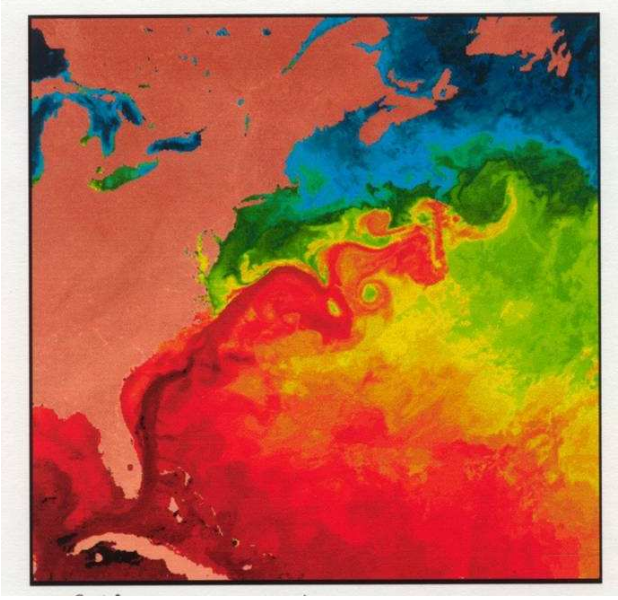

FIG. 2: Sea Surface Temperature (SST) picture of the Gulf Stream. Red colors denote regions with warm water masses, blue colors denote cold regions. The Gulf Stream can be clearly seen with its red meandering structures, flowing from Cape Hatteras towards the East. picture taken from: http://seawifs.gsfc.nasa.gov/OCEAN_PLANET/HTML/oceanography_remote_sensing.html

from the fundamental point of view, as the skeleton of the fluid dynamics, as also from the point of view of applications: the geometrical structures act as avenues and as barriers for transport, so that important time-scales such as residence times, mixing times, and even the amount of transport, are determined by their positions and persistence.

With the help of the Kantz-Grassberger equation ($D_m = 2 - \kappa/\bar{\lambda}$ for a two-dimensional system, with D_m beeing the dimension of the manifold, the (average) Lyapunov exponent $\bar{\lambda}$ and the escape rate κ) [34] a connection between these geometrical properties of the manifolds and the dynamics of the system can be established: by measuring the (fractal) dimension of one of the manifolds, we can determine the system's Lyapunov exponent and with it the chaoticity of the system. The problem, however, is that in closed 2 dimensional systems we cannot get any other dimension than that of the system's full phase space (e.g. $D_m = 2$ for a two-dimensional system). Thus, the method seems to fail for closed systems. Another possibility for calculating the Lyapunov exponent $\bar{\lambda}$ is

to measure it directly from the rate of separation of two nearby particles. Note, that the separation rate of any pair of nearby particles is characterized by a different local Lyapunov exponent depending on the local properties of the flow. Consequently, the local Lyapunov exponent does not have to coincide with the global one. In order to get the global, or average, Lyapunov exponent, one has to follow these particles for a long time.

In the year 2000 we developed an efficient algorithm with which it is possible to obtain fractal dimensions of subsets of the system's stable and unstable manifolds even in closed systems [77]. This so-called method of 'leaking' which is basically consisting of the definition of a leak in the closed flow through which particles can escape out of the system, turned out to have a rather broad range of applicability [76]. First of all, as mentioned, its basic feature lies in visualizing subsets of the system's chaotic saddle along with its fractal manifolds. We found that the dimension of the visualized structures, and thus of the escape rate of the particles out of the system, is depending on the size and even of the position and shape of the leak [77]. This sensitive dependence gives more insight about the systems basic geometrical and dynamical properties. Also, the extracted structures of the subsets of the unstable manifold are closely resembling the structures traced out by superimposed chemical or biological reactions ([35], Chapter III B). Furthermore, they show the "roads of transport" which are of importance e.g. in oceanography to get informations about water exchange, carrying different oxygen or salinity concentrations (Chapter IV B), or in atmospherical dynamics to see e.g. transport barriers due to which the ozone hole is existing. We will show some possible applications to oceanography performing numerical simulations of the Mediterranean Sea in monitoring the movement of particles and so visualizing the resulting Lagrangian structures at different depth of the Sea (Chapter IV B).

Furthermore, on the example of mixing dynamics in the Earth mantle, we demonstrate that our method of visualizing transport routes and mixing properties in flows also works in flows with irregular time-dependence and high viscosity (Chapter IV D).

II. BASICS OF CHAOS

This chapter gives a short overview of the basic terminology used in chaos-theory, providing definitions of terms used in the next chapters. For a broader introduction to nonlinear dynamics see Ref. [26, 29, 83].

A **deterministic dynamical system** is a system which evolves in time - with time beeing either a continuous (the system can then be called a flow) or a discrete variable (the system is a map) -. Beeing deterministic in the mathematical sense means that a well defined end-point is belonging to every starting point. Consequently, the evolution of the system can be forecasted (is deterministic) when knowing the intitial conditions exactly.

A basic assumption for chaotic motion is that the system is **nonlinear**. The characteristics of a nonlinear dynamical system can be described by the reaction of the system on a stimulus (outer force): take for example a pendulum. If we apply a certain force to it, bringing it out of its equilibrium point, and compare its motion (response) with the one resulting from a force which is twice as large as before, then we will see that the response-motion (amplitude) is twice as large as before, too. In this case, the system is said to be linear. If the response is not linear, thus in this example larger or smaller than the double, then consequently, the system is said to be nonlinear. A small change in a parameter of a nonlinear system can lead to drastic changes in the dynamical behavior of the system.

Having **chaos** in a dynamical system, we find a characteristical exponential growth of uncertainties. Due to the exponential divergence and because the ability of measuring the state of a dynamical system is finite (finite precision), the forecasting of motion in a chaotic system is only possible for a finite time. Long term predictions become impossible, statistical tools have to be used in order to give the probability of the evolution of the system.

A common tool for the description of a chaotic system is the use of the **phase-space** representation. Phase-space is spanned by N independant variables which can be given by a set of N first-oder differential equations. In other words, the actual state of the system is fully determined by a point in phase-space. The use of phase-space was introduced in the 1800's by Henri Poincaré (actually, the name 'phase-space' was introduced by J.W. Gibbs around 1900, Poincaré himself used the word 'state space').

Using the phase-space representation, we can identify the two basic classes of dynamical systems: non-conservative and conservative ones. In **non-conservative systems**, the area (or volume)

in phase-space is not conserved. It is either decreasing (system is approaching an equilibrium state, e.g. due to damping forces) or increasing (self-excitational systems). Former ones are also called **dissipative systems**. Their characteristical decreasing area in phase space results from the fact, that as the system evolves, trajectories in phase space will be attracted by certain points or regions in phase space. Their final point / region where they end up is called an **attractor** (Fig. 3). Attractors are defined as bounded subsets in phase-space with zero volume, attracting trajectories. The ensemble of initial points wherefrom trajectories are going towards the given attractor is the **basin of attraction** of that attractor.

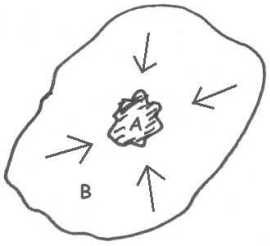

FIG. 3: Attractor (A) with its basin of attraction (B). Particles beeing within the basin of attraction will be attracted by the attractor.

An infinite number of attractors can exist at the same time in a dissipative system. Their basins of attraction can have complicated structures and might be intertwined in each-other. The basin-boundaries, the basin of attraction and also the attractors themselves can be of fractal type which means that their dimensions have a value which is not an integer - the origin of fractals goes back to Mandelbrot in the 1980's -.

Characteristical for **fractal** objects is that they have large surface-to-volume ratios. Remember, that usually the surface-to-volume ratio is well defined with the surface beeing proportional to the volume$^{-2/3}$. Anyway, there exist exceptions as we can see in the examples of the froth of fresh beer -has a large surface but almost no contents- or in the fine structures of catalysts as e.g. the human lung , where the goal is to have the largest surface possible -in order to provide large surfaces for the reactions- together with the smallest volume. For the human lung, this is realized by over twenty generations of branching of the blood circulation vertebrates. Due to the resulting fine fractal structure, the human lung has a surface as large as a tennis-court (measured on a microscopic level), but on the same time only occupying a volume of a view litres.

The mathematical construction of a fractal is about to have an infinite set of points achieved by recursive operations. One well-known generated fractal structure is the **Cantor Set**, consisting of

a starting line element of unity length whereform the middle third part is removed. From the two remaining parts, again the middle-thirds will be removed (Fig. 4). Continuing this procedure, the structures of the resulting object will be self-similar -same structure arises at different scales- and have a not-integer dimension of $D = 0.63$.

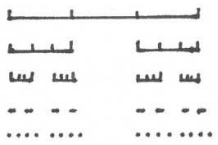

FIG. 4: Construction of a Cantor Set. Beginning with an interval of e.g. unity length (uppest row), successively the middle third will be removed of the remaining parts.

Attractors which have a fractal dimension are also called **strange attractors**. In two-dimensional phase-spaces, attractors can consist of stable fixed points or they can be limit cycles. **Fixed points** are points where particles stay forever. For a two-dimensional flow, beeing a system described by $\dot{\mathbf{x}} = \mathbf{f}(\mathbf{x})$ with $\mathbf{x} = (x_1, x_2)$ beeing the independant variables and $\mathbf{f} = (f_1, f_2)$ functions determining the evolution of the variables, the time-derivatives at a fixpoint FP are zero: $\dot{\mathbf{x}}_{FP} = 0$. In maps however, where x_1, x_2 are discrete variables with $(x_{n+1}, y_{n+1}) = \mathbf{M}(x_n, v_n)$ ($\mathbf{M}$ beeing a function), fixpoints can be identified as places where a point is mapped into itself: $\mathbf{x}_{FP} = \mathbf{M}(\mathbf{x}_{FP})$ with $\mathbf{x}_{FP} = (x_{FP}, v_{FP})$.

To determine the kind of fixed point (Fig. 5), we have to evaluate the partial derivatives of the evolution functions $\mathbf{f}$ and $\mathbf{M}$. With J beeing the Jacobian matrix

$$J = \begin{pmatrix} f_{11} & f_{12} \\ f_{21} & f_{22} \end{pmatrix}, \tag{1}$$

the eigenvalues λ_+ and λ_- for the flow are calculated from

$$\begin{vmatrix} f_{11} - \lambda & f_{12} \\ f_{21} & f_{22} - \lambda \end{vmatrix} = 0 \tag{2}$$

(the calculation for the eigenvalues for a map is analogously). Depending on the values of $\lambda_\pm$, the following types of fixpoints may exist:

	$Re\lambda_\pm = 0$	$Re\lambda_\pm < 0$	$Re\lambda_- < 0 < Re\lambda_+$	$Re\lambda_\pm > 0$
$Im\lambda_\pm = 0$	$--$	node	hyperbolic point	repellor
$Im\lambda_\pm \neq 0$	elliptic point	spiral attractor	$--$	spiral repellor

A **node** or a **spiral attractor** can only exist in systems with dissipation. They belong to the class of stable fixpoints since they are purely attracting. Therefore, both are denoting end-points for trajectories in phase-space. A completely different behavior is represented by **(spiral) repellors**. They are opposites to the node and spiral attractor since they do only repell trajectories. They are belonging to the class of unstable fixpoints. For comparison, stable fixpoints are like sinks, unstable fixpoints act like sources.

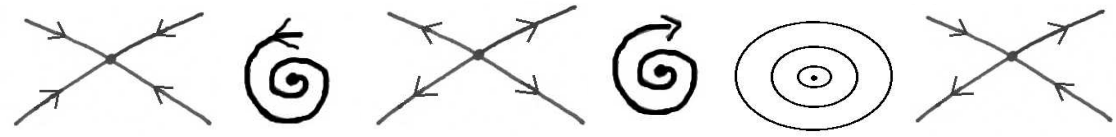

FIG. 5: Different types of fixed points. From left to the right: node, spiral attractor, repellor, spiral repellor, elliptic point and hyperbolic point.

In contrast to these fixpoints are the **ellipic points** which are neither attracting nor repelling. They consits of a fixed point with closed trajectories around it which are ellipses. Elliptic points do typically occur in Hamlitonian system (we will come to these systems soon). **Hyperbolic points** (also called **saddle points**) are repelling and attracting. Having one attracting and one repelling direction they are structurally stable. The attracting direction is also called the **stable manifold** of the hyperbolic point, the repelling direction is the **unstable manifold** (Fig. 6). Trajectories will

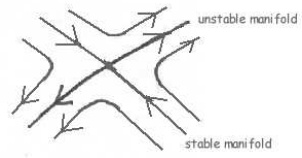

FIG. 6: Hyperbolic point with its stable and unstable manifolds. Trajectories which are not exactly either on the stable or the unstable manifold have the shape of hyperbolas.

be governed along the stable manifold towards the fixpoint. During their movement on the stable

manifold, the trajectories approach each-other with the rate λ_-. Trajectories are taken away from the hyperbolic points on the unstable manifolds where they separate / diverge with the rate λ_+. In general, lines which are governing trajectories towards a fixpoint are called the stable direction (or manifold), the ones taking trajectories away from the point are the unstable directions (or manifolds).

Beside the elliptic points, hyperbolic points are the only fixpoints which can exist in **conservative systems** which are characterized by having a constant phase-space volume.

Furthermore, in a phase-space with two or more dimensions, it is possible to have periodic behavior, represented by closed loop-trajectories -**limit cycles**- in phase-space. These loops can be either approached by trajectories or they can repell trajectories.

It is important to highlight that in two-dimensional phase-spaces of time-continuous systems, chaos cannot exist: in a **closed system** thus the phase-space is limited and any trajectory started in that region stays there for all times (motion is restricted to a finite area), there are only two possibilities for a trajectory. Either, it approaches an (attracting) fixed point, or it goes towards a limit cycle (Poincaré-Bendixson theorem). Due to the closeness of the system, any other dynamics would lead to a crossing / intersection of trajectories which is prohibited ("no-intersection theorem"). In other words, for time-continuous systems described by differential equations, we need to have at least three phase-space dimensions for the appearance of chaos. In contrary to that, maps can already display chaotic motion when only having one dimension.

In this thesis, we want to concentrate on conservative systems. Therefore, we will now take a closer look on the characteristical dynamics of that type of systems.

In **conservative systems**, no dissipation exists. A phase-space volume of initial conditions remains constant for all times. Conservative systems (with a phase space of dimension two) are also called **Hamiltonian systems**. That name goes back to the 19th century to Sir William Hamilton who described the time-evolution of conservative systems. The evolution of such a Hamiltonian system is completely given by a set of 2N coupled differential equations with the positions q_i and momentum p_i of its $i = 1...N$ particles:

$$\dot{q}_i = \frac{\partial H(q,p)}{\partial p_i}, \dot{p}_i = -\frac{\partial H(q,p)}{\partial q_i}. \tag{3}$$

The Hamiltonian function H usually represents the total energy of the system which is conserved. The state of the system is completely given by the N_i independent variables q_i ($i = 1, ..., N$)

which determine the degree of freedom N of the system. At this point, we should also mention **Liouville's theorem** which, in it generalized form, is the following:

$$\sigma = \left(-\frac{\partial f_1}{\partial x_q} + \frac{\partial f_2}{\partial x_2} \right) = -div\mathbf{f}. \tag{4}$$

For the special case of having a Hamiltonian system it states that volume in phase-space remains constant, thus $div\mathbf{f} = 0$. Therefore, and as explained above, attractors and repellors cannot exist in conservative systems.

Integrable Hamiltonian systems display only periodic or quasiperiodic behavior, chaotic motion cannot exist. Their phase-space is organized by elliptic points separated by separatrices which belong to hyperbolic points (separatrices are the stable and unstable manifolds of the hyperbolic points, separating phase-space regions with qualitatively different kinds of motion) (Fig. 7). The

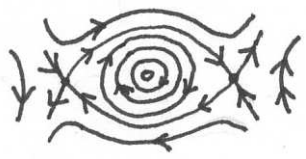

FIG. 7: Organization of phase space for an integrable system, corresponding to the phase-space picture of a frictionless pendulum. The pictures shows one elliptic point surrounded by separatrices associated with the hyperbolic points on the left an right.

elliptic points themselves are surrounded by closed loops, resulting from resonant motion of trajectories around the elliptic point. The closed loops are projections of a higher dimensional object: in the three-dimensional space, they correspond to closed **tori**.

If we now perturb our Hamiltonian system a bit, making it **nearly integrable**, the following will happen: due to the perturbation, constraints of the motion begin to diminish and trajectories will begin to move more freely through the phase-space as the perturbation increases. Hence, the 'organized patterns' due to the tori (elliptic and hyperbolic orbits) will be slowly destroyed.

For the destiny of the tori (in a two-dimensional phase space), we have to distinguish between two types of them where both are characterized by their **winding number** $\omega = \nu_1/\nu_2$. The winding (or rotation) number tells us about how many times the trajectory moves around the small cross section of the torus (ν_1) while it moves one time around the large circumfere of the torus (ν_2) (Fig. 10). Now, ω can be either a rational number which means that the resulting motion is periodic, or in the other case it can be irrational resulting in a quasi-periodic motion.

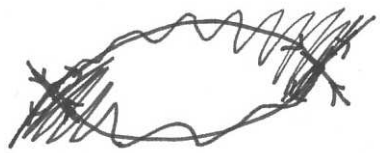

FIG. 8: Organization of phase space for a nearly integrable system: the in the integrable case exactly overlapping manifolds of two connected hyperbolic fixpoints begin to oscillate. Particles moving on these manifolds will exhibit irregular motion.

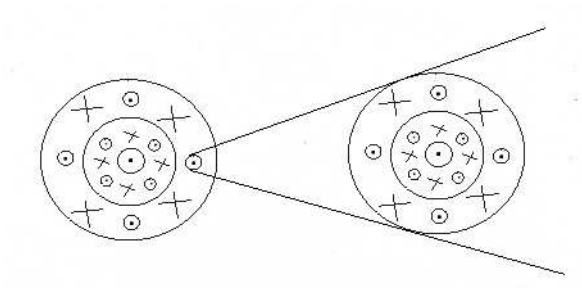

FIG. 9: Selfsimilar structures of tori in the vicinity of elliptic points. Left picture shows the organized patterns in a slightly perturbed system with its elliptic and hyperbolic points. Right picture shows a blow-up of an elliptic point with its surroundings.

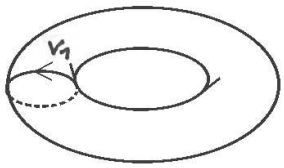

FIG. 10: Schematic of a torus. Particles moving on a torus exhibit a spiraling motion due to the movement along the small cross section (ν_1) and the circumfere (ν_2) of the torus.

As soon as our system now feels a perturbation, tori associated with rational winding numbers begin to break up. They split into pairwise hyperbolic and elliptic points -together with their associated families of higher order elliptic and hyperbolic points (Fig. 11, 9). Around the elliptic points, quasiperiodic motion will arise, whereas chaotic motion appears in the vicinity of the hyperbolic points. A crucial point is that between any two of the invariant curves around the elliptic points in our two-dimensional phase-space, elliptic- and hyperbolic points of some higher order exist. And around each of these secondary elliptic points are again closed curves between which a new set of elliptic and hyperbolic points of an higher iterate exist. This process continues

indefinetely (Fig. 9).

If the applied perturbation is small, then only tori with a rational winding number will break. Irrational tori might be deformed a bit. Kolmogorov, Arnold and Moser found in the 1970's a

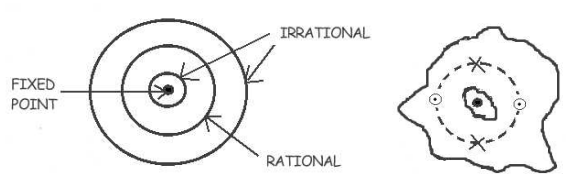

FIG. 11: Breakup of tori under the influence of a small perturbation. Left picture shows the torus before applying a perturbation, right picture shows how the torus with a rational winding number broke up into elliptic and hyperbolic points. The irrational tori still exist, showing some slight deformations.

theorem which states that some tori (**KAM-tori**), in particular those with an irrational winding number survive for a given (small) amount of nonintegrability of the system.

In phase-spaces with only one degrees of freedom, they can segregate regions in the phase-space, keeping some organization for the trajectories in phase-space.

As the system will be more and more perturbed it developes to a **nonintegrable** system. Then, all the tori will slowly break up and trajectories are able to move off them, displaying chaotic motion. Now, there opens the possibility that the trajectories move freely within the whole phase-space since no motion-restricting tori are existent any more. This kind of system is called an **ergodic system**. In our case, it is a fully chaotic system and therefore also called a **hyperbolic system**, because its dynamics is (only) influenced by the existence of an infinite number of hyperbolic points.

All of these hyperbolic points have their own stable and unstable manifolds, along which particles' motion takes place. For a closed system which is fully chaotic (hyperbolic) these manifolds are then space-filling, having an integer dimension corresponding to the dimension of the system. This is not the case for open systems. In an **open system** trajectories are not restricted to a certain region, they may come from infinity, enter the chaotic region which has a finite size, and then leave the chaotic region again. Consequently, there are stable manifolds governing particles into the chaotic region, and unstable manifolds along which particles can leave the chaotic region again. The manifolds are in this case not space-filling and have a fractal dimension. The common parts / intersections of the stable and unstable manifolds are the **chaotic saddle**. In other words,

it is the ensemble of all exisiting hyperbolic points and periodic orbits. The chaotic saddle is not attracting and is of fractal type, comparable with a double Cantor-Set. Trajectories which are exactly on the chaotic saddle will remain on it forever, exhibiting chaotic motion. Trajectories which are slightly off the chaotic saddle stay there only for a limited time, displaying transiently chaotic motion.

An open system can be for example a flow around an island, where the chaotic region is located in the wake of the island. In a closed flow however, particles stay forever within a bounded region. Numerically, closed flows can be constructed by superimposing periodic boundary conditions to a space-periodic system, so that e.g. a particle leaving the system on the right border will re-enter it again on the left.

III. THE LEAKING METHOD

A. Background

The description of transport of certain fields or particles by a flow is done by the application of statistical methods to the motion of fluid particles, i.e. to Lagrangian dynamics. Lagrangian dynamics provides a possibility to analyze a system by calculating the motion of particles, requiring only the velocity fields of the system.

Having a velocity field $\mathbf{v}(\mathbf{r}, t)$ which is smooth in space and $d \geq 3$ ordinary differential equations $\dot{\mathbf{r}} = \mathbf{v}(\mathbf{r}, t)$ (or $d \geq 2$ for time dependent flows), the Lagrangian dynamics can be chaotic.

Motion in chaotic systems is organized by different types of fixed points. In two dimensions, there is the possibility of having attractors, repellors or saddle points (for more details see Chapter II). We will focus on the saddle points, since we mainly work with conservative (thus volume preserving) systems, where no attractors or repellors can exist.

Saddle points play an important role in the chaotic motion of particles. The large sensitivity to perturbations and slight variations of initial conditions, is a result of the for chaotic systems characteristical exponential divergence of two nearby particles, created by saddle points. The ensemble of points in phase-space wherefrom particles are moving towards the saddle point is called the stable manifold, whereas the ensemble of those points from which particles move away from the saddle point is the unstable manifold of the saddle point. Trajectories of particles which are not *exactly* on either the stable or the unstable manifold have the shape of hyperbolas. Due to this fact, the points are also called hyperbolic points.

Particles following the direction of the stable manifold of the saddle point will converge, but their trajectories diverge exponentially along the saddle point's unstable manifold. These rates of convergence and divergence are characterized by the local Lyapunov exponents $\lambda_-(\mathbf{r})$ and $\lambda_+(\mathbf{r})$ of the hyperbolic point, with the separation Δ with time t at point $\mathbf{r}$ as $\Delta x(\mathbf{r}) = e^{\lambda_\pm(\mathbf{r})t}$.

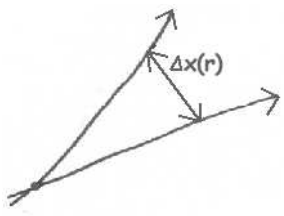

FIG. 12: Exponential divergence of two nearby particles.

In practice, every chaotic system is consisting of an infinite number of hyperbolic fixed points. Together they form either a chaotic attractor, or, for area-preserving systems as we want want to focus on here, the system's chaotic saddle. Each of its hyperbolic points is characterized by its own local Lyapunov exponent.

To have a measure of the chaoticity of the whole system, we can calculate the *average* Lyapunov exponent. The system is chaotic, if it has at least one positive average Lyapunov exponent (the number of existing average Lyapunov exponents corresponds to the dimension of the phase space). The sum of the average Lyapunov exponents is restricted to be zero for Hamiltonian systems, resulting in a volume preserving dynamics due to the same rates of convergence and divergence, e.g. for a two-dimensional system $\bar{\lambda}_+ = -\bar{\lambda}_-$.

Experimentally, we can get quick insight into the local distribution of Lyapunov exponents by placing any passive tracers in the system, concentrated to one place like in a droplet of dye. This droplet will then be squeezed along the stable manifold and stretched along the unstable manifold. Accordingly, the droplet will become a kind of material line, becoming thinner, squeezed by the local exponential factor of $\lambda_-(\mathbf{r})$, and longer, stretched with the local Lyapunov exponent $\lambda_+(\mathbf{r})$, with every iteration or time-step.

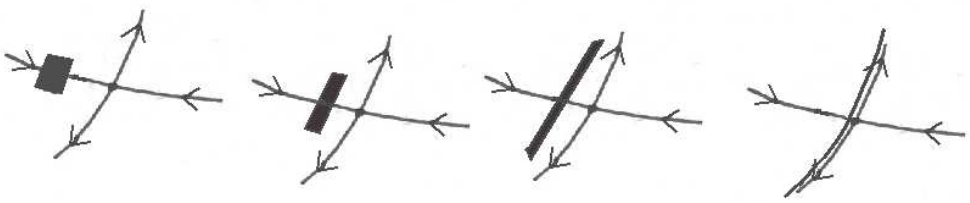

FIG. 13: Development of a droplet of dye, initially overlapping with the stable manifold of an hyperbolic point. As time goes on (from left to the right) the blob of dye will be squeezed in the direction of the stable manifold and stretched along the unstable manifold which will be approached.

Note that for Hamiltonian systems, on which we will focus here, the area of the droplet will remain constant during every iteration due to the Lypunov exponents which are opposite in sign.

The longer this process of stretching and folding goes on, the more accurately do passive particles trace out the unstable manifold. In closed flows, however, the visualization of the unstable manifold by the accumulation of passive tracers on and around it will only hold for a short time. Assuming that we have a fully hyperbolic and ergodic system, the manifolds are fully space-filling. Particles will consequently be spread in the whole system, covering it (and the space-filling un-

stable manifold) homogenously, so that no dynamical structures of the system can be seen any more.

But common flows are usually not perfectly hyperbolic, which means that not every point in the system has a well-defined contracting and expanding direction. Those points are then elliptic points, e.g. existing in KAM (Kolmogorov-Arnold-Moser) islands. However, for highly chaotic systems it is a good approximation to treat them as fully hyperbolic.

Apart from the possibility of visualizing structures of the unstable manifold of the system's chaotic saddle for a limited time, we can also obtain the chaotic saddle's stable manifold if we perform the same experiment, but with a backward running time.

For both manifolds, the crucial point is to find the proper length of the simulated time: taking too short time-spans, the particles might not cover accurately the invariant sets (parts of them could still be on the stable manifold or the chaotic saddle, while others are already on the unstable manifold). Simulating for too long times, particles are spread all over the system, if the system is fully hyperbolic, and not showing any structures.

The visualization of a system's manifolds is known to be easier in the case of *open* chaotic flows where the time-dependent region of the flow is restricted to a finite domain, called the mixing region. Particles' trajectories are asymptotically free before entering and after leaving the mixing region. They can exhibit chaotic motion if their trajectory overlaps with the invariant set. Then, they will move in the mixing, or scattering, region and will be trapped for some characteristical time-span τ, tracing out the system's unstable manifold.

First experimental evidence of chaotic scattering in a fluid wake was given by Sommerer et al [80]. Using a moving cylinder in a strongly stratified fluid, they created a periodically time dependent velocity field in the wake (scattering-) region. They showed that there exist unstable

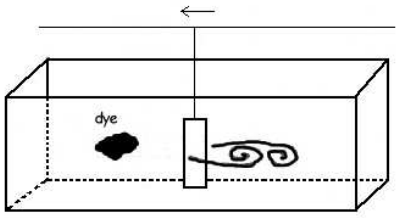

FIG. 14: Chaotic scattering of dye in the wake of a cylinder. The cylinder moves from the right to the left, in front of it a droplet of dye will be inserted.

periodic orbits in the wake of the cylinder: particles moving on or close to the stable manifold

spend a long time shadowing the chaotic saddle in the wake, then leaving it along its unstable manifold.

Due to the opennes of the system and thus the finite time particles spend on (or close to) the manifolds, the by the particles traced out structures of the manifolds of the chaotic saddle are always filamental and not space-filling, as in closed chaotic systems. Moreover, the traced out structures are then fractals.

The dimension of these fractal structures can be measured directly, giving a description of the strength of chaos in the system (the stronger, the larger the fractal dimension). In other words, the more chaotic the system is, the more hyperbolic points exist, around which particles bounce around in the wake, spending a longer time in the scattering region, tracing out denser structures.

This can also be measured by the time-delay function or the average lifetime τ of transient chaos [82]. It depends on the impact parameters of the initial conditions of particles and has an irregular appearance with singularities for particles started on the chaotic saddle's stable manifold. Experimentally, it can be measured e.g. by recording the intensity of dye which left the scattering region, as done by Sommerer et al. Alternatively, one can measure the number of particles which still did not leave the scattering region in dependence on the simulated time. The emptying process is then described by the escape rate $\kappa = 1/\tau$.

Numerically, the escape rate can be found quickly by distributing a large number of particles N_0 homogenously in the scattering region (alternatively, they can be also concentrated in one spot in or in front of the scattering region, but in this case one has to ensure that the position of the particles overlaps with the chaotic saddle's stable manifold) and then measuring the decay of the remaining particles N_t by time t which is exponential: $N(t) = N_0 e^{-\kappa t}$. The inverse of the escape rate gives the ideal length of simulation time for getting the most possible structures of the manifolds. The escape rate itself gives a measure of the strength of the chaotic saddle: the larger it is, the more unstable the saddle and the faster is the emptying process.

The escape rate κ is a global measure of instability of the system's chaotic saddle. It is related to the local properties describing value of the average Lyapunov exponent $\bar{\lambda}$ by the Kantz-Grassberger equation: $D_m = 2 - \kappa/\bar{\lambda}$, where D_m is the information dimension. It describes the fractality of the manifolds. Both manifolds have the same fractal dimension if the system is Hamiltonian, since for a conservative system having $\bar{\lambda}_+ = -\bar{\lambda}_-$, resulting in $D_{sm} = D_{um}$ (with D_{sm} denoting the dimension of the stable manifold, and D_{um} the dimension of the unstable manifold, respectively). Note that the chaotic saddle always has a lower dimension ($2(1 - \kappa/\bar{\lambda})$) due to the

fact that it only consists of the common part of its stable and unstable manifolds.

But let us come back to closed flows. Here, if the system is highly chaotic (fully hyperbolic), particles' motion is ergodic as explained above. This implies that both manifolds and also the corresponding chaotic saddle are space filling, their dimension is an integer, corresponding to the full phase-space dimension. In other words, we dont get any information about the structures of the manifolds of the chaotic saddle, apart from the transient structures traced out by passive tracers, or structures traced out by active particles. Latter one means, that the particles carry certain properties, as e.g. different concentration values which decay by time.

Experimental evidence for the movement of particles along the saddle's unstable manifold in closed flows has been shown by Voth et al [87], building on an experiment performed by Rothstein et al [71]. They used a two-dimensional (density stratified) fluid flow and a time-periodic magnetic forcing, affecting a conducting layer above an array of permanent magnets. Tracer particles (e.g. dye) are moving upon a nonconducting upper layer. The resulting flow field is a time-periodic vortex array. Using time-periodic square or sine wave forcing, there is no mean flow. Due to this, persistant patterns can emerge: initially, half of the upper layer is filled with dye. After some transient time, the concentration field reaches a nearly steady state, the by different concentrations traced out structures appear at same phases of the forcing. As passive tracers, the dye is spread in the whole system after some transient time. But due to the additional property of carrying different (decaying) concentrations, we can still identify structures with the help of concentration gradients. These gradients appear due to the continuous stretching and folding of the fluid and are aligned with the stretching field, thus showing structures of the unstable manifold. Voth et al gave evidence for this by also calculating the past and future stretching fields of the flow, measuring particle displacements. They found that these past and future stretching fields, beeing nothing but the stable and unstable manifold of the flow's chaotic saddle, are corresponding to the gradients of the dye. They are material levels or lines, having their origin in hyperbolic fixed points, organizing the evolution of inhomogenities in the flow and giving insight into the geometrical structures governing the mixing dynamics. These visualized structures of the unstable manifold are the 'roads of transport', since particles are moving on them, tranporting certain properties along them.

Thus, the visualization of the manifolds is an important task not only for theoretical purposes, but also for real experiments. For example, for mixing processes, it is important to know about the 'roads of transport', along which certain properties as e.g. temperature, oxygen or pollutants are transported. Furthermore, for mixing processes, it is also important to know about the mixing

strength itself, measured by the Lyapunov exponents. They quantify mixing by beeing a measure of particle separation, depending on the global properties of the flow only.

The efficiency of mixing on the local scale can be characterized by the finite time Lyapunov exponents (FTLE): depending on the initial position, the motion of every particle is determined by its individual FTLE. However, in the asymptotic time limit, all particles will diverge and converge with the same exponential rate $\bar{\lambda}$.

Another possibility of characterizing mixing is to monitor the growth of material filaments. Measurements of this kind have been done e.g. by Neufeld et al [51]. Recent investigations have been done by Alvarez et al [2] who measured the growth of material lines and found that the filament lengths $L_n$grows much faster than one would predict whith using the average Lyapunov exponent $\bar{\lambda}$: $L_n \approx e^{\bar{\lambda}n}$. The explanation for this is that for finite time, the local Lyapunov exponents do not correspond to the average one. Instead, there is a nonuniform stretching field due to the different local Lyapunov exponents. Alvarez et al found that the exponential growth rate of the filamental length is detemined by the topological entropy exponent θ: $L_n \approx e^{\theta n}$, with $\theta > \bar{\lambda}$.

Plotting the FTLEs at certain instants of time gives a picture about the stretching (converging) field when simulating forward (backward) in time. Many investigations about the FTLE exponents have been performed, one of the latest was done by Lapeyre [40] who computed the spatial distribution of FTLEs in freely decaying $2d$ turbulence. Lapeyre confirmed that filaments with the largest FTLEs coincide with the (turbulent) flow's invariant manifold. Indeed, calculating the FTLEs is one approach to find the geometrical structures, the stable and unstable manifolds, which are guiding the global mixing.

Another approach to calculate the manifolds directly is based on starting a droplet on a stagnation point of the velocity field and then following its motion forward and backward in time, finding approximations of the stable and unstable invariant sets. However, the difficult task is first of all the existence of such a point and its identification. A refinment of this method was done with developing analytical tools with which finite time invariant manifolds in two-dimensional velocity fields could be identified [21].

All in all, the visualization of structures of the manifolds of the flow's chaotic saddle is a challenging task in closed flows. When not working with active particles, rather long and complicated analytical and /or numerical methods are used. In this chapter, we want to propose a new method which provides filamental structures of the manifolds in a computationally very fast and cheap way.

B. Introducing Leaking in 2d flows

this chapter is published in:

'Dynamics of leaking Hamiltonian systems',

J. Schneider, T. Tél, Z. Neufeld

Physical Review E (Ref[77])

As discussed above, in closed chaotic Hamiltonian systems the detection of manifolds is a rather challenging task. Apart from the possibility of using active tracers so that their different concentration gradients show filaments of the underlying manifolds when the system is covered enterily by the tracers, other methods are all based on analytical calculations.

Examples for the former one were given in the background of this chapter. The maybe easyest example for the latter one, the active tracers, is a numerical experiment by Pierrehumbert [63], using a so-called resetting-algorithm for studying chaotic stirring in fluids. He studied passive advection by two-dimensional incompressible closed flows in an example of the double-periodic area-preserving sine-map. A resetting forcing is applied in two finite regions (resetting domains) of the flow. Tracer particles which enter one of the two domains of the flow get a concentration value or color associated with that region. For example, the left region will give particles a black color, while the right one will color them white. The given color will be carried by the particle

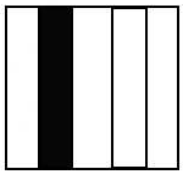

FIG. 15: Two resetting domains in a two-dimensional closed flows which is initially homogenously filled with particles. Left resetting domain (black stripe) will color particles entering it black, right resetting region (white stripe) will give particles a white color.

until it enters the other region where the color is changed again. Due to this resetting-forcing, all particles will carry one of the colors after some finite time.

This resetting forcing mimicks changes of properties carried by particles in our environment, as can be seen e.g. in thermal convection, where the temperature of the fluid parcels will be re-setted if they reach the hot (upper) or cold (lower) boundary / region. The resetting algorithm can also

be considered to be an elementary model of chemical reactions, since the fluid particles can have certain properties that they will loose by reaching one of the pre-selected regions. After returning from there, they therefore behave differently from the point of view of chemical activity, which is marked by the change of their colors. Thus, this simple algorithm is sufficient to make clear filamentational patterns visible in the flow.

A recent discovery [50] in the field of real chemical reactions superimposed on closed flows shows that the product distribution can be filamental inspite of the fact that the passive problem has a Hamiltonian chaotic dynamics. The chemistry is visualizing in this case the unstable filamentation.

Furthermore, the advantage of the use of the resetting forcing is that the structures traced out by differently colored particles are fractals, equivalently to patterns created by tracer advection in open flows.

An upgrade of this algorithm is the so-called Leaking method which we developed end of 2000. It consists of considering a finite region which is, in contrary to the one by Pierrehumbert, an exit out of the system. With this cutting out of a finite region in the phase-space of the flow, the leak, through which an escape of particles is possible, we open up the formerly closed chaotic Hamiltonian system. This then leads to transiently chaotic behavior and to an escape of nearly all particles out of the system.

The possibility of leaking to generate chaos with a finite lifetime in the case of a billard was already mentioned in the classical paper by Pianigiani and Yorke on transient chaos [62]. Later this problem was discussed in detail in the context of fractal exit boundaries [5], of geometrical accoustics [41], as well as in the context of ergodicity [42] with fixed holes of exit. Another, more recent, reason for studying the motion in leaked systems is the Ott-Grebogi-Yorke (OGY) method of controlling chaos [55] in which a control region is defined inside of which the dynamics is changed to achieve control [58]. Furthermore, leaking can be relevant in many problems of celestial mechanics and cosmology, where gravitating bodies are considered to be point masses: by taking into account their finite sizes, the probability of collisions becomes nonzero. The simplest way of discussing this effect is to take out particles from the process after having hit other ones. This corresponds to leaking the phase space around the center of large bodies with arbitrary momenta. A leaking method has also been applied for analyzing the chaotic structure of the mixmaster cosmological model [48]. A problem of great technological relevance is the design of heterostructure devices: in the ballistic regime, these nanoscale structures are, from the point

of view of the electron's motion, billiards, leaked at the positions of the leads [78]. Characteristics of the transiently chaotic classical motion in these open billiards (such as, e.g., the escape rate) are known to be related to the statistics of the measured conductance fluctuations. In these investigations, the size of the leak is typically small and its position is unchanged.

Here, our aim is to understand the dynamics of closed chaotic Hamiltonian systems in more detail, in particular, to visualize their space-filling unstable foliation. We emphasize that the appearing transiently chaotic behavior is always related to the presence of a chaotic saddle which governs the motion of the long-lasting transients. The chaotic saddle, made visible by the leaking, is necessarily a subset of the original invariant space-filling set and can thus be considered as a skeleton of it. Furthermore, we want to study whether the characteristics of the generated transient chaos changes by changing the orientation of a large leak. In the chaotic region of closed Hamiltonian systems where the natural measure is uniform, one might expect that the escape process depends on the area of the leaked region only. Instead, we find that there is an essential dependence on the orientation even if the area is fixed. This dependence can be considered as a fingerprint of the unstable foliation of the chaotic region, which is not visible as a phase-space structure in the closed case but becomes observable by the smallest amount of leaking. We point out that the anisotropy of this foliation, together with the finite size of the leak, is responsible for the observed orientation dependence.

1. Numerical procedure

In contrast to previous studies, we investigate the effect of large leaks and take a band crossing through the full phase space as the leak. Its center is chosen to be the center of the phase space. One freely changeable parameter is then the width ϵ of the band in the x direction which also measures the area and the angle θ of its axis relative to a fixed direction. The analysis is carried out in the spirit of the theory of transient chaos [82]: the basic aim is to identify the set of never-escaping orbits, a nonescaping chaotic set, the so-called chaotic saddle, along with its stable and unstable manifolds. The characteristic number to be measured is the escape rate κ versus ϵ and θ. The invariant sets are determined by means of the method described in [39]. We start with a large number N_0 of particles initially distributed in the full phase space uniformly. All the nonescaping particles are followed over a large number of iterations, say n. For large enough N_0 and n, the initial coordinates of the nonescaping particles should trace out the stable manifold, their final positions

after n steps of the unstable manifold, and the midpoints at time $n/2$ of the chaotic saddle itself. The reason for this is that from regions outside of eventually existing KAM (Kolmogorov-Arnold-Moser) tori all initial points exit with the exception of a fractal set of measure zero. Therefore, points spending a long time in the leaked system must be those that came close to the chaotic set. The points still inside after n steps are thus either on the chaotic saddle or are already about to leave it. If so, they are practically on the unstable manifold. A long time ($n/2$ steps) earlier they must have been around the saddle, and initially around the stable manifold. The basic quantity we use to measure the degree of openness is the escape rate κ from the chaotic saddle. The number of $N_n - N_\infty$ of surviving points after n steps (N_∞ stands for the never-escaping points due to the presence of KAM tori) should decrease after a large number of steps as $exp(-\kappa n)$. The escape rate was determined by measuring the number $N_n - N_\infty$ of survivors and fitting a straight line to the $ln(N_n - N_\infty)$ versus n curve.

2. The Baker map

As a very simple example in which no KAM tori can be present, we take the area preserving baker map [56]:

$$x_{n+1} = \begin{cases} cx_n, & y \leq 1/2 \\ 1 + c(x_n - 1), & y > 1/2 \end{cases}$$

$$y_{n+1} = \begin{cases} ay_n, & y \leq 1/2 \\ 1 + a(y_n - 1), & y > 1/2. \end{cases}$$

For guaranteeing the area-preservation, the parameters are chosen as $a = 2$, and $c = 1/2$ (rate of stretching equals squeezing). The dynamics of the baker map is defined on the unit square and works as the following: the lower half square is compressed along the x axis to its half and is stretched along the y axis by a factor of 2 so that the left lower corner, the origin, is kept fixed. The upper half square is transformed in a similar way but the upper right corner, the point $(1, 1)$, is left unchanged during this process. The system is known to be fully hyperbolic, all local Lyapunov exponents are $\ln 2$, and therefore no stability islands (no elliptic points) are present. The natural distribution is uniform on the full square.

Figure 16 shows the saddle and its manifolds in the case of a leak with a width and area of $\varepsilon = 0.1$ and located at angles $\theta = \pm 25^\circ$ relative to the vertical line going through the midpoint of the unit square. The leak is clearly visible as a white band. There are much more white bands

present: in the plot of the stable (unstable) manifold these are the pre-images (images) of the leak, and in the plot of the saddle both the pre-images and the images are present. Although the baker map is thought to be symmetric around the midpoint of the square, its action on a full line crossing the unit square is not. This is quite clear in the first images of the leak (bands of second largest width in Fig. 16c, 16f), but the effect is even stronger in the case of the first pre-images (bands of second largest width in Fig. 16a, 16d). The pre-images of left and right tilted bands are completely different. The inverse map transforms the left (right) half square on the lower (upper) half square.

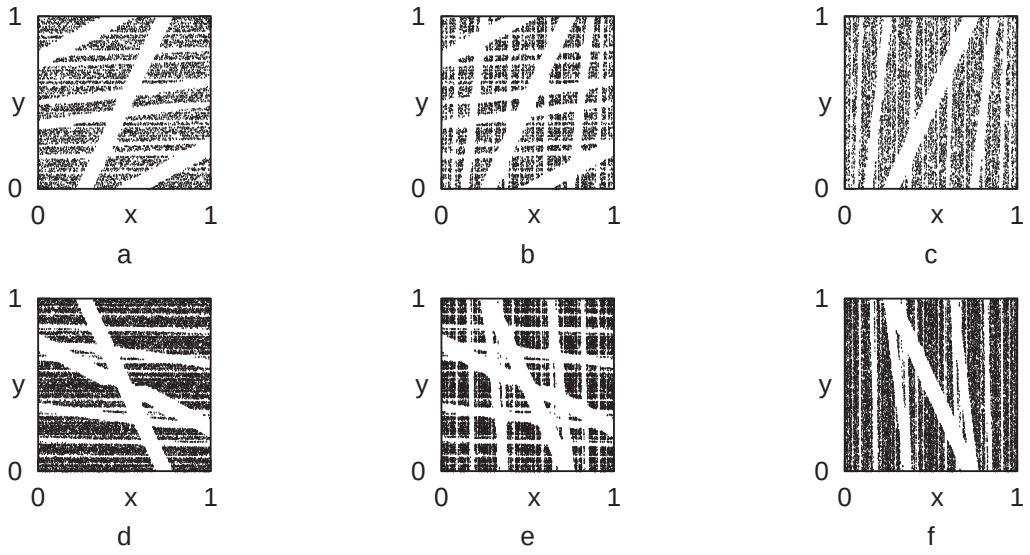

FIG. 16: The stable manifold, the chaotic saddle, and the unstable manifold of the leaked baker map with $\varepsilon = 0.1$ in the case of a tilted leak with angle $\theta = 25$ (a),b),and c)) and $\theta = -25$ (d),e),and f)). The parameters of the simulations are $N_0 = 10^6$, $n = 40$. The different contrast of the pictures is due to the different decays: the number of remaining particles is $N_{40} = 9537$ ($N_{40} = 22399$) in the 25° (-25°) case so that the escape rate is $\kappa(25^\circ) = 0.11$ ($\kappa(-25^\circ) = 0.09$).

Therefore, the lower part of the 25° leak is mapped on a band around the lower right corner, while that of the -25° leak is mapped on a band around the lower left corner of the second quadrant(!),

etc.. More importantly, the first pre-image of the 25° leak does not overlap with the leak, but there is an overlap in the other case. Thus, the total area of the leak and its first pre-image is larger for the positive angle case than for the negative one. This asymmetry is kept by further iterations leading to different values of the escape rate: $\kappa(25^\circ) > \kappa(-25^\circ)$. The difference in the escape rate can be deducted from the darkness of the invariant sets, too, since we used the same number of initial conditions and therefore more points (smaller escape rate) imply darker figures.

Fig. 17 is an overview of the chaotic saddles for the same width but at other angles θ. The completely different textures at angles of opposite signs are striking. The dependence of the escape

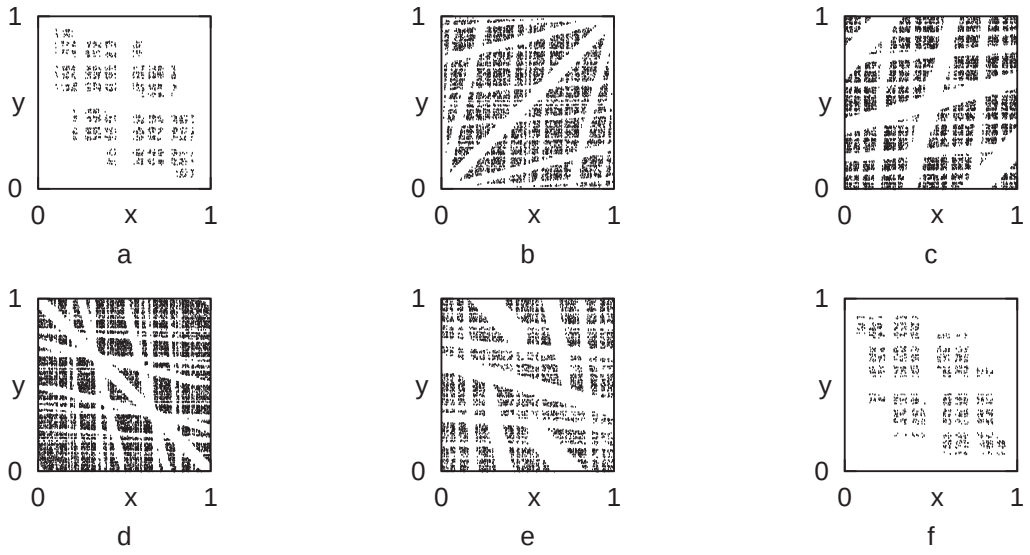

FIG. 17: The chaotic saddles of the leaked baker map with $\varepsilon = 0.1$ at leak angles $\theta = 0^\circ$ (a) 45° (b), 75° (c), and $\theta = -45^\circ$ (d), -75° (e), and $\mp 90^\circ$ (f). The parameters of the simulations are $N_0 = 10^6$, $n = 40$. In order to ensure that the leak area is always ε, at leak angles $\theta = \pm 45^\circ$ (parts b), d)) we added tiny leak pieces around the corners not crossed by the main band, as if the map were periodic. Contrast differences can be observed again.

rate on both parameters is summarized in Fig. 18. The escape rate belonging to very narrow leaks

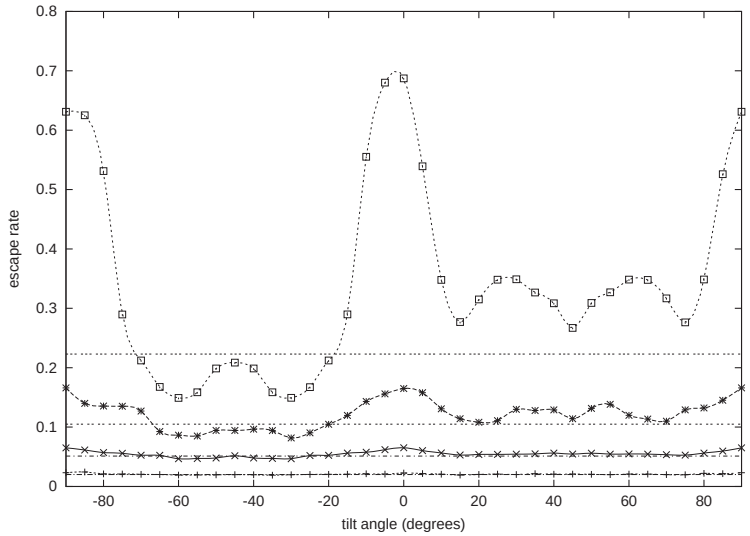

FIG. 18: The dependence of the escape rate on the tilt angle at different widths $\varepsilon = 0.02$ (+), 0.05 (x), 0.1 ($*$), 0.2 (squares). Horizontal lines correspond to the values $\kappa = -\ln(1-\varepsilon)$.

is nearly orientation independent. In addition, the value of κ is then close to the total relative area of the leak, which is ε in our case. Orientation dependence becomes considerable by $\varepsilon = 0.1$, and the amount of fluctuations around the mean is increasing with increasing area. In all cases the naive expectation $\kappa = -\ln(1-\varepsilon)$ is close to or below the average escape rate over all the angles.

3. *The Sine map*

Next we consider the sine map introduced in [63]. It is a double periodic map defined on the unit square whose action is the subsequent application of two sinusoidal displacements: one in the x, the other one in the y direction. The explicit form of the map is

$$x_{n+1} = x_n + a\sin(2\pi y_n + \phi_n) \mod 1,$$

$$y_{n+1} = y_n + a\sin(2\pi x_{n+1} + \phi_n) \mod 1. \tag{5}$$

We will use the amplitude $a = 0.6$.

First, all the phase variables will be taken to be zero: $\phi_n \equiv 0$. In this case the map represents a typical, closed Hamiltonian system [49, 63] containing islands of integrability and broken KAM tori (cantori).

These regions are clearly visible in the invariant sets (Fig. 19) since due to the homogeneous initial distribution, points starting in these regions escape very slowly or do not escape at all. Hence

the very dark structures appearing in the plots. Again, the asymmetry due to the leak orientation is clear.

In the escape rate versus ε and θ diagram of Fig. 20 we see again that leaks with small area have the weakest orientation dependence. In these cases the escape rate is well approximated by the area ε of the leak. At larger areas, however, fluctuations become stronger. It can be read off

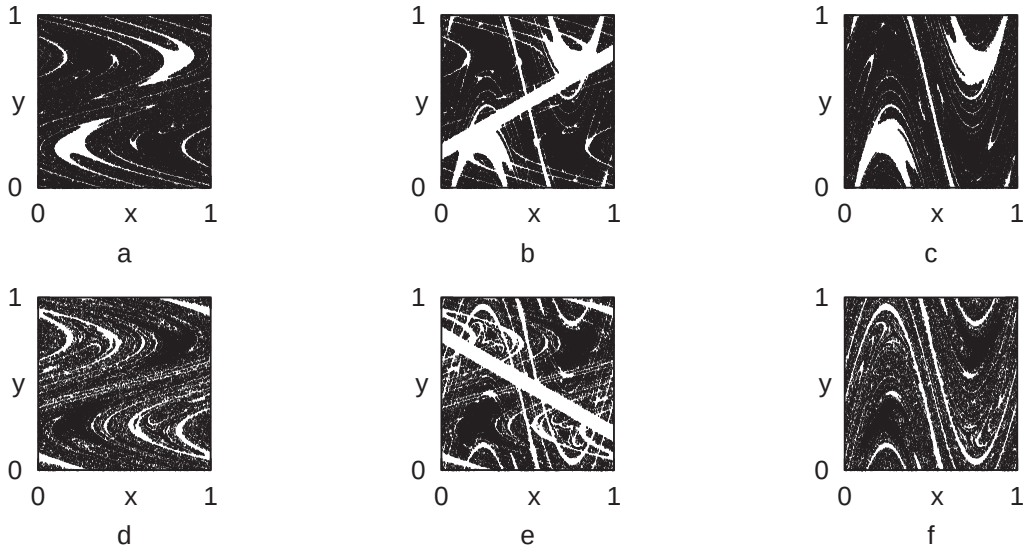

FIG. 19: The stable manifold, the chaotic saddle, and the unstable manifold of the leaked sine map with $\varepsilon = 0.1$ in the case of a tilted leak under angle $\theta = 60$ (a),b),and c)) and $\theta = -60$ (d),e),and f)). In order to stronger emphasize the stable and unstable foliation, in parts a),c),d) and f) we do not show the leak. The leak is, however, clearly visible in the plots of the chaotic saddles (parts b) and e)) as the widest white band. The parameters of the simulations are $N_0 = 1 \cdot 10^5$, $n = 20$.

from Fig. 20 that leak angles coinciding with the slope of the local unstable and stable foliation ($\theta = -20^\circ$ and 70° in the sine map, and 0° and $\pm 90^\circ$ in the baker map) always belong to a local maximum of the escape rate (which is a global one in the baker map). No simple rules have been found for predicting the angles of the other local maxima. In this case the $\kappa(\theta)$ diagram exhibits

an invariance under translations with $90°$.

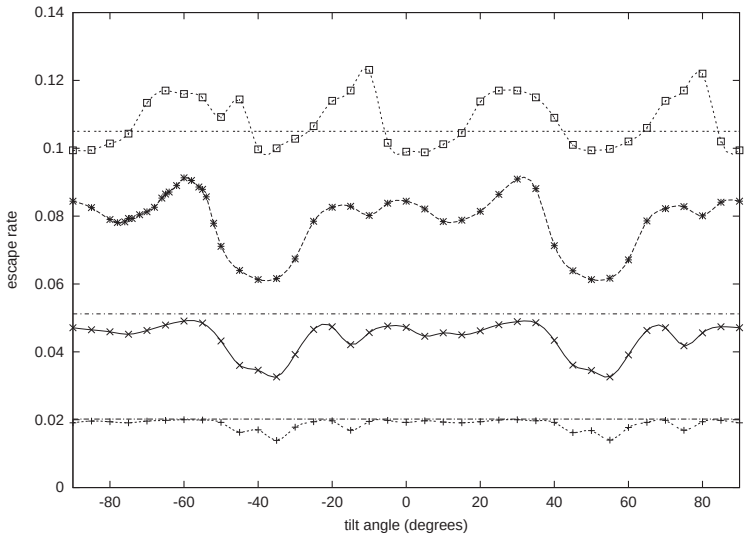

FIG. 20: The dependence of the escape rate on the tilt angle at different widths $\varepsilon = 0.02$ $(+)$, 0.05 (x), 0.1 $(*)$, 0.2 (squares). Horizontal lines correspond to the values $\kappa = -\ln(1-\varepsilon)$. The one belonging to $\varepsilon = 0.2$ is beyond the frame.

The naive expectation $\kappa = -\ln(1-\varepsilon)$ is now *above* the average escape rate over the angles. In the case of the largest area investigated it is much larger than any of the measured escape rates. We attribute this to the presence of the KAM tori and cantori, and to their remnants after leaking. These surfaces are known to be sticky and the long time decay from their neighborhood is not even exponential, but of power law type [11]. We are interested in the intermediate time behavior which is found to be still exponential but the presence of these surfaces makes also the effective escape rate κ smaller than in cases without tori. This is why the naive expectation becomes now an upper bound. In fact an even larger upper bound follows if the total surface of all the KAM regions are added to ε.

These qualitative findings are valid for any shape and location of the leak. We carried out numerical experiments also with two-band leaks under various angles and at different locations.

As shown in the experiments by Rothstein et al [71], persistent patterns arise in periodically driven flows when taking sampling snapshots in phase: after a certain transient time, a steady mixing pattern is created and repeats itself with every period. As already shown above, patterns created by tracer particles are nothing but the structures of the unstable manifold. So it is easy to understand that for the manifolds, obtained with our method of leaking, the same rules hold: for time-periodical systems the visualized structures of the manifolds are the same, no matter how

long we simulate. The structures may become less detailed the longer we simulate corresponding to the decaying contrast of the mixing patterns in Rothsteins experiment. But this can be compensated by using the more particles the longer the simulation has to run (although you will need an incredible huge amount of particles when choosing too long times, and the computational expenses are usually not worth to do so. So, as you can see, it is an important point to choose a proper simulation length τ, having the most possible structures in the manifolds with the smallest computational costs).

When taking snapshots of the mixing patterns out of phase the patterns of the tracers will change substantially. It is like taking snapshots of non-periodically, thus randomly or chaotically, forced systems (it does not matter in this case wether the snaphsots are in phase or not). The same is true for the structures of the manifolds we obtain by leaking: even for systems with chaotic time-dependence, we get clear filamental structures of the manifolds. But in this case, the structures do not resemble each-other in the snapshots, they change in time.

4. The random sine map

The random version of the sine map is obtained by considering random phases, i.e, by taking the values ϕ_n of (5) at any instant of discrete time n from a stationary ensemble from the range $(-\pi, \pi)$. The map remains area preserving with these phases, too, but the presence of the random perturbation leads to the disappearance of any invariant tori [30, 63]. This might, however, be observed in numerical simulations on long time scales only. In the fluid dynamical context, the random version of the map represents the advection problem in an incompressible (smooth, non-turbulent) flow with an aperiodic (chaotic) time dependence. The basic difference relative to the previous cases is that the chaotic saddle and the manifolds are no longer independent of the number n of iterations taken, not even for large values of n. Their shapes are changing with n (since the random phases do so) but their fractal dimensions do not. Therefore, the plots look qualitatively similar irrespective of the value of n used. Fig. 21 shows the invariant sets. The former dark spots are no longer present because of the disappearance of coherent phase space structures.

Considering the dependence of the escape rate on the orientation, we find (Fig.22) that the fluctuations are reduced. This can be interpreted by observing that the random phases indicate a shift of the filamentation in a certain direction. Since the leak is fixed, the filamentation under it is time-dependent, and hence an averaging procedure is carried out. This leads to a much weaker

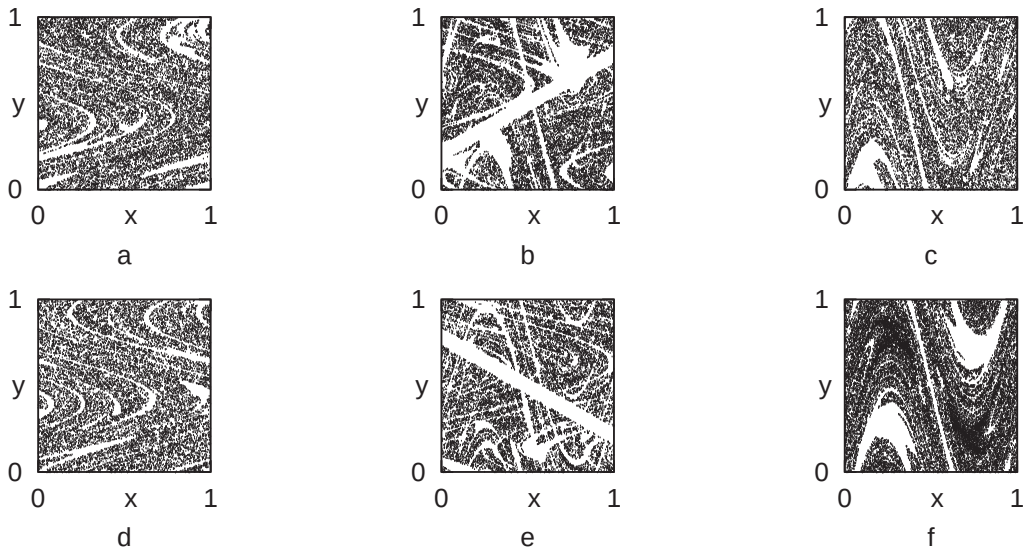

FIG. 21: The same as Fig. 19 for the random sine map. The topological structure is similar but the difference in contrast is greatly diminished.

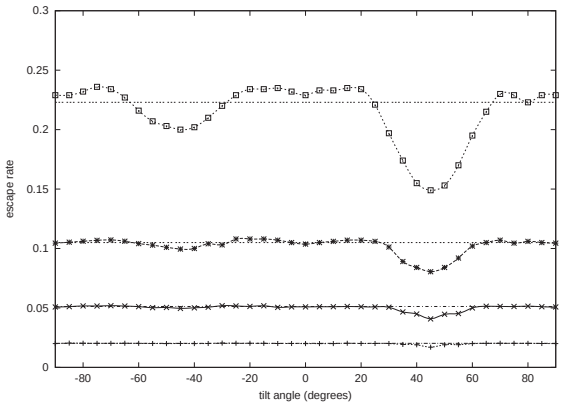

FIG. 22: The dependence of the escape rate on the tilt angle at different widths $\varepsilon = 0.02$ (+),0.05 (x), 0.1 ($*$), 0.2 (squares) for the random sine map. Horizontal lines correspond to the values $\kappa = -\ln(1-\varepsilon)$.

orientation-dependence than in the nonrandom case.

In addition, the value of the escape rate comes closer to the naive expectation $\kappa = -\ln(1-\varepsilon)$

since sticky phase space surfaces are efficiently destroyed by the randomness of the phase.

Note, that there are two minima of the κ versus tilt angle curve shown in Fig. 22 extracted from simulations carried out over 20 time steps. By following ensembles of particles over longer times and deducing κ as the asymptotic decay rate, we observe that the minimum values become closer to each other, and to the naive expectation as well; the curve becomes better smoothed out. It is worth mentioning that by randomly choosing the position of the center of the leak along the x or y axis (at fixed tilt angle) and by using the nonrandom sine map, the orientation dependence of the escape rate fully vanishes and this can already be seen over short time scales.

5. Conclusions

From the point of view of the application of the resetting algorithm [63] described in the introduction, our results imply that the patterns depend not only on the size of the resetting region but on its orientation, too. This dependence disappears, however, if the flow is sufficiently random, or sufficiently chaotic.

Another implication of our findings can be a proper interpretation of transient droplet patterns in closed flows. The initial droplet is compact, its dimension is 2. As time goes on, the droplet is stretched and folded (its area is unchanged) and becomes elongated along the unstable filamentation of the flow. There might be an instant of time, where the shape of the droplet is similar to the unstable manifold of the leaked flow with a certain width and orientation of the leak (Fig. 23d is quite similar to 23e). This does not mean, however, that the droplet's shape is the same on *all* scales as the unstable manifold. It does not have in any instant a well-defined fractal dimension [11]. In fact, its form appears to be denser already after three more steps (Fig. 23f). The only stage where its dimension is well defined [11] is that of the asymptotic state reached after an infinitely long time, when it fills the full chaotic region (and its dimension is 2 again).

In a general hydrodynamical problem, it is natural to find regions of qualitatively different flow features (like e.g. jets, recirculating regions, eddies, etc.). One can then select one of these regions and consider all others as leaks in order to determine the escape rate, which is a measure of material exchange of this region with its surroundings. Small values of the escape rate mark regions with large lifetimes of water which might therefore be of specific biological relevance.

The last property we discuss is the relation to filamental chemical or biological product distributions in closed flows. We have considered a very simple chemical reaction, the decay of

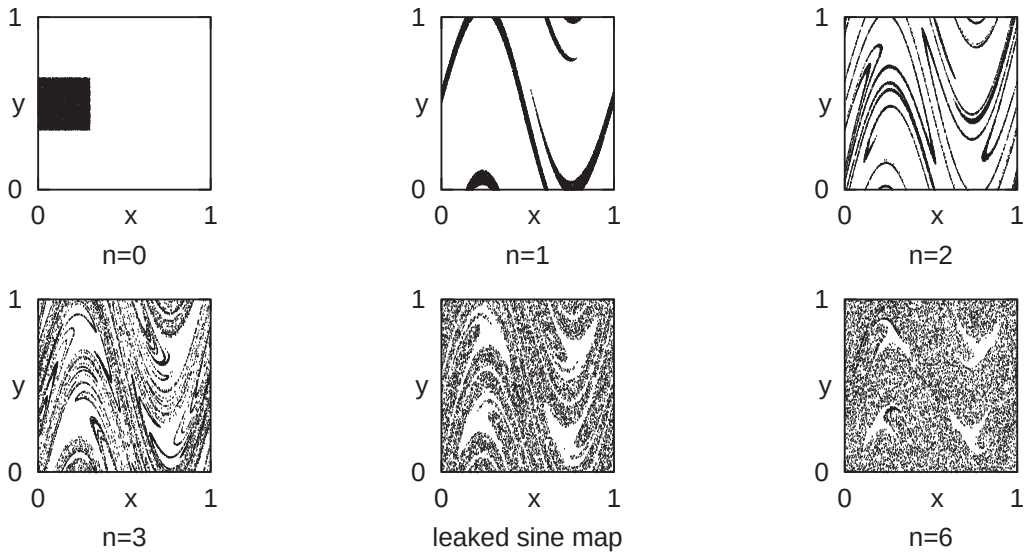

FIG. 23: The shape of a square droplet at time $n = 0$ (a), $n = 1$ (b), $n = 2$ (c), $n = 3$ (d), and $n = 6$ (f) in the nonrandom sine map. Part e) is the unstable manifold of the chaotic saddle obtained by leaking the map with two identical bands parallel to the y-axis of width $\varepsilon = 0.1$ with midpoints at $(0.25, 0.5)$ and $(0.75, 0.5)$

the concentration C of some chemical constituent towards a background value superimposed on the random sine map as a hydrodynamical flow. The chemical field $C(x, y)$ is generated by the mapping

$$C_{n+1} = S(x_n, y_n) + bC_n, \tag{6}$$

$$x_{n+1} = (x_n + a \sin(2\pi y_n + \phi_n)) \mod 1,$$

$$y_{n+1} = (y_n + a \sin(2\pi x_{n+1} + \phi_n)) \mod 1,$$

where $S = S_0 + S_1 \sin(2\pi x) \sin(2\pi y)$ is the fixed source distribution and the parameter b ($b < 1$) is a measure of the decay rate. In each step the chemical concentration decays by a factor b (in our case $b = 0.5$) and receives an input $S(x, y)$ according to the local source concentration. Then

the fluid parcels are advected by the random sine map ($a = 0.7$). Fig. 24 shows the concentration

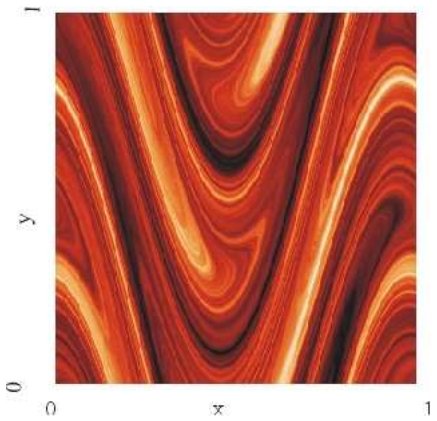

FIG. 24: Chemical concentration field of problem (6) obtained by iterating the sine map with random phases at $a = 0.7$. Bright colors indicate regions of high concentration.

distribution obtained in this way. It has a striking filamental structure since the parameter values correspond to a state beyond the smooth-filamental transition defined and described in [50]. In the left picture of Fig. 25 only the regions of high concentration ($C > 1$) are plotted. The boundary between black and white regions, corresponding to an iso-concentration surface, shows a subset of the unstable foliation. It is therefore not surprising that the unstable manifolds of the leaked passive system, which is also a subset of the unstable foliation (right picture of Fig. 25b), trace out a similar structure. In general, biological or chemical active processes always accumulate along the unstable manifold of a chaotic saddle [85], which serves as a backbone for the active process. Hence, by leaking the underlying Hamiltonian system and visualizing the unstable manifold of the chaotic saddle, we are able to reconstruct, mimic or even forecast structures traced out by active processes, for example structures related to phytoplankton distributions in the Gulf Stream [50, 76].

In conclusion, the geometric structure of the unstable foliation of a closed Hamiltonian problem is the origin of the strong dependence of the escape rate on the orientation of the leak. Local maxima of this function correspond to the direction of the unstable or of the stable foliation. The randomness of the dynamics is smoothening out the orientation dependence. The method can also be used to indicate the presence of KAM islands since the effective escape rate in non-random cases is then smaller than the naive expectation. Measuring the escape rate of leaked area preserving systems can give a useful piece of information about the unstable foliation of the closed system, whose fingerprints otherwise only appear as instantaneous droplet shapes or as backbones

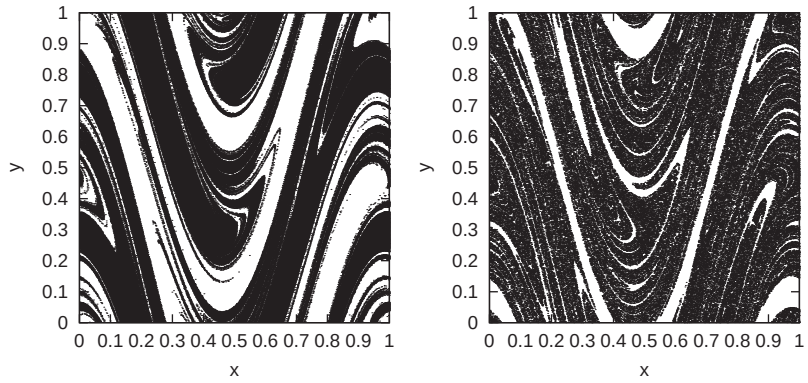

FIG. 25: Left picture: The concentration distribution of problem (6) in the random sine map after 10 steps of iteration starting from an initially homogeneous distribution. Black regions correspond to concentrations higher than the treshold value C_{th} = 1 . Right picture: The unstable manifold of the chaotic saddle in the leaked passive problem obtained by using the same random sequence. The leak is taken as 0.1 .

of chemical product distributions.

Our findings might have relevance beyond the field of hydrodynamics, too. For mesoscopic devices in the ballistic regime, we predict a strong dependence of the escape rate and hence of conductance fluctuations on the actual position of the leads (at fixed width) along the wall of the billiard.

Indeed, the result that the escape rate depends sensitively on the choice of the leak / the boundary of the system has been verified with numerical experiments about ray dynamics in a paraxial optical cavity where ray-splitting is present [66].

C. Fractal structures due to leaking in 3d non-Hamiltonian systems

this chapter is part of a publication in:

'Opening up fractal structures of three dimensional flows via leaking'

I. Tuval, J. Schneider, O. Piro, T. Tél

Europhysics Letters (Ref [84])

In this section, we study the behavior of time-periodic three-dimensional incompressible flows modelled by three-dimensional volume-preserving maps in the presence of a leak. The dynamics of passive impurities transported by a three-dimensional incompressible fluid flow is conservative, the volume occupied by the particles remains constant under the evolution. There are situations, however, in which a peculiar type of dissipation comes to the scene. Consider for example the following problem: the air of a room in which a controlled flow pattern has been established needs to be cleaned. A purifier system installed at a specific location is to be chosen in order to maximize its eściency. In a simplified view, we can think of the purifier as a volume of the space where the impurities are eliminated of the system without perturbing the flow. We are then facing a 'leaking' dynamics in which trajectories evolve preserving the volume until they reach a specified region of the space where they disappear. Our problem is then deeply related to the investigation of the changes expected in the residence time of the particles in the allowed phase space (the room) as we modify the shape and location of the leak (the purifier design).

The purpose of our work here is to perform the first study of this kind for a conservative but non-hamiltonian dynamical system, namely, volume preserving three-dimensional maps describing the basic features of incompressible time periodic flows. Apart from the applications, the study of leaked volume-preserving maps in three dimensions poses a few challenging questions to the theory of dynamical systems. For example, a key dynamical objects to understand leaked systems as well as many other open dynamical systems such as those describing scattering processes, are the so-called chaotic saddles and their associated stable and unstable manifolds. The chaotic saddle represents the set of points that never escape through the leak either forward or backward in time. The stable (unstable) manifold is the union of points which converge towards the chaotic saddle in the forward (backward) dynamics, and can also be interpreted as the complement of the union of all the pre-images (images) of the leak.

In 2D Hamiltonian systems the preservation of volume implies that the two Lyapunov exponents must be equal in magnitude and opposite in sign. Consistently with this, the invariant

manifolds of the leaked system present some sort of statistical time reversal symmetry. For example, the fractal dimension of the stable and the unstable manifolds are the same. New to 3D maps, however, is the fact that generically, the maps present either two positive and one negative expansion rates or viceversa. Consequently, a leaked 3D map is *not* a direct analog of a scattering problem since it is non-hamiltonian, although the original system is volume preserving, but only for a particular choice of parameters -when one of the Lyapunov exponents is exactly zero - is it also time-reversal invariant. Here we investigate the impact of these features on the dimensionality and other statistical properties of the filamentation. Some of these questions turn out to have unexpected importance from the point of view of applications.

An interesting case, for example, is the analysis of magma flows from petrological data. Lavas often present a freezed form of the Lagrangian structures of these flows that can then be studied by image processing. Part of the processing may consist of band-pass filtering the greyscale levels of the images which is an indirect way of introducing leaking. Some empirical results [61] show that the resulting fractal dimensions of the structures are strongly correlated with the mixing effciency of the corresponding magma flows. In this case, however, leaking does not imply a physical escape out of the system, rather it means that regions with a certain property (i.e. greyscale level) are filtered out. Considering the concentration as the filtering criterion, the same approach can be applied to the analyzis of chemical reactions in flows (see III B 5).

As a paradigm of this type of three-dimensional systems, we use the family of ABC and ABC-related maps [8]: $\mathbf{T}(x_n, y_n, z_n) \longrightarrow (x_{n+1}, y_{n+1}, z_{n+1})$, with

$$\begin{aligned} x_{n+1} &= x_n + Asin(z_n) + C'cos(y_n) \\ y_{n+1} &= y_n + Bsin(x_{n+1}) + A'cos(z_n) \\ z_{n+1} &= z_n + \omega_z(x_{n+1}, y_{n+1}), \end{aligned} \tag{7}$$

with $\omega_z = Csin(y_{n+1}) + B'cos(x_{n+1})$.

Using the concepts from Hamiltonian mechanics, the first two spatial variables x and y are representing actions while the third one, z, is an angle variable.

In the integrable case, when the amplitudes are all zero ($A = B = A' = C' = 0$), the trajectories lie on lines where the actions (x, y) are constant. Motion there is now due to the angle variable z. For small perturbations (small amplitudes), the lines coalesce into invariant surfaces. In other words, the phase-space is splitted up by several tori lying parallel to the z-axis. A raising of the amplitudes results in a shrinking of the tubes (KAM tori) and in a spreading of the chaotic

motion of particles in phase-space.

Although the ABC map is the solution of the Navier-Stokes equation in the presence of a rather artificial space-time periodic forcing [19], it has been shown to capture the essential features of more realistic three-dimensional time-periodic flows [8] whose geometries are relevant to geophysical and environmental applications. This family of maps displays a range of dynamical behavior that goes from nearly integrable to strongly chaotic ones that in some sense can be considered the equivalents in three dimensions of those found in even dimensional conservative Hamiltonian dynamics.

In the following, we will focus on the highly chaotic case, where no large scale sticky integrable regions are found numerically, and we will investigate the effect of introducing leaking regions. As an example, we define a rectangular box lying parallel to the $x-y$-plane of width of $\epsilon = 0.5$, centered at $z = \pi$, cutting through the whole system in z, as the leak. Particles which enter the leak during the simulations escape the system. Remaining particles then trace out fractal structures, which have a dimension less than 3, the dimension of the whole accessible space. Starting with a large number N_0 of particles initially distributed in the full phase space uniformly, all the nonescaping particles are followed over n number of iterations. For large enough N_0 and n, the initial coordinates of the nonescaping particles should trace out the stable manifold, their final positions after n steps the unstable manifold, and the midpoints at time $n/2$ the chaotic saddle itself [13]. For iterating $n = 17$ times, we obtain the chaotic saddle as shown in Fig. (26). In order to have a better view on the three-dimensional structure, the chaotic saddle is represented in slices of the system centered at different y. It can be seen in the pictures, that the sine structures appear both in the x and in the z direction.

As a tool of visualizing dynamical properties of the particles in the leaked ABC map, we calculated their residence times. A 2D slice of this function is depicted in Fig. (27a): regions with large lifetimes (particles need long times to reach the leak) are denoting regions close to the stable manifold, thus the structures traced out by the long-living particles practically coincide with the ones of the stable manifold. The residence times depend sensitively on the size and on the position of the leak [77]. For a fixed size of the leak, such as the purifier, calculations of the residence or escape times will give the optimal location for an efficient particle exchange.

Fig. (27b) depicts the chaotic saddle, refined with the PIM-triple method [53]. The method is based on so called PIM (Proper Interior Maximum) triples: three points (a, c, b) in a straight line segment such that the interior point c has the maximum residence time. Once a PIM-triple is

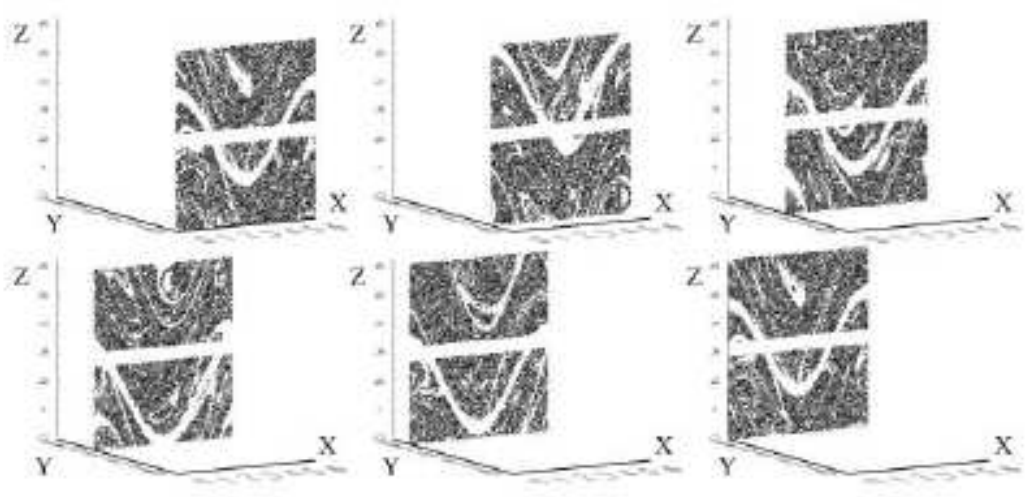

FIG. 26: XY slices of the chaotic saddle for the leaked ABC map with $A = B = C = 1.6$. The leak is centered at $z = \pi$ with a width of $\epsilon = 0.5$. The number of initially distributed particles is $N_0 = 5000000$. The width of slices is 0.08π.

found, is used to approach the stable manifold of the chaotic saddle, looking for refined segments in (a, b) that contain closer PIM-triples. This constitutes an iterative scheme to approach the stable manifold. Initial conditions on the stable manifold in the $x - z$-plane at $y = 0$ are then evolved $n/2$ times to obtain the chaotic saddle. A slice (with the width of 0.01π) of this three-dimensional saddle is plotted in the figure. Slices of its unstable and stable manifolds are plotted as well (Fig. (27c,d) respectively). If the chaotic saddle has a large dimension, this implies that the emptying process is slow, that is, the location or size of the purifier is not optimal. The visualization of parts of its otherwise space-filling three dimensional unstable manifold is an important step to obtain the stretching filamentation [57], i.e. the routes of efficient transport, in a system. Furthermore, visualizing different subsets of the unstable manifold by defining different leaks (different shapes, positions or sizes) corresponds to mimicking different concentration layers, traced out e.g. by chemical or biological processes or by magma mixing processes.

We have computed the fractal dimensions of the unstable and stable manifolds of the chaotic saddle of the leaked map. We have used both the correlation dimension and the generalization of the Kaplan-Yorke formula for the information dimension. We investigated the case $A = A' = B = B' = C = C' = 1.6$. Analogously to the $2D$ case, the stable and unstable manifolds have then the same dimension. We obtained

$$\lambda_1 = +0.775; \lambda_2 = +0.001; \lambda_3 = -0.776.$$

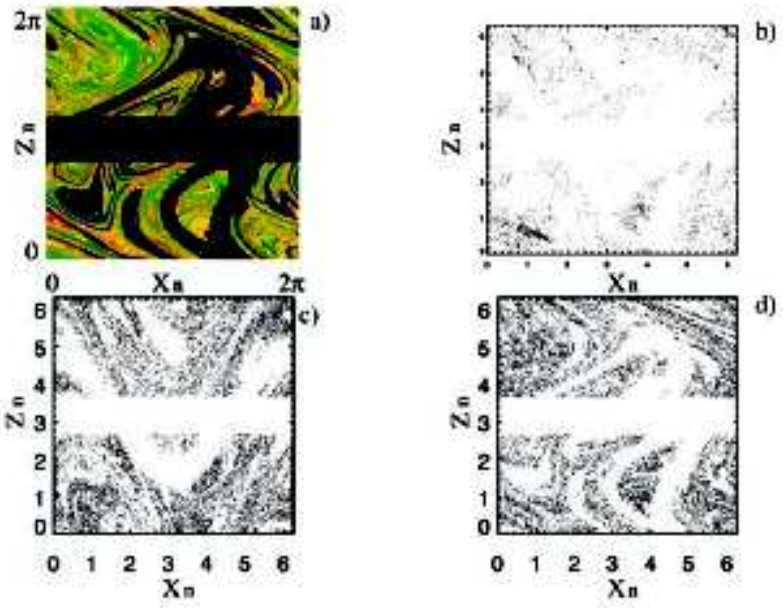

FIG. 27: (a) XZ slice of the residence time function for the same parameters as in Fig.26. The leak is centered at the same z-value but with a width of $\epsilon = 1.0$. Dark colors mean small residence times, while light colors represent higher values. (b) XZ slice of the chaotic saddle re.ned with the PIM-triple method. (c) and (d) the associated unstable and stable manifolds, respectively. The average mean residence time τ of the associated chaotic transient is used to obtain the fractal dimensions, and its value is $1/\tau = 0.192$. All the slices are for $y = 0$.

$$D_u = 2.752, D_s = 2.751, D_{saddle} = 2.50.$$

In the more interesting case when the Lyapunov exponents of the map are all nonzero new characteristics of the manifolds appear in comparison to the $2D$ case. Now, the manifold related to the two exponents of equal sign (i.e. the unstable manifold if the system shows 2 positive Lyapunov's, and the stable one in the case of two negative Lyapunov's) is locally a surface, while the other one is a line. Due to the foldings generated by the chaotic dynamics, their global form is a curtain like and a filamental fractal, respectively. The former possesses a larger dimension than the other one.

The topological difference in the manifolds can also be seen in the ABC map. In the particular case of the ABC parameters as $A = 3.6, A' = 1.6, B = 4.6, B' = 0.06, C = 5.06, C' = 0.6$. Then, the map has two negative and one positive exponent. Consequently, the dimension of the stable manifold is larger than of the unstable manifold.

$$\lambda_1 = +2.53, \lambda_2 = -0.9, \lambda_3 = -1.63.$$

$$D_u = 2.864, D_s = 2.91, D_{saddle} = 2.774.$$

The geometrical difference of both manifolds is visible in these approximately two-dimensional slices (Fig. (28)).

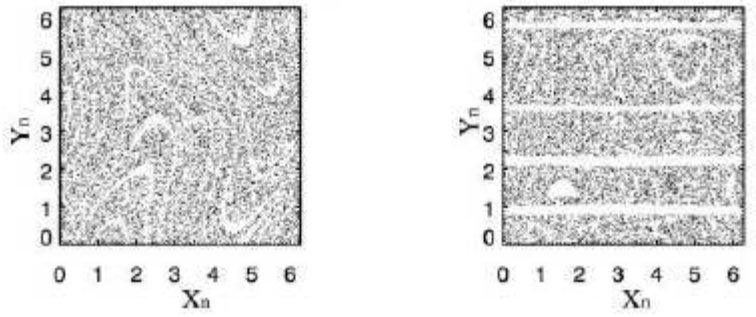

FIG. 28: XY slices (for a value of $z = 0.8\pi$ above the leak) of the stable (left) and unstable (right) manifolds for the asymmetric ABC map . The leak is a rectangular box parallel to the XY plane and centered at $z = 0.3\pi$ with a width of $\epsilon = 0.25\pi$. The width of the slices is 0.01π. The mean residence time values are $1/\tau = 0.227$.

Note, that the nonlinear ABC map has manifolds which are not translation invariant, but their structures are intertwined. Therefore, the above explained geometry of the manifolds (curtain and filamental like) cannot be seen so easily. In any case, the different size of the dimensions is clearly visible in the figures. The structures of the stable manifold appear to be filamental in this cut while the unstable one is a cloud of points without any systematic filamentation and consistently with the lower fractal dimension of the latter manifold.

In conclusion, the proposed application of the method of leaking is shown to provide insight into the phase space structures of chaotic 3D incompressible flows. In the example of the ABC map, which represents a general class of 3 dimensional systems, it is shown to be a fast and suitable way in quantifying physical and geophysical systems. The performed example of measuring the fractal dimension in the highly chaotic ABC map with 3 non-zero Lyapunov exponents is in agreement with the theory: the manifold related to the Lyapunov exponents with equal sign has the larger dimension.

Fractal structures have recently been shown [61] to be quantifiers of mixing effciency in magma processes. In the case studied by Perugini et al, frozen magma flows were found to be suitably modelled by the ABC-flow. The use of these parameters results in a flow where non-integrable

(chaotic) regions co-exist with intergrable islands (KAM-tori). Such imperfect mixing-structures, where well-mixed regions (active regions) co-exist with badly mixed regions (coherent regions), were observed e.g. in frozen lava flows from the island of Lesbos. Numerically, to obtain fractal structures and so to be able to characterize the mixing-strength in the active regions, we propose to leak the model-system. Otherwise, similar structures have numerically been reproduced only by following a dye droplet in closed 3D flows, which, however do not possess a fractal dimension other than 3

A characterization of the mixing structure is essential to understand the basic dynamics of magma mixing processes in the Earth. We will take a closer look on the dyanmics of magma in the Earth's mantle in Chapter IV D.

IV. APPLICATIONS IN ENVIRONMENTAL FLOWS

A. Background Oceanography

The ability of modelling fluid flows, especially the dynamics of and in oceans, has attracted wide interest and has a large importance: $2/3$rd of our planet is covered by water, 97% of those are oceans. The oceans (Atlantic, Pacific and Indian Ocean) are all connected with each-other, forming one global fluid system. This system is always in motion due to the forcings of the sun, the moon (tidal forces), the rotation of the Earth, and by wind. These forcings keep major currents and circulations in the oceans alive. For example, the largest warm-water currents are the Gulf Stream and the Kuro-Shio. The currents guarantee the exchange of tropical warm water and cold water from the poles. In the Atlantic Ocean, for example, the thermohaline circulation ensures Europe's mild weather. A key role in the thermohaline circulation plays the Gulf Stream: warm water masses from the Carribean Sea are flowing along the east american coast. They leave it as the Gulf Stream towards the Atlantic Ocean at Cape Hatteras (NC, USA), having a width of approximately 50km and an average surface speed of around 5km/h. After around 1500km it looses its shape of a bundled current. Then, parts of the water masses pass the coasts of north-western Europe, reaching a final destination: Greenland. During its travel and especially around Greenland, the surface water is cooled down and so the salty tropical water sinks near Greenland down to a depth of $2-3$ km, then making its way back to the tropics as a cold deepwater current.

The driving forces of the thermohaline circulation and with it the Gulf Stream are atmospheric circulations (wind, around the tropics from the east, and from west to the east in the mid-latitudes) and the northward increasing Coriolis force. The so-called pumping-mechanism, which is keeping the whole thermohaline circulation alive, is the sinking of salty water at cold temperatures due to a higher density than the surrounding freshwater at the same temperature. The more water is sinking, the more water will be pumped to the North at the sea-surface. A slight change of the salt-water content of the ocean around Greenland, for example due to global warming and the resulting heavier snow fall and melting of Greenlands ice-coast, could already disturb or even disupt the circulation. If this circulation would collapse, the weather in the concerned regions would change dramatically.

The understanding of the dynamics of the oceans and their interactions with our environment is therefore a major concern. Also, the knowledge about the complex ocean system is important

to be able to maintain and protect the inhabitants of the oceans: the oceans provide a huge living-environment for around 250000 different species, from whales and fishes down to microorganisms. Whereas the smallest organisms are often passive ones, thus they are not able to swim but will be advected by the surrounding water, larger species can move in the water independently from the currents to places they find food, as e.g. some microorganisms (as plankton). The existence of microorganisms and their role in our climate dynamics shouldnt be underestimated: Billions of small phytoplankton organisms which are usually of a size of around $0,02$mm are producing more than a half of the oxygen at our planet. Concerning the fish-population, it is important to know about the dynamics in the oceans to locate main transport currents, upwelling / freshwater zones, which are populated by prey for fish, thus attract fishes.

There are different approaches to study the dynamical structures of oceans: one possibility is to take a look on gradients of passive scalar fields in the oceans. These can be, for example, temperature-gradients, salinity, oxygen distributions or even the distributions of passive small organisms. Often, there exist snapshots of such gradients taken by satellites which can give us a first impression about the local dynamics of the ocean. The gradients align with the main transport direction and thus with the system's unstable manifold, as explained in the Introduction.

Another possibility is to access the dynamical structures directly by measuring the velocity fields to find the main transport direction. This can be done for example by releasing drifters and keeping track of their motion. The recorded trajectories can give some insight about the underlying dynamics. But often, the recorded trajectories of the drifters are heavily intertwinded and it is rather difficult to get any information out of these so-called Spaghetti diagrams. Also, due to the high costs of floats or drifters there are not many floats/drifters and measurements available.

Out of different measurement techniques and observations, numerical simulations have been developed with the aim of modelling and also forecasting the dynamics of flow-systems as the oceans.

How can we model such hydrodynamical systems?

Analogously to classical mechanics, the basic equation and starting point is Newon's law: $\mathbf{F} = m\mathbf{a}$. The force per volume is then: $\mathbf{F} = \rho\frac{d\mathbf{v}}{dt}$. In a co-moving frame, the change $d\mathbf{v}/dt$ of the velocity of a particle is given by: $\frac{d\mathbf{v}}{dt} = \frac{\partial\mathbf{v}}{dt} + \mathbf{v}\nabla\mathbf{v}$. The internal force, causing the velocity-change of the particle in the system, is due to a pressure gradient: $\mathbf{F}_i = -gradp$. Putting everything

together in Newton's law results in Euler's equation:

$$\frac{\partial \mathbf{v}}{\partial t} + (\mathbf{v}\nabla\mathbf{v}) = -\frac{1}{\rho} gradp - \mathbf{g}. \tag{8}$$

The Euler equation describes strongly idealized flows. Including the viscosity force, the gravitational force and the Coriolis force, we finally get the fundamental equation for hydrodynamics, the Navier-Stokes equation:

$$\frac{d\mathbf{v}}{dt} = -\frac{1}{\rho} gradp + \nu\nabla^2\mathbf{v} - 2\mathbf{\Omega} \times \mathbf{v} - \mathbf{g}. \tag{9}$$

The second term on the right hand side represents the viscosity force $\mathbf{f_v} = \nu\nabla^2\mathbf{v}$, with $\nu = \lambda/\rho$ beeing the kinematic viscosity which can be treated as a constant, and λ beeing the dynamical viscosity. g is the gravitational constant. The third term, $\mathbf{F} = -2\mathbf{\Omega} \times \mathbf{v}$, is the Coriolis force which can be neglected if the system is not rotating or if it is on the rotating Earth but not having a size comparable with the radius of the Earth itself.

Furthermore, working with incompressible flows, the density becomes $\rho = const$ and the continuity equation $\frac{\partial \rho}{\partial t} + div(\rho v) = 0,$ so that $divv = 0$.

Now, the Navier-Stokes becomes for a two-dimensional problem:

$$\frac{\partial v}{\partial t} + u\frac{\partial v}{\partial x} + v\frac{\partial v}{\partial t} = -\frac{1}{\rho} gradp + \nu\nabla v. \tag{10}$$

Solutions (exact ones or approximations) of the Navier-Stokes equation are represented by a streamline-function Ψ:

$$d\Psi = 0 = \frac{\partial \Psi}{\partial x}dx + \frac{\partial \Psi}{\partial y}dy. \tag{11}$$

The solutions are constant along the streamlines and the closeness or density of the streamlines is giving a measure about the velocity of the particles along the streamlines: the closer one streamline to the other, the higher the velocity of the particles:

$$v_x = \frac{\partial \Psi}{\partial y}, \quad v_y = -\frac{\partial \Psi}{\partial x}. \tag{12}$$

For beeing able to compare results from obeservations, es e.g. the recorded trajectory of a drifter, we need to derive an equation of motion for tracers. Let us consider that the tracer's density is the same as the one of the surrounding fluid, it's size is diminishable (pointlike) and it adopts the velocity of the underlying fluid instantaneously. Then, the velocity of the tracer is:

$$\dot{r}(t) = \mathbf{v}(\mathbf{r}(t), t).$$

With a known streamfunction, the advection equation becomes:

$$\dot{x} = -\frac{\partial \Psi}{\partial y}, \quad \dot{y} = \frac{\partial \Psi}{\partial x}. \tag{13}$$

This is a canonical set of equations and corresponds to the Hamiltonian equations.

B. Oceanography - The Gulf Stream

this chapter is published in:

'Extracting flow structures from tracer data'

J. Schneider, T. Tél

Ocean Dynamics (Ref [76])

A method of visualizing structures in closed chaotic flows out of homogenous particle distributions is presented in the example of models of a meandering jet. The possibility to apply the algorithm to analyze buoy data, and a comparison with the finite time manifolds is discussed.

Chaotic advection and the related mixing processes in environmental flows have been widely studied in recent years [15, 28, 57, 61]. Advection in the Gulf Stream attracted special attention since mixing there can change important features such as temperature and salinity distributions [18], or it can affect distributions of nutrients [1] or of pollutants such as oil [16]. For describing the basic dynamics of the Gulf Stream, Bower proposed a two-dimensional kinematic model [6], since the Stream appears two-dimensional along isopycnal surfaces. Samelson [72] (see also Cencini et al. [9]) introduced time-dependence in that model to simulate mixing processes. Dutkiewicz and Paldor [14] enhanced mixing via the interaction with a spatially fixed eddy which perturbs the velocity field of the meander. del-Castillo-Negrete and Morisson [12] (see also Rogerson et al [68], Yuan et al [90]) replaced the models by a dynamically consistent one, compatible with the quasigeostrophic equation, where chaotic advection is due to Rossby waves in the Bickley jet. The basic dynamical mechanism responsible for chaos is in all the models the nontrivial time dependence of the velocity field, which alone is sufficient to convert advection to be chaotic [56].

It is worth mentioning that inspite of the barotropic nature of these models, variations in their parameters parametrise changes in the depth of the oceanic jet (see [90]), the models therefore reflect certain baroclinic effects, too.

Mixing, or Lagrangian dynamics in general, can be made visible by tracer particles, which will be treated as pointlike particles with the same density as the surrounding fluid [36]. Such tracers

could be for example plankton or chemical substances (for reactive flows see the Focus Issue on Active Chaotic Flow [86]) or buoys. In environmental flows, chaotic mixing generates filamental sructures which give informations about the underlying dynamics. Gradients of the temperature field (SST) and of the potential vorticity can be used to detect these filaments.

In experiments, a simple method of getting structures out of closed flows without any biological or chemical reactions is to add dye particles [71, 87]. In closed flows (flows in closed basins) which are sufficiently chaotic, idealized tracer particles will trace out structures of the flow for a short period, but after a certain transient time, they will be distributed homogeneously. The advection dynamics is area or volume preserving due to the incompressibility of the flow, and the asymptotic distribution in such systems is uniform over the chaotic region [56].

The question which arises here is whether it is possible to get again some structure out of this homogenous distribution of particles in closed flows. Can we extract some information about the complicated Lagrangian dynamics of the system, which is completely described in the Eulerian sense by the set of smooth streamlines, out of this state? Here, we propose the method of leaking [77] which is shown to provide a kind of fingerprint of the closed system's advection dynamics.

1. Time-periodic kinematic model

The model of Bower [6] and Samelson [72] describes a meandering jet flowing eastward (to the right) whose velocity field is described in a frame co-moving with the jet:

$$\Psi(x,y,t) = \Psi_0 \left[1 - \tanh \frac{y - A\cos(kx)}{\lambda\sqrt{1 + k^2A^2\sin^2(kx)}} \right] + cy. \tag{14}$$

Here, A is the amplitude, λ sets the jet's width, k stands for the wavenumber and c is the phase speed. We handle this model as a closed flow, by imposing periodic boundary conditions in x. The velocity is the highest in the middle of the stream (jet) and decreases towards the edges (corresponding to the decreasing density of the streamlines). Idealized tracer particles, which are point-like and adopt the velocity of the fluid at once, follow exactly the instantaneous streamlines. In the used co-moving frame, the stream is clearly divided into three regions: into a central jet flowing to the right, into an outer flow of a small negative average velocity and into closed recirculation cells at the edges (see Fig. 29a).

The tracerst' equations of motion can be derived from the streamfunction:

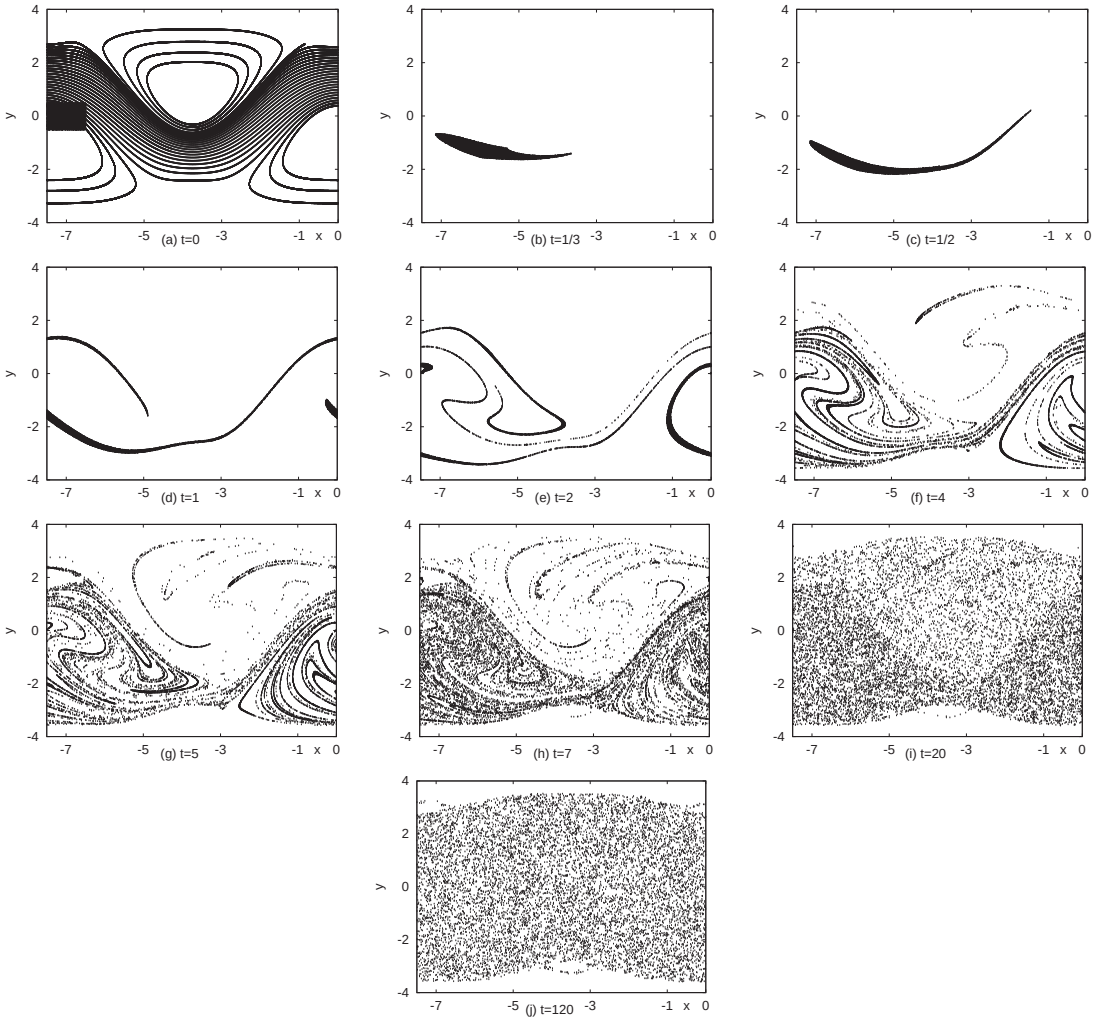

FIG. 29: Evolution of a droplet in the kinematic model equations (14,15, 16) of a meandering jet. A droplet of dye, consisting of 10000 particles uniformly distributed on the black rectangle shown in the first frame (a) evolves in time as shown in frames (b, t=1/3), (c, t=3/4),...(j, t=120). The upper left panel ((a) $t = 0$) also shows the streamlines of the unperturbed flow in the background. Stretching and folding characteristic for chaotic motion can be seen (e.g. at (e) $t = 2$). At some instant (e.g., t=4) the dye traces out a filamental structure which is smeared out after some more time. After $t = 120$ periods, all dye particles are distributed homogenously in the whole flow. Used parameters are: $\Psi_0 = 1$, $A_0 = 1.2$, $c = 0.12$, $\lambda = 1$, $k = 2\pi/7.5$, $\sigma = 0.3$, $\theta = \pi/2$, $\omega = 0.4$. Time is measured here and in all the following captions in units of the flow's period $2\pi/\omega$.

$$\dot{y} = v_y = \frac{\partial \Psi}{\partial x}, \quad \dot{x} = v_x = -\frac{\partial \Psi}{\partial y}. \tag{15}$$

Introducing a simple time-dependence, e.g. varying the amplitude of the streamfunction peri-

odically in time with the period $T = 2\pi/\omega$:

$$A = A_0(1 + \sigma\cos(\omega t + \theta)), \tag{16}$$

where ω is the perturbation frequency, σ the perturbation amplitude and θ a constant phase shift, tracer particles do not move along the streamlines. This perturbation corresponds to a periodic change of the amplitude/width of the Gulf Stream [72].

For a perturbation amplitude of $\sigma = 0.3$ ($\omega = 0.4$, $\theta = \pi/2$), the motion of tracer particles is already highly chaotic. With the dimensionless parameters used, model (14), (16) correspond to a jet of width 40km, speed 1 m/s, wavelength 260 km, and of perturbation period 8 days (see [9]). The chaotic regime lies between the lines $|y| < y_0$, where $y_0 = 3.5$. After long times, particles can then move freely within the whole width of the stream, no region of the flow is preferred. This can be demonstrated by monitoring the motion of a droplet in the chaotic flow [Fig. 29]. Starting a droplet of dye consisting of $N = 10000$ particles, the droplet will be deformed: it will be stretched and folded, as it is characteristic for chaotic motion. Asymptotically, all particles are distributed homogeneously in the whole stream. Can one extract some local information out of the homogenous state?

To this end we apply the method of leaking, described in Chapter III B: two lines will be defined inside the stream, parallel to the mean flow direction, for example at $y = y_c = 2.7$ and $y = -y_c$ (for keeping the symmetry of the stream). Particles which cross these borders outwards will be treated as escaped ones, and are taken out of the flow. Thus, the borders serve as a kind of semi-permeable walls which only allow the particles to leave the stream. In this way, the formerly closed system is opened up by leaking, and escape of particles is possible.

Starting out of a homogenous particle distribution, particles which have not yet escaped over a certain time will trace out filamental structures (see Fig. 30) if we analyse these trajectories as described in Section II. Comparing the traced out structures with the streamlines of the unperturbed flow [Fig. 29, panel (a)] shows, that they still hold some similarity, even if the motion of particles is highly chaotic: the central jet is clearly visible and the structures on the edges are somewhat resembling the recirculation cells.

The traced out structures are not only filamental but have a fixed fractal dimension less than 2, too. Varying the width of the leak, results in a change of the fractal dimension: if the area of the leaks increases, i.e., if $y_0 - y_c$ increases, the fractal dimension of the system decreases. Thus, the traced out structures are more rarified. On the other hand, by decreasing the width of the leaks

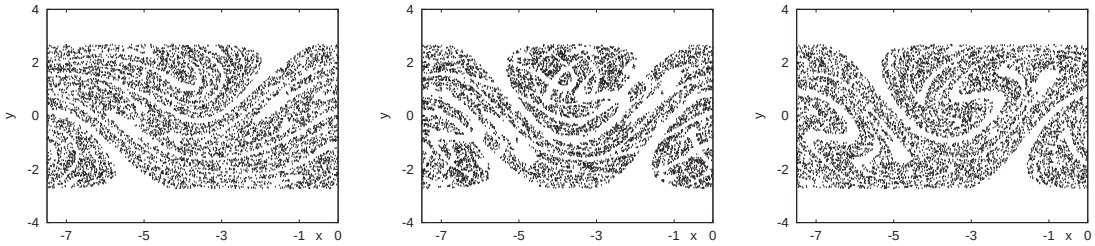

FIG. 30: Filamental structures in the leaked flow (1)-(3) traced out by not escaped particles after applying the analysis of Section II. The left panel shows the converging filamentation, i.e. the stable manifold of the chaotic saddle: only those initial ($t = t_0 = 0$) positions out of an initially homogenous particle distribution ($N_0 = 50000$) on the region $[-7.5 : 0][-2.7 : 2.7]$ are plotted which do not escape during $\tau = 20$ periods. The right panel shows locations of the not yet escaped particles after $\tau = 20$ periods, which trace out the stretching filamentation, i.e., the unstable manifold of the chaotic saddle. The panel in the middle depicts the chaotic saddle itself, obtained from the points taken at $t = \tau/2$ and coincides with the intersection of its stable and unstable foliations.

towards zero $(y_c \to y_0)$, more particles remain in the system and their traced out structures fatten and become denser. They reach a dimension of $d = 2$ for a leak of zero area, and the filamentation becomes then space-filling.

According to a general result [56, 82] the deviation of the fractal dimension d of (any of) the manifolds from unity is the ratio of the reciprocal value of the average lifetime and the positive Lypunov exponent λ of the chaotic advection in the leaked system. By using the estimate mentioned in the previous section, we obtain the relation $d \approx 2 + \ln(1 - \Delta)/\lambda$ where Δ is the area ratio of the leak, which is proportional in our case to $y_0 - y_c$.

Measuring the residence time, i.e. how long it takes for particles (initially homogeneously distributed in the whole flow) to leave the flow through the leaks, results in Fig. 31. Short residence times (dark blue regions) stand for locations where particles escape rapidly from the flow. Positions with large residence times (red colors) correspond to an approach towards one of the never escaping orbits. Points with large residence times must therefore be close to the *converging* foliation, i.e.,to the *stable* manifold (compare with Fig. 30a).

A surprising application of leaking a flow is in connection with the patterns traced out by reactions taking place in the same flow. Such patterns may appear due to strong concentration gradients in atmospheric chemistry, e.g. in ozone concentrations, or can be observed in ocean plankton dynamics. The basic mechanisms to generate them are the compression of the fluid ele-

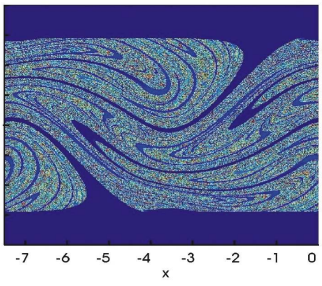

FIG. 31: Residence times. Particles starting from the dark blue regions need the shortest time to escape. Light blue denotes places where the residence times are within 4 and 7 periods. Colors towards red (residence time larger than 40, up to 99 periods) denote places with increasing residence times. $N_0 = 600800$ particles were used, initially distributed over a grid of mesh-size $\delta = 0.01$ in the same region as in Fig. 30.

ments towards the stable foliation of the flow, with the consequence of increasing local gradients, and the stretching of the fluid elements along the unstable filamentation of the flow. The concentration is then smoothened out along the unstable filamentation due to the experienced stretching [25]. Here, as an example, we will consider a biological reaction by superimposing a model of plankton dynamics on the two-dimensional meandering jet described above.

Particles are assumed again to be point-like. They are active, can react with each-other, but do not modify the flow. In the examined model, the temporal evolution of the phytoplankton, its nutrient and the zooplankton is determined by advection-reaction-diffusion equations (see [43] for details). Nutrients are distributed in the flow and are eaten up by phytoplankton, which then grow in number. These biological reactions make complex filamental structures appear, marked by different phytoplankton concentrations, shown in Fig. 32. Due to stretching, the concentration is smoothly changing along the unstable foliation, but not so along the converging one. Therefore, directions corresponding to low concentration gradients trace out a part of the *unstable* foliation of the *passive* problem (compare Fig. 32 with the right panel of Fig. 30). Since the backbone for an active process is in general the unstable filamentation of the passive dynamics [85], it is not surprising that structures of the unstable manifold got by leaking the reaction free flow show striking similarities with those traced out by the active particles in the closed flow. Thus, by leaking a closed flow and studying the not yet escaped passive particles we can mimic structures similar to ones which appear in active processes. For a chemical model see [77].

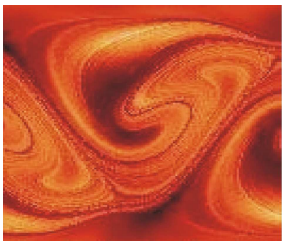

FIG. 32: Structures traced out by phytoplankton in a plankton model superimposed on the meandering jet. Picture taken from: C. Lopez, Z. Neufeld, E. Hernandez-Garcia, P.Haynes (2001) Physics and Chemistry of the Earth B 26: 313-317, with the kind permission of the authors. Note the similarity with the stretching/unstable foliation shown in the right panel of Fig. 30.

2. *A chaotically time dependent flow*

The temporal periodicity of the flow model used above seems to be a strong restriction. Flows changing quasiperiodically or chaotically in time, but characterized by smooth streamlines in space form an interesting class of flows which received recent attention. Since on snapshots taken with some sampling time, the velocity field appears to be a random (but not necessary weak) perturbation of the initial one, such flows are called random flows [30, 52, 63]. Two-dimensional random flows can be considered as elementary models of two-dimensional or geostrophic turbulence. A surprising feature of random flows is that tracer patterns generated by them are shown to exhibit - inspite of the randomness - *clean* fractal structures which can be described by the theory of random maps [69, 81, 89].

To test how a random perturbation changes the stable and unstable filamentation in the meandering jet model, we modify the amplitude of the sinusoidal driving in (16) by adding a random shift to the average amplitude $\bar{\sigma}$ after each period $2\pi/\omega$ of time. We thus take the streamfunction defined by (1) and (3) with

$$\sigma = \bar{\sigma} + \delta\sigma_n, \tag{17}$$

where $\delta\sigma_n$ is a random number distributed uniformly in the range $[-0.05; 0.05]$ and kept constant over the nth period. The results obtained with the method of leaking are shown in Fig. 33. Inspite of the fact that the random perturbation is not weak (its amplitude is one third of the average value $\bar{\sigma} = 0.3$), the filamentation remained clean. The actual shape of all the patterns is similar to what we see in the nonrandom case (Fig. 30), but minor details can be different (like e.g. the precise

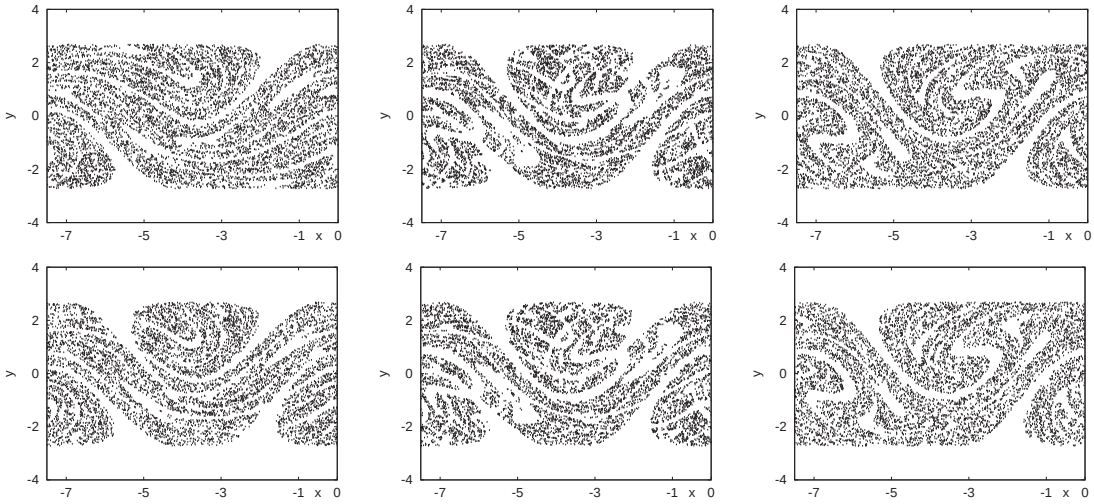

FIG. 33: Filamental structures in the random flow model of the meandering jet (equ. 14-17) opened up by leaking. The average driving amplitude is $\bar{\sigma} = 0.3$, the same as in Fig. 30, but there is a random variance around it of half-width 0.05 (see (4)). The panels show the points of the orbits not escaping over $\tau = 20$ periods at times $t = 0$, $t = 10$, $t = 20$ and $t = 1$, $t = 11$, $t = 19$. The left, middle and right columns correspond to the stable foliation, the chaotic saddle, and the unstable foliation, respectively. Note that the plots above each other are not the same due to the aperiodic time dependence of the flow. Initial conditions (apart from the number of particles started: $N_0 = 100000$) and leak are the same as in Fig. 30.

form of the largest white tongues). Furthermore, all the patterns depend on the actual snapshot taken (see Fig. 33 d,e,f) which is due to the fact that the flow is not periodic. (In the periodic case the location of the points of the nonescaped orbits is the same for $t = t_0$ and $t = t_0 + 1$, for $t = t_0 + \tau/2$ and $t = t_0 + \tau/2 + 1$, and for $t = t_0 + \tau$ and $t = t_0 + \tau - 1$.) The theory of random maps also implies [30, 52] that the fractal dimensions of the manifolds and the chaotic saddle do not depend on the snapshot taken. The similarity of the structures on subsequent snapshots indicates that the filamentation remains qualitatively the same as in a periodic flow. Thus, the method of leaking the flow for visualizing its stable and unstable filamentation is applicable to random flows, as well. Note that the shape of the stable foliation does not depend on the observed time span τ, but it does depend on the instant (t_0) of the initialization of particles. The shape of the unstable foliation and the chaotic saddle depend both on τ and t_0.

3. A dynamically consistent model with barriers

Instead of the kinematic model, we consider now a dynamically consistent (nonrandom) model of the jet derived by del-Castillo-Negrete and Morrison [12] which takes into account the conservation of potential vorticity in leading order. The flow is defined in a frame comoving with the slower wave of wavenumber k_2 by the streamfunction

$$\psi = -\tanh y + c_2 y + \epsilon_1 \cosh^{-2} y \cos(k_1 x - \Omega t) + \varepsilon_2 \cosh^{-2} y \cos k_2 x \tag{18}$$

where $\Omega = 2k_1/3\sqrt{1-3\beta/2}$ with β as the beta parameter, and $k_{1,2}^2 = 2(1 \pm \sqrt{1-3\beta/2})$, $c_2 = 1/3(1-\sqrt{1-3\beta/2})$. With these parameters, the model exhibits bounded chaos interwoven with integrable regions (KAM tori).

The new feature of this flow is the appearance of a transport barrier around the jet which is a kind of coherent structure. Due to this barrier, there is no need of leaking the flow on both sides since there is anyhow no communication between the lower and the upper part of the jet. Therefore, the filamentations are independent of each other in these two regimes. We apply an escape condition across the line $y = -y_c = -1.7$ only, and carry out the same procedure as in the first subsection in order to visualize the filamentation in the lower part. For simplicity we only show the endpoints of the nonescaped orbits in Fig. 34, corresponding to the unstable foliation. The pattern seen is somewhat different from the previous cases because of the central barrier. Note,

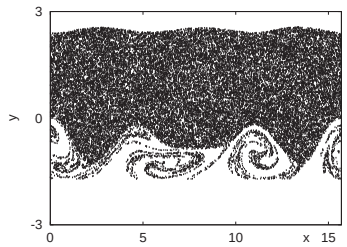

FIG. 34: Filamentation in the dynamically consistent model 18 of the jet. The endpoints of orbits which do not cross the line y=-1.7 over a time period of 3 times $2\pi/\Omega$, trace out the unstable filamentation below the centerline of the jet. The leaking of the system does only affect the lower part of the jet due to the transport barrier in the middle, no structures become visible in the middle and in the upper part. The initial condition was a uniform distribution of $N_0 = 50000$ particles in the slab $-1.7 \leq y \leq 2.5$ over the spatial period $3 \cdot 2\pi/k_2$. Parameters: $\varepsilon_1 = 0.1$, $\varepsilon_2 = 0.3$, $\beta = 0.614$ ($k_1 = 1.6$, $k_2 = 1.2$, $c_2 = 0.24$, $\Omega = 0.3$).

that the visualized structures of the eddies are corresponding to the spirals Yuan et al [90] found

in their patchiness plots. Now, we can see that these structures (unstable manifold) are indeed created by the underlying motion, composed of the rotation in the eddies and of the motion of the co-moving frame.

The leaking method proposed here, for visualizing structures in the flow, is applicable for all parameter ranges and implies also an applicability in 3 dimensional systems.

4. Discussion

The method proposed here is based on following tracer trajectories. The models used were chosen to be close to realistic flows in the oceans or atmosphere. In particular, parameters are taken to roughly correspond to those of the Gulf Stream. Our method can thus be applied to oceanic flows in which the motion of floats are monitored over a long period of time: by selecting a region of observation smaller than the full region accessible by the tracers, and keeping only those trajectories which stay within this region over a long period, the spaghetti diagrams (Fig. 35) clean out and a filamentation appears by plotting the initial and the final positions of the not yet escaped tracers. The basic limitation in practice is set by the number of tracers used. We

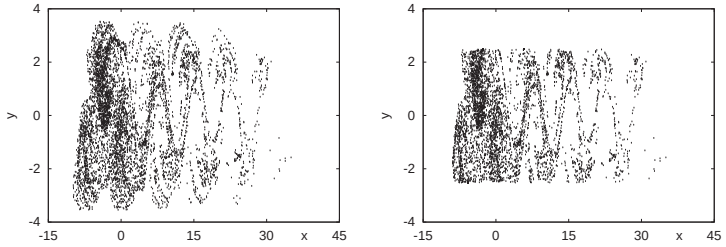

FIG. 35: Spaghetti diagram. Time continuous trajectories of $N_0 = 1200$ tracers in model 14-16, started homogenously distributed in the region $[-7.5 : 0][-2.5 : 2.5]$, depicted over a time-interval of $\tau = 5$ periods. Right panel: Trajectories staying in the leaked region $|y| \leq 2.5$ over 5 time units. The kinematic model is taken with the same parameters as in the first figures.

carried out simulations to check what the smallest number of tracers is by which the first signs of filamentation optically appear. In our first model, this number was found to be on the order of 1200 (see Fig. 36). There is therefore hope for applying this method to visualizing Lagrangian patterns in the ocean if the number of tracers available will grow on the order of one thousand. The visibility of the structures depends somewhat on the initial particle distribution (see Fig. 36, right panel).

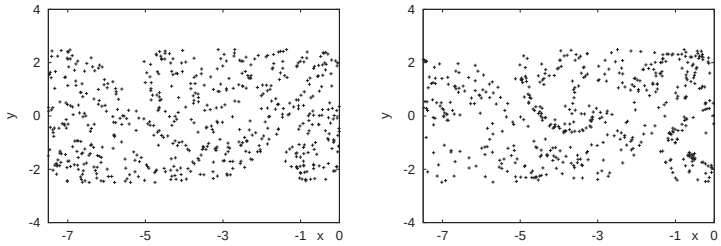

FIG. 36: Unstable filamentation traced out by a "small" ensemble. Left panel: Same data is used as in Figure 35 (same τ, N_0 and initial distribution) but represented according to the leaking method described in the main text. Only the end-points of trajectories at $\tau = 5$ have been plotted. Trajectories which go further than $y = \pm 2.5$ are not depicted. Endpoints are plotted over the basic wavelength $L = 7.5$ of the stream after applying periodic boundary conditions in x. Right panel: Same as left panel, but now the particles were initially distributed in a stripe at $-0.5 \leq y \leq 0.5$ over one wavelength ($-7.5 \leq x \leq 0$).

Next we compare our method with another one aiming to determine the so-called finite time or effective manifolds [22, 23, 31, 37, 47, 65, 73, 90]. The latter can be applied to any aperiodic flow, also to flows which become stationary after some time. The purpose is to identify the analogs of saddle (hyperbolic) points in these flows, and after finding some of them to determine a finite segment of their stable and unstable manifolds. In the knowledge of these, the lobe dynamics [4, 70, 88] can be applied to quantify fluid transport over a finite period of time. The applicability of our method, in contrast, requires that the flow does not change its basic character over a longer period of time (it does not die out), although its temporal behavior can be chaotic, too. What we gain by the existence of such a fluid dynamical 'steady state' is the applicability of the theory of chaotic systems which implies that not only a few, but a large number (an infinite number in principle) of hyperbolic never escaping orbits can be present. All the midpoints (taken at time $t = t_0 + \tau/2$) are of this type, and form the chaotic saddle of the leaked flow. The fractal foliations related to times t_0 and $t_0 + \tau$ can be considered as stable and unstable manifolds, respectively, they, however, do not belong to a few isolated fixed points, but to the *full chaotic set*. Thus, we get a better characterization of the main transport/stretching directions of the system, and by means of a much simpler and faster method, than the one needed by reconstructing the finite time manifolds of only a few hyperbolic points. Our method thus always provides a fractal foliation. In the cases of decaying fluid activity it cannot be applied and then the effective manifolds are necessarily nonfractal objects.

In conclusion,by leaking, i.e., by cutting out a finite region of a closed chaotic flow, and thus

making an escape of particles possible, we can visualize fractal filamental patterns out of a formerly homogenous tracer distribution. As pointed out, by visualizing the unstable manifold we are also able to reconstruct or mimic structures which will be traced out by active processes., e.g. by phytoplankton or pollutants in the flow.

C. Oceanography - The Mediterranean

this chapter is a result of a cooperation with:

V. Fernández and E. Hernández-García

IMEDEA (CSIC, UIB)

1. introduction

Ocean currents transport water in such a way that parcels initially close become distant after some time (*dispersion*). Eventually water masses of different origins are put into contact, allowing them to interchange their contents of heat, chemicals or nutrients (*mixing*). These two processes, dispersion and mixing, have a profound impact on the physical, chemical and biological dynamics of the ocean. The rapid development of Lagrangian techniques [44] is enhancing our understanding of them. For example, floater experiments, that directly track the motion of the water parcel on which the floater has been deployed, reveal irregular trajectories and strong dependence of them on the precise position and timing of the release. The influence of coherent structures on the trajectories, such as trapping by eddies, is also observed.

One of the theoretical frameworks that is being used to understand the above phenomena comes from the mathematical study of dynamical systems [88]. This approach identifies the main dynamical structures (hyperbolic points, stable and unstable manifolds, elliptic points and tori, ...) that provide the skeleton organizing the full set of particle trajectories. Irregular trajectories and sensitive dependence on initial conditions are interpreted as the direct manifestation of the chaotic nature of fluid trajectories in the ocean. Coherent structures such as eddies and fronts are also linked to well studied objects in the dynamical systems approach.

Although techniques for the identification of dynamical structures in time-periodic velocity flows are well established since long time ago [57, 88], the consideration of aperiodic flows, as occurring in the turbulent ocean, is much more recent. A variety of methods are being tested on more or less idealized dynamical systems [22] and some of them applied to realistic geophysical settings [32, 37, 38]. A particularly simple methodology was proposed in [77] and applied to idealized geophysical flows in [76]. The so-called *leaking method* consists in identifying the initial positions of particles that leave a given spatial region within a long enough interval of time. Alternatively, starting positions of trajectories which end in a given region can also be

identified. In both cases, the geometrical structures of these sets of positions are related to objects of dynamical relevance (stable and unstable manifolds, and exchange basins). In the context of chaotic dynamical systems, they are shown to have a fractal structure, i.e. fine details with self-similar properties at arbitrarily small scales. The meaning of this in the ocean context is that these sets will show a fine filamentary structure which resembles satellite observations of sea surface temperature or ocean color images. From a practical point of view, the fine structure is the responsible for the different fate of trajectories starting in close and apparently equivalent positions. The manifolds revealed by the leaking method allow the identification of the *roads to transport* between sub-basins, as well as the *barriers to transport*. The method was originally developed to display the geometry of the transport structures. But it also gives readily the relevant time scales for exchange from selected regions, an information of evident oceanographic interest [7].

Here, we apply the leaking method to a realistic surface velocity field of the Mediterranean Sea obtained from a primitive equation ocean model. The method can be applied to three-dimensional velocity fields [84], but we restrict here to a single horizontal layer (neglecting the third spatial dimension is in this case a good approximation since the vertical velocity components are three orders of magnitude smaller than the horizontal components). Transport structures in the Western Mediterranean are identified and time scales for transport between basins calculated. We also consider the seasonal variability of these time scales.

2. Mediterranean sea surface circulation

The Mediterranean Sea is a semi-enclosed basin connected with the Atlantic Ocean via the Strait of Gibraltar. It is divided in two principal basins (the Western and the Eastern Mediterranean). The main oceanographic characteristic of the Mediterranean Sea as a whole is that it is an evaporative basin (evaporation exceeds precipitation), and the deficit of water is supplied by the inflow of Atlantic waters (AW) from the Strait of Gibraltar. This is considered the main forcing mechanism of the Mediterranean circulation. In a simplified view, AW coming from the Strait of Gibraltar flow eastward along the north African coast, forming the so called Algerian current. When this current reaches the Strait of Sicily, it bifurcates, one branch follows a cyclonic (anti-clockwise) path around the Western Mediterranean Basin, while the other branch crosses the Strait of Sicily into the eastern basin where it also follows a cyclonic path.

The eastern and western Mediterranean themselves can be divided in several sub-domains (sub-basins) separated by topographic features (straits or channels) and clearly characterized by different patterns of circulation and by different forcing mechanisms (e.g heat fluxes, wind stress, river discharge, etc). Indeed, each of the sub-basins present a highly seasonal variability dependent on the local forcing variability. This fact makes the Mediterranean surface circulation to be depicted as different gyre systems connected by seasonal currents. The interaction between the local (sub-basin) circulation and the general circulation, and the connections between sub-basins, is still an open field of research of the Oceanography in the Mediterranean Sea [3].

3. The ocean circulation model

In this study, we have used the Mediterranean version of the DieCAST (Dietrich for Center Air Sea Technology) numerical ocean model [17]. DieCAST [13] is a primitive equation, z-level, 3D, baroclinic ocean model that has been applied to the Mediterranean Sea with realistic coastlines and topography. It is based on hydrostatic, incompressible and rigid lid approximations. A complete description of the model setup can be found in [17] and here we will only summarize some of the main properties of the model setup. The horizontal resolution is $1/8$ degrees while the vertical direction is discretized in 30 levels. We use a single year forcing (perpetual year) repeated each year, based on climatological wind stress and climatological surface temperature and salinity [13]. Horizontal eddy viscosity and diffusivity are specified to be constant of $A_h = K_h = 10m^2s^{-1}$, respectively) and are represented by a Laplacian operator. Vertical viscosity and difffusivity are based on [59], with background vertical viscosity and diffusivity set at near-molecular values (0.01 and 0.002 cm^2s^{-1}, respectively). Tracer and momentum time step is 15 minutes. Model outputs are stored as instantaneous values each model day.

We used for this study the Eulerian model velocity data corresponding to years 18 to 21 of a simulation starting from rest and winter climatological conditions. Therefore, we consider that the model has reached a stationary state for the surface circulation after 17 years of run [17].

4. Lagrangian diagnostic - Extended Leaking method

The method we propose to get the transport structures between two sub-regions is based on chaos theory and makes the Lagrangian routes of transport visible. Therefore, we apply an ex-

tended version of the leaking method, the exchange method: out of the whole western basin of the Mediterranean we choose two sub-regions between which we want to calculate the transport properties.

One of the two sub-regions will be filled up randomly with particles. Then, their motion will be simulated. In contrast to the original leaking method, particles are free to leave their starting region and to move in the whole system. But in the moment they (eventually) enter the second sub-region, the simulation of their motion will be stopped. Those particles are then treated as exchanged ones. Consequently, when marking the initial positions in the starting box wherefrom a particle could reach the target box, we get the exchange basin of the starting box with the target box: any particle started within that basin will hit the target box.

Furthermore, when plotting the endpositions of the not-exchanged particles, we can visualize the main (cyclonic) routes of transport of the western Mediterranean.

Particle integrations are computed using up to four years of the previously stored Eulerian velocity 2D fields provided by the DieCAST numerical model.

Motion of particles is calculated by integrating the Eulerian velocity fields in 0.5 hour time-steps, using a linear interpolation in time. In space, we use a bilinear interpolation method to compute velocities in between the gridpoints. Motion of particles is followed as long as they do not enter a defined target region (they exchanged with the other sub-region).

We should note that we neglect the vertical velocity component and consider only the two-dimensional velocity field.

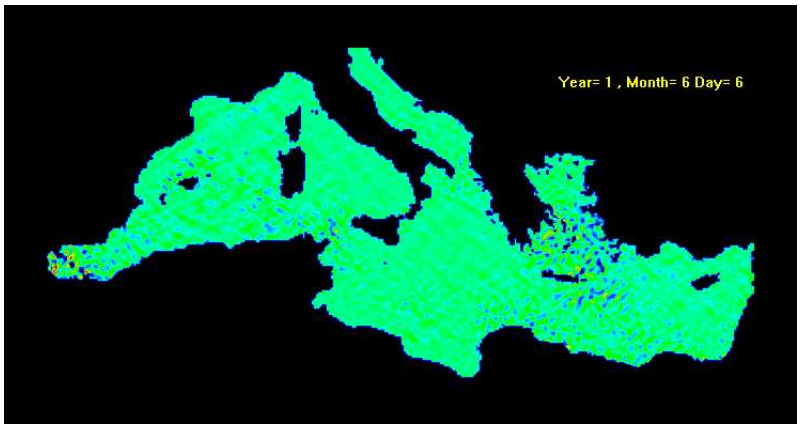

FIG. 37: Divergence field. Dark blue colors denote downwelling places while red colors are upwelling zones.

This is a good approximation if we consider that the w values are three orders of magnitude smaller than the horizontal velocities (except in areas of deep water formation, which are not resolved by the actual model configuration).

5. Results without diffusion

We used the Eulerian two-dimensional velocity fields at the second layer of the Mediterranean model to compute the trajectories using the methodology explained above. The reason for using the second layer is because the velocity is exactly zero at the coast and so we diminish problems with particles getting sticked to the coast.

However, we should note here that particle trajectories computed with this method are depending on the model layer from which we take the Eulerian velocity. Particles in the top layer are faster than in the layers below (due to the direct wind stress effect) and our results, which are computed from the second model layer (equivalent to 16 m deep), may not be directly compared with observations from surface Lagrangian drifters.

6. Horizontal exchange between sub-basins in the Mediterranean Sea

One of the applications of the previously described methodology is to study the surface exchange of particles between adjacent sub-basins in the Mediterranean Sea.

The sub-basins can be defined by boxes which are filled randomly with a high number of particles (N_t), and then, their trajectories can be analyzed. If a particle crosses the common boundary of the two boxes (in other words, it 'exchanges to the adjacent box'), the simulation of the movement of that particle will be stopped and the number of not exchanged particles started in that box, N_t, will be decreased accordingly by one at that time t. Therefore, the number of not exchanged particles decreases with simulated time t; out of that data, the exchange rates between the two defined regions can be calculated.

North-South exchange in the Western Mediterranean

The connection between the northern and southern sub-basins of the western Mediterraenan (Balearic and Algerian sub-basin respectively) particularly deserves our attention. In nature, the southern part, the Algerian sub-basin, is filled with Atlantic Waters (AW) coming from Gibraltar. Meanwhile, the northern sub-basin, the Balearic, is mainly occupied by much older and saltier

Mediterranean Waters. However, there is observational evidence of exchange of surface waters between these two basins with a marked temporal variability [64] that will be studied here.

To quantify this meridional water exchange with the Leaking method we define two boxes, one representing the northern sub-basin, and other representing the southern sub-basin of the western basin of the Mediterranean from the western coasts until the islands Corsica and Elba, excluding the basin around Gibraltar. Both boxes are therefore defined to have an area from 0 to 9E in longitude and from 36 to 39N in latitude for the southern and from 39N to 44.5N for the northern one. We consider a borderline between both boxes at 39N latitude. A particle is considered to exchange from North to South, and viceversa, if it crosses the common borderline at latitude 39N. This latitude is rather ambiguous but we have considered it to be at Ibiza channel latitude where mostly of the water exchange occurs [64].

Filling the southern (northern) box with initially $N_0 = 200000$ particles and calculating for a time-span of 4 years, we obtain the following average exchange rate from S to N (N so S): $\kappa = 4.94 \cdot 10^{-3}$ ($\kappa = 2.64 \cdot 10^{-3}$), corresponding to an average exchange time of 202 days (378 days).

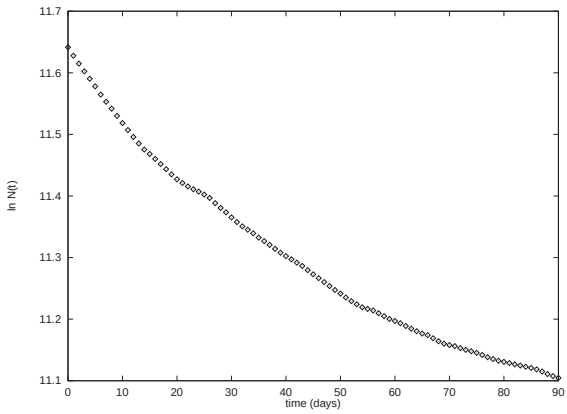

FIG. 38: Graph for calculating the exchange rate κ in the example for the exchange in summer of the first simulated year. The vertical axis is logarithmic, showing the number of particles N which did not exchange with the other box at time t. The horizontal axis displays the time t. Fitting a straight line on the graph gives the exchange rate.

The seasonal exchange rates κ (for every 3 months) averaged each season over four years are shown in the following table:

	N to S	S to N
I	$2.93 \cdot 10^{-3}$	$7.25 \cdot 10^{-3}$
II	$2.19 \cdot 10^{-3}$	$4.76 \cdot 10^{-3}$
III	$2.88 \cdot 10^{-3}$	$4.52 \cdot 10^{-3}$
IV	$2.57 \cdot 10^{-3}$	$3.23 \cdot 10^{-3}$
	yearly avg:	yearly avg:
	$2.64 \cdot 10^{-3}$ (378days)	$4.94 \cdot 10^{-3}$ (202days)

Exchange rates of the 2nd layer (no Lagrangean diffusion), averaged over 4 years. Rates are in $1/day$. I,II, III and IV corrresponds to winter, spring, summer and fall.

The first thing we can infer from the table is a seasonal variability of the exchange rates. Comparing the northward with the southward flux, we see that the one from South to North is higher than from the North to the South. This result corresponds to the fact that in the northern basin the water is much 'older' and saltier. Due to the denser water masses the main flux in the northern basin is in deeper layers than in the southern basin. Therefore, with measuring fluxes in the 2nd layer (16 meter deepness), the flux of less saltier water from the Atlantic contributes the main part to the exchange rates, whereas only a fraction of the North-South fluxes of the saltier water masses can be measured.

7. stable and unstable manifolds

To get more insight into the above results, we studied motion of particles in both of the boxes in more detail, particularly we investigated the initial and final positions of the particles realeased in each of the boxes. The ensemble of those particles which will take part in the exchange with the other box (within the simulated time-span) were initially located in the exchange basin of the box they are exchanging to.

Fig. 39 shows a sequence of the exchange basin towards the northern box for particles launched in the southern box. As can be seen, the shape (and density) of the exchange basins changes each

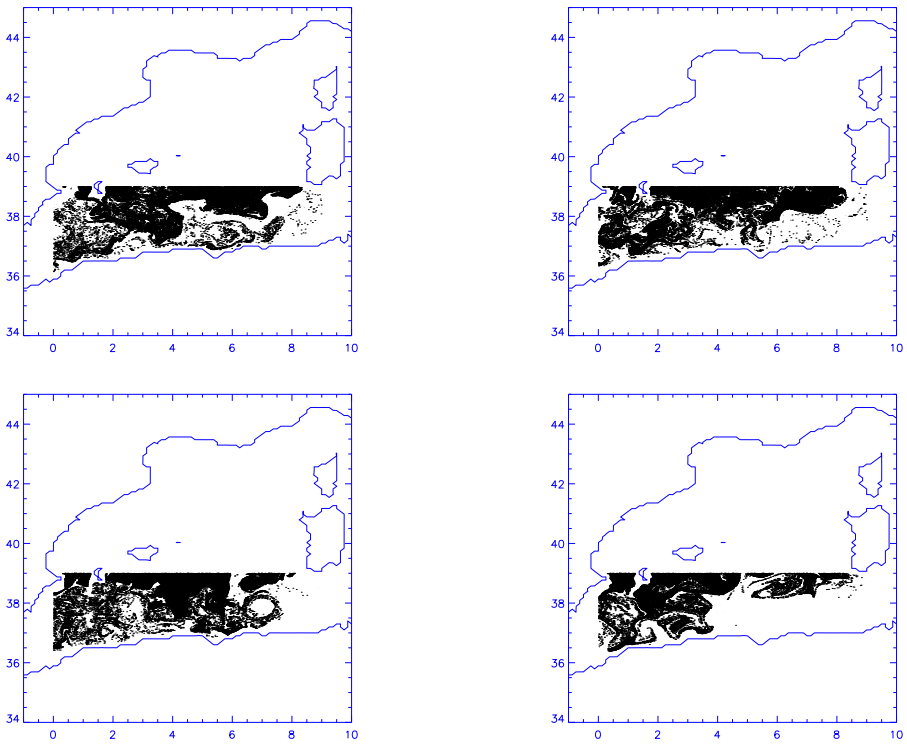

FIG. 39: Exchange basin towards the northern box in the south. Upper left: winter, upper right: spring, lower left: summer, lower right: fall.

season, according to the seasonal dependence of the exchange rates. Also, the exchange basin is smallest in fall in correspondance to the calculated exchange rates in Table 1. Some nice filamental structures can be seen in the pictures, going like fingers from the common borderline of the two-boxes into the southern box. These fingers grow in time into the southern box, 'attracting' more and more particles. Also, it can be realized that the exchange basin mostly does not include the water masses around the eastern Algerian coast. Particles started there will be transported eastward by a strong eastward current and vortices. Indeed, this can be seen when plotting the endpositions of those particles which where initially not located within the exchange basin from the South towards the northern box. Fig. 40 shows the endpositions of those particles started in the southern box in summer, simulated for one season. As can be seen in the picture, particles which did not go to the northen box but left their southern box followed the strong algerian current towards the East. Shortly before reaching the Strait of Sicily, the current splits into two parts: one going into the Tyrrhenian Sea, circulating only in the western basin of the Mediterranean, the other one following the strong coastal current along the african coast into the eastern basin of the

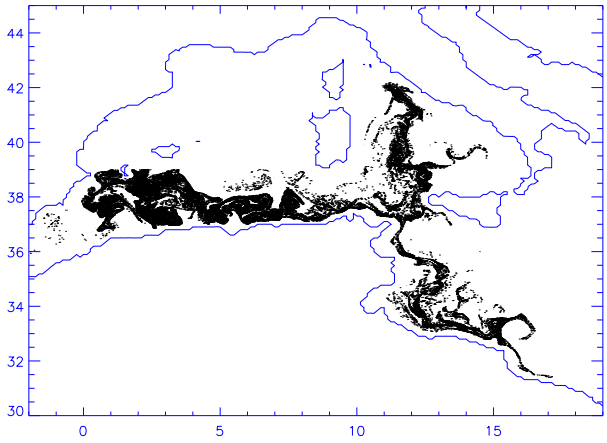

FIG. 40: Endpositions of particles launched in summer in the South which did not exchange to the North.

Mediterranean. However, some particles are still in their initial southern box. They seem to be trapped in several vortices around the african coast, only transported slowly towards the East with the main current. Note, that vortices do also play a role in the South-North transport. As can be seen in in Fig. 39, the exchange basins in summer and fall show some vortex structures which seem to trapp particles in the South and transport them into the northern area.

Fig. 41 shows a sequence of the exchange basins as Fig. 39, for particles launched in the northern box exchanging towards the southern box . In comparison with the exchange basin from South to North, here the basin is more restricted. Particles which exchange with the southern box are initially mostly located in the lower half of the northern box. Due to the smaller exchange basin, the exchange rates shown in Table 1 are also smaller. Note, that in all pictures in Fig. 41 the exchange basin does not include a channel west of Mallorca where in fact a strong current is transporting particles from the South to the North.

The endpositions of those particles which exchanged from the northern towards the southern box are shown in Fig. 42. Some particles are tracing out the same structures as particles launched in the South: both are showing the routes of transport of the main circulation in the western basin, partly going into to eastern basin of the Mediterranean. Note that particles which are located in the end in the South do not show any vortex structures. Therefore, the vortices seem to be formed only in the vicinity of the African coast where they trapp particles (particles initially located in the vortex will be transported by them for a longer time).

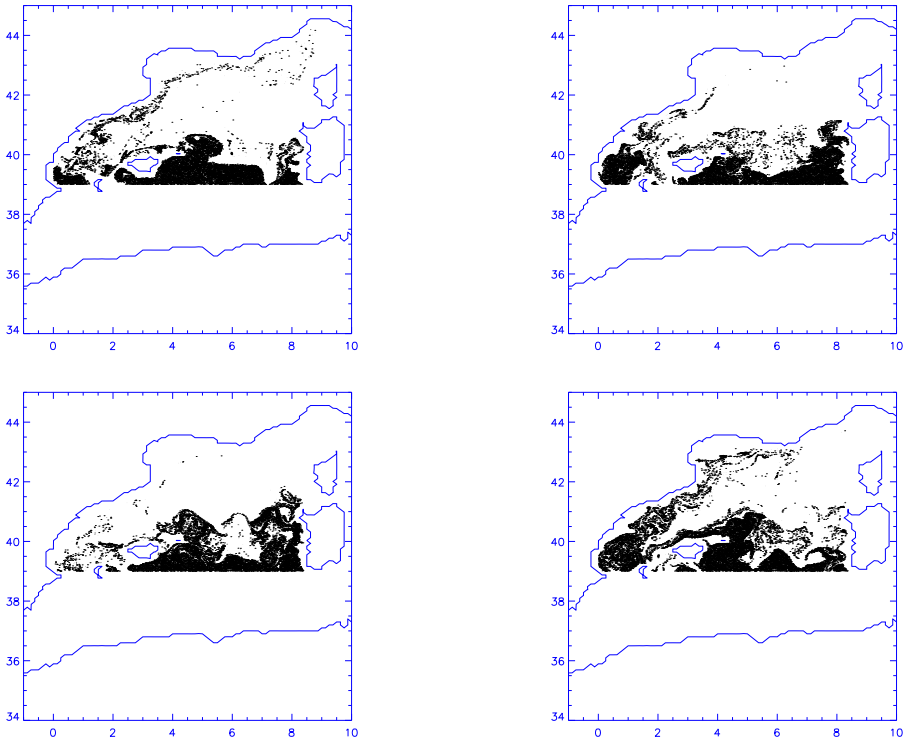

FIG. 41: Exchange basin towards the southern box in the north. Upper left: winter, upper right: spring, lower left: summer, lower right: fall.

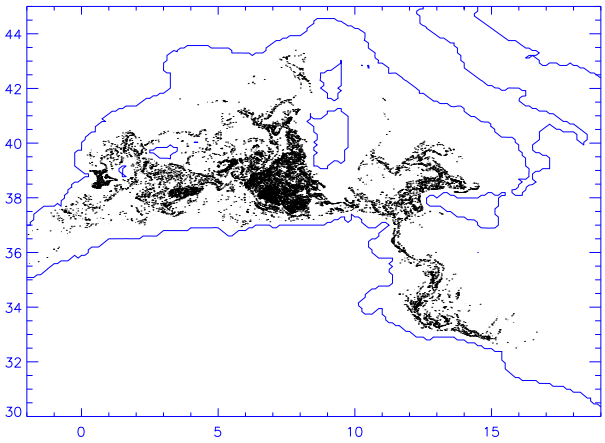

FIG. 42: Endpositions of particles launched in fall in the North which did exchange to the South.

Note, that the traced out structures do not resemble the distribution of downwelling zones in Fig.37. This confirms that there are no strong attracting regions present. However, particles sink more or less continuously down to deeper layers and would reach a new layer within the

simulated time. Thus, the simulations are a first approximation to real observable structures in the Mediterranean.

Results adding Lagrangian diffusion

Next, we will add diffusion to the particle motion. The Lagrangian diffusion is chosen according to the ones suggested by Okubo [54] and is comparable in size with the Eulerian diffusion:

according to Okubo, the apparent diffusivity K_a is depending on the scale of the diffusion l: $K_a = 0.0103 l^{1.15}$. With the average spatial resolution of $l = 12km$ of our model, we get $K_a = 0.036 km^2/h$. The resulting diffusion will be added to the velocity of the particle: $\dot{x} = \dot{x} + \sqrt{2K_a dt}\Gamma$, where Γ is a random value out of a Gaussian distribution and dt the time-step used ($dt = 0.5h$).

Adding Lagrangian diffusion, the motion of the particles will speed up a little bit and the resulting in higher exchange rates:

	N to S	S to N
I	$2.92 \cdot 10^{-3}$	$7.09 \cdot 10^{-3}$
II	$2.30 \cdot 10^{-3}$	$6.04 \cdot 10^{-3}$
III	$2.99 \cdot 10^{-3}$	$6.13 \cdot 10^{-3}$
IV	$3.16 \cdot 10^{-3}$	$4.44 \cdot 10^{-3}$
	yearly avg:	yearly avg:
	$2.84 \cdot 10^{-3}$ (352days)	$5.92 \cdot 10^{-3}$ (169days)

Exchange rates of the 2nd layer, using Lagrangian diffusion (Okubo), averaged over 4 years. Rates are in $1/day$. I,II, III and IV corrresponds to winter, spring, summer and fall.

Above table shows the averaged seasonal exchange rates when using Lagrangian diffusion. As expected, the exchange rates are now slighlty higher than the ones without diffusion (see first table). The characteristical minimal value in the exchange rates from North to South is still in spring and for the South-North exchange in fall as for the exchange rates without diffusion (Table 1). With Lagrangian diffusion, a particle will need almost one year to go from the northern box to

the southern one and a bit more than a half year to go from the southern box to the northern.

Note that the exchange basins of the South-North exchange are resembling to the ones we got

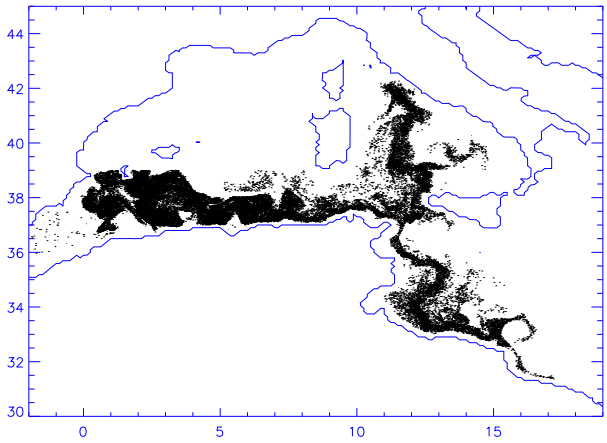

FIG. 43: Endpositions of particles with diffusion launched in summer in the South which did not exchange to the North (analogously to Fig.40)

without diffusion, but now the fine structures are destroyed (Fig. 43). Also, if we take a look on the endpositions of particles launched in the South which did not exchange with the northern box, we can see that particles are more spread.

8. Conclusion

We visualized the exchange basins between a northern and a southern sub-basin in the western Mediterranean, finding complex structures and a seasonal variability in the geometry.

We calculated the time-scales of transport between the two basins. Again, we found a seasonal variability in agreement with the visualized different exchange basins. Also, we found that the South to North transport is faster (202 days in average) than the transport from the North to the South (378 days in average). The explanation for this strong difference lies in the fact that we restricted our simulations to a layer in 16 meters deepness. Since during the cyclonic circulation in the Mediterranean water masses become saltier and sink down to deeper layers, the main transport flux of water masses from North to South is expected to be in a deeper layer than 16 meters.

Furthermore, we investigated the change in the dynamics when adding Lagrangean diffusion. We found that the transport rates become, as expected, higher (169 days in average for the South-North, 352 days in average for the North-South transport, respectively). The resulting visualized

filamental structures are smeared out due to the diffusion, but the large-scale structures, showing the routes of transport, remain.

To conclude, we have shown in the example of the Mediterranean Sea that with the extended leaking method (the exchange method) we are able to identify and characterize dynamical structures in aperiodic realistic flows. The method allows us to visualize the exchange basins and transport routes in a very fast and efficient way. The knowledge of these structures is crucial for forecasting purposes: active or passive tracers released on places belonging to the exchange basins, such as for example an oil spill, will spread towards the target region.

D. Geology

this chapter is a result of a cooperation with:

J. Schmalzl and T. Tél

University Münster and ELTE Budapest

In this chapter, we will go into the Earth's interior and we will take a closer look on the convection in the Earth's mantle.

This convection is comparable with a Rayleigh-Bénard convection and is the mechanism behind tectonic activities on Earth. Investigations about the Earth's structure have been carried out by remote-sensing techniques, e.g. with seismology and also by geochemical observations of isotope ratios of basaltic rocks at mid-ocean ridges and oceanic islands. It has been found that inhomogenities within the Earth's mantle exist. The survival of these heterogenities in the Earth mantle is determined by the mantle convection itself.

In the following, we take a closer look on the mixing properties of the Earth's mantle in a two-dimensional high Rayleigh number convective flow model whose time dependence is strongly aperiodic. To get insight into the dynamical structures, the system is leaked or opened up by defining a smaller region of the flow, so that a particle is considered to be escaped if it leaves this region. By means of an ensemble of nonescaped tracers we are able to characterize mixing and transport processes by visualizing the converging and stretching filamentations (stable and unstable manifolds) in the flow. Therefore, transport routes within the large-scale convection in the Earth's mantle can be characterized.

1. Introduction

Geochemical observations from oceanic island basalts (OIB's) and mid-ocean ridge basalts (MORB's) reveal that the Earth's mantle is heterogenous in composition on different length scales (e.g. [24]) and that these heterogeneities must have existed for a long time. In contradiction to these findings are quantitative mixing studies which indicate that the present day Earth's mantle is convecting vigorously enough to erase initial heterogeneities well within the age of the Earth (e.g. [10, 27]). This has led to the conclusion, that the Earth mantle must have some form of layering. Most investigators favour a depleted and well mixed upper layer which is seperated by the seismically distinct 670km boundary from a poorly mixed and enriched lower layer. In recent years

however seismic observations and geodynamic investigations have revealed a significant mass exchange between upper and lower mantle. Therefore, the traditional models have come under siege. Alternative models have been proposed which consider blobs of geochemically different material which are advected by the flow. Most models proposed however favour some form of geochemical layering in the lower mantle. The proposed scenarios are often accompanied by 2D numerical simulation which start from a given set of initial conditions which the authors consider feasible for the earth mantle. A potential problem with the mixing models which try to explain the geochemical evolution is the arbitrary choice of the initial heterogeneity. Because the mixing properties of convective flow vary strongly in space this can potentially result in misleading mixing rates. A more general tool to characterize mixing by chaotic advection would thus be benificial.

Here, we will consider a two-dimensional Rayleigh-Bénard convection as a model of a vigorously convecting Earth's mantle. We will visualize dynamical mixing structures of the flow to see wether, in spite of the turbulent behavior of the flow, badly mixed regions do exist in which chemical heterogenities could survive.

Our method is based on the idea of considering a subregion of the flow and investigating how Lagrangian particle trajectories escape from or enter into it. This offers a possibility for opening up local properties of the transport process.

2. Chaotic advection and mixing

The basic dynamical mechanism responsible for chaos is the time dependence of the spatially smooth velocity field, which can be sufficient to convert advection to be chaotic [56]. Chaotic advection has been widely studied in recent years [15, 28, 57, 61]. Mixing, or Lagrangian dynamics in general, can be made visible by tracer particles treated as pointlike particles with the same density as the surrounding fluid [36]. Chaotic mixing generates filamental structures which give information about the underlying dynamics.

In the case of imperfect mixing, dense blobs of one kind of material (heterogenities) survive. They are islands within the chaotically mixed flow, co-existing with strongly mixed regions. Such structures have been found by Perugini et al [61], examining the state of frozen lava flows on small scales (meters). The origin of the badly mixed islands is either the finite lifetime of the flow (fluid motion stops after some time) [22, 88] or the presence of regions of quasi-periodic (non-chaotic) advection [57].

In a long lasting flow, however, whose time dependence itself is chaotic, such transport barriers are typically not present [63]. Then, all structures will be smeared out and disappear finally after some transient time τ. The advection dynamics is area or volume preserving and the asymptotic distribution of tracers in such systems is uniform [56]. Mixing in this case is very efficient. It has nevertheless an intriguing structure characterized by two sets of filamentation: converging and stretching ones. In order to visualize these otherwise hidden structures we apply the method of leaking [77] which is shown to provide a kind of fingerprint of the closed system's advection dynamics and which is able to characterize different mixing regions of the flow.

3. Models and results

Convection in a very viscous incompressible flow is defined by the conservation laws for mass, momentum and energy [46, 67]:

$$\nabla \underline{u} = 0,$$

$$\eta \nabla^2 \underline{u} + \rho \underline{g} = \nabla p$$

$$\frac{\delta T}{\delta t} + \underline{u} \nabla T = \kappa \nabla^2 T.$$

Here $\underline{u}$ is the velocity field, ρ is density, p is pressure, $\underline{g}$ is acceleration due to gravity in $-z$ direction, η is dynamic viscosity, T is temperature and κ is thermal diffusivity. We assume an incompressible Boussinesq fluid with constant physical properties, except that density is linearly dependent on temperature:

$$\rho = \rho_0(1 - \alpha(T - T_0))$$

where ρ_0 is the density at $T = T_0 = 0$ and α is the coefficient of thermal expansion. The equations are non-dimensionalized by the depth scale d, temperature scale ΔT and timescale d^2/κ. The dimensionless equations are then completely specified by the Rayleigh number

$$Ra = \frac{\rho g \alpha \Delta T d^3}{\kappa \eta}$$

with ΔT being the temperature difference between upper and lower boundaries. Internal heating is assumed negligible.

A primitive variable formulation was used for the calculations. The thermal convection is studied in a two-dimensional rectangular domain with an aspect-ratio of 4. We use a Rayleigh

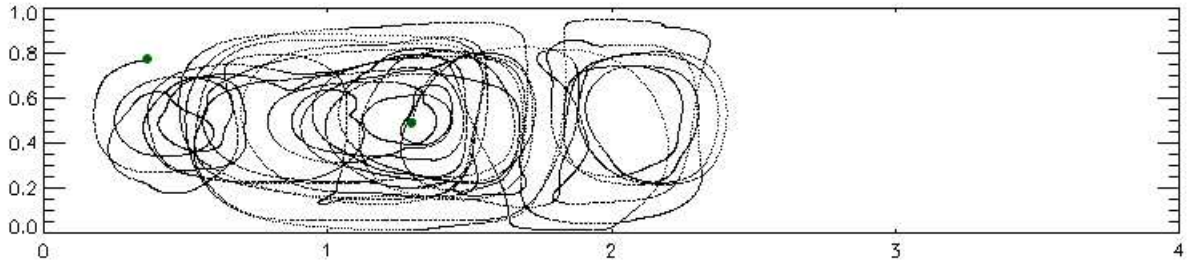

FIG. 44: Chaotic particle trajectory for a tracer started at $x = 1.3, y = 0.5$, simulated for 283 time-steps.

number of $Ra = 10^7$, an infinite Prandtl number and stress-free boundary conditions. Therefore, on horizontal and vertical bounding surfaces, the normal component of velocity and the tangential components of traction are set to zero. The side walls are insulating and the top and bottom surfaces are set to the constant non-dimensional temperatures 0 and 1, respectively. The resolution of the model consists of $50x254$ elements with grid refinements at the top- and bottom boundaries in order to resolve the thin boundary layers.

Velocity components are obtained on a regular mesh at discrete time levels $t_i, i = 1, 2, ...$ (where $t_i = t_{i+1} - t_i$). The Lagrangian particle paths are calculated by post-processing the velocity-data from the model, using a 4th order correct Runge-Kutta method to integrate particle locations from time level t_i to time level t_{i+1}, using the average of the velocity fields at those two levels, and

$$\delta_t x = u(x, y), \delta_t y = v(x, y).$$

The accuracy of calculated tracer paths is discussed by [75]. In time-dependent flows the solution of these equations is typically chaotic [Fig. 44: chaotic particle trajectory]. In the simulations, up to 300000 particles have been used.

For identifying the main routes of transport in chaotic flows experimentally or numerically, a droplet can be placed in the system which will then trace out parts of the main dynamical structures. However, in *closed* chaotic flows the dye will be spread homogenously in the whole system after some transient time τ. Applying the method of leaking as described in Chapter III B, we are able to visualize the dynamical structures of the system and to identify regions with high mixing rates. Therefore, a rectangular region is defined inside the flow in which idealized tracer particles are initially homogenously distributed Fig. 45: particles which cross the borders of the rectangular regions outwards will be treated as escaped ones and are taken out of the system. In this way, the formerly closed system is opened up by leaking, and an escape of particles is possible. Fig. 45

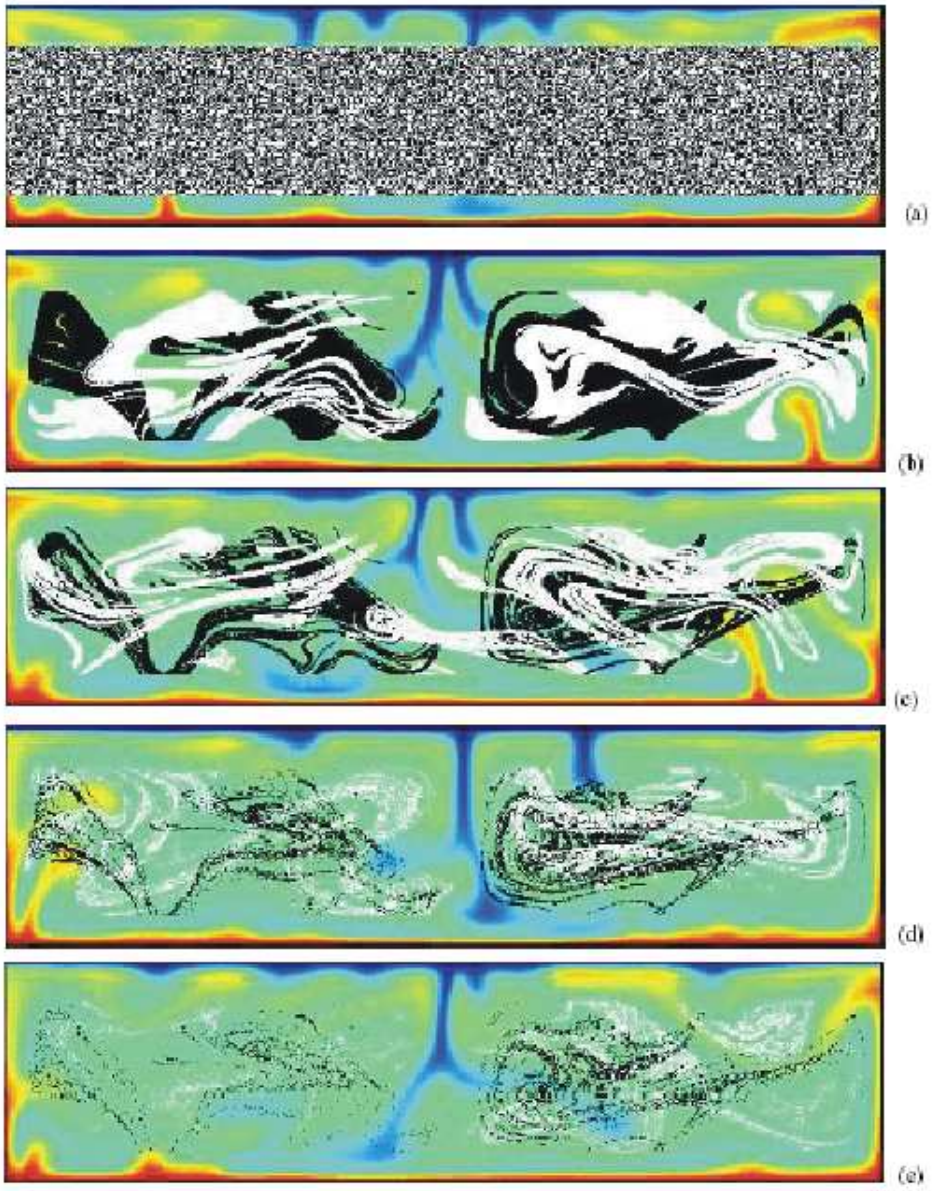

FIG. 45: Sequence of snapshots of the temporal evolution of passive particles in a domain with two convection cells. Top: a smaller rectangle (sub-region) is initially homogenously filled with tracers. Subsequent panels depict the evolution of the tracers, showing the actual position of the tracers in white and their initial positions in black.

shows a sequence of plots for increasing values of the time span τ representing the set of initial (black) and final (white) positions of trajectories which did not leave the selected region over τ. White points, representing the actual position of the tracers at time τ, accumulate along the main transport direction (unstable manifold).

The longer the simulated time τ, the more particles leave the rectangle, thus more and more 'stripes' appear in the initially homogenous (black) distribution. (The loss of structures over very long times is due to the finite number of particles used in the simulation.) The process is similar to gradually removing meat from a backbone. The backbone, the asymptotic fractal shape, is the stable manifold of a never escaping set, the chaotic saddle, existing in the pre-selected rectangle.

The set of white and black points, representing the initial positions of the particles with the white endpoints (stable manifold), becomes more and more rarified and filamental with increasing time.

Note, however, that the resulting distribution of tracer particles is not filamental everywhere. There are some regions within the convection cells where tracers seem to accumulate. Especially in the right convection cell, there are some denser blobs (in white and in black their corresponding starting positions). Also, particles seem to be mixed faster in the left than in the right convection cell.

The topology of the flow can also be seen in the temperature filed which is color coded in the background of Fig. 45. The flow pattern is similar to that of a two-cell problem, since most of the time two convection cells exist, in which the location of the wall between the cells moves chaotically in time, allowing cross-cell mixing.

The midpart of the convection cell and the regions around the side-walls are regions of strong up- and down-welling, where the streamlines, which are similar to the temperature lines, are approximately vertical. In the view of this, we can say that the Lagrangian patterns (the manifolds) have completely different structures than the Eulerian ones (the streamlines). In particular, the latter ones are not fractals. Nevertheless, there are some global relations between them. The stable manifold, for example, cannot penetrate the up- and down-welling regions (Fig. 45 b-e) since points initially situated there are quickly transported towards the horizontal walls (towards the leaks), and thus cannot remain in the pre-selected rectangle.

We can infer from the sequence of plots in Fig. 45 that mixing occurs mainly within each cell and cross-cell mixing is less dominant -in panel (c) we can see the less frequent situation where particles (white) are crossing the cells- corresponding to the results reported by [74].

Mixing of a smaller part of one cell with its surroundings is shown in Fig. 46. From the intertwined black and white structures, denoting the initial position of particles leaving the box to the left or to the right, respectively, it can clearly be seen that particles within that box mix vigorously. But note again, that there exist some regions where the structures are more blob-like

than filament-like.

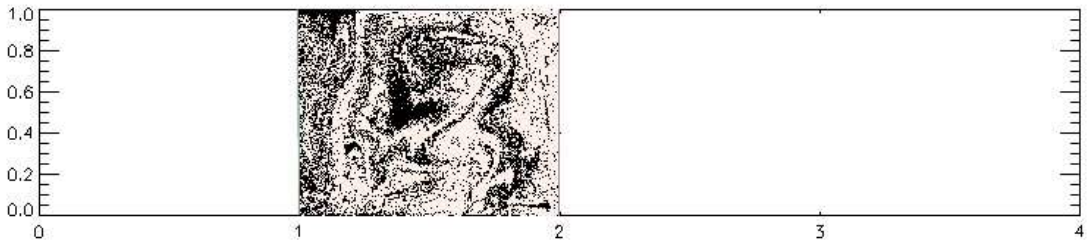

FIG. 46: Mixing of tracers out of a box, showing the initial positions of particles leaving the box towards the left (black), and particles leaving the box to the right (white).

In general, mixing strength can be determined by measuring the fractal dimension of the mixing structures. Due to the before mentioned topological invariance of the flow, however, the fractal dimension D_0 can be shown to remain unchanged [30, 52]. This fact, that the dimension of the, once established, pattern remains fixed is a crucial point for the ability of characterizing the strength of mixing processes: the value of the fractal dimension is a measure of the mixing strength of the given pre-selected region. Thus, for fully chaotic flows as in this model of the Earth's mantle, we get a measure of mixing strength which is *independent* of the initial distribution of material / particles: would we have chosen an initially non-uniform distribution of the particles in the pre-selected region, or only in a sub-region of it, the filamental structure would be the same after sufficiently long time.

Fig. 47 helps to give insight into the meaning of the stable and unstable manifolds. Here, again a smaller pre-selected region is shown, but we have identified another box, too, with the purpose of making initial conditions of trajectories in this box visible who enter the other box up to time τ (these trajectories are then not followed any longer). The blue region, denoting starting positions of particles which reached the other box, increases as time goes on and approaches the black filaments (denoting initial points wherefrom particles did not leave the first box). In the same time, the black filaments become rarified, since the particles slowly leave the starting box. After some longer time, both the blue and black filamental regions approach each-other.

This experiment can be seen as a simulation of the mixing of two spatially separated regions (starting and target region) with distinct material composition. It shows that two such reservoirs do mix (blue filaments), but there is the possibility that some material blobs remain over a long time in their starting environment / reservoir (black blobs).

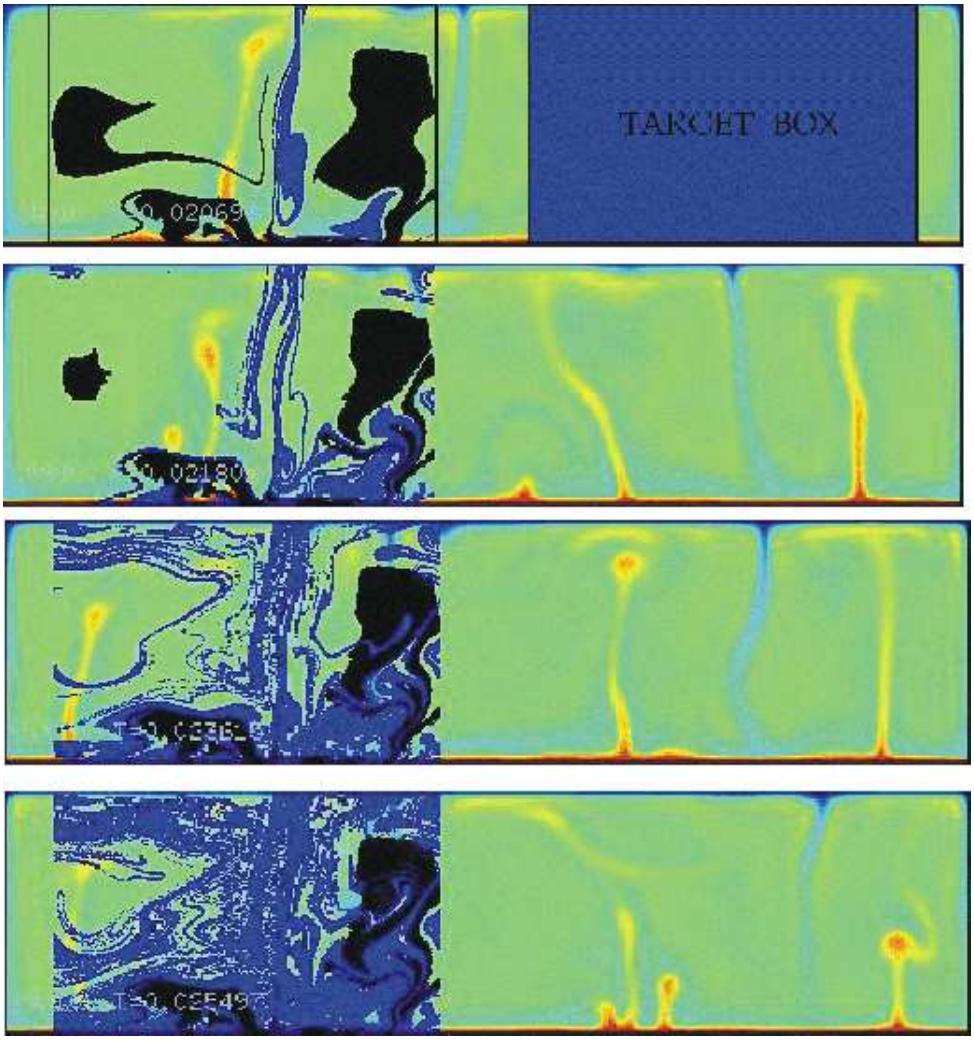

FIG. 47: Starting positions of particles in a box (left) which did exchange into the right target box are shown in blue. Black points in the starting box denote places wherefrom particles badly mix with their surroundings (did not leave their starting box).

In theoretical terms speaking, this numerical experiment shows that particles $close$ to the stable manifold can reach a new region / box and any other region of the flow. Whereas particles starting on the stable manifold stay in the pre-selected region. Thus, nearby points can depart to large distances. A pair of points from which one is on the stable manifold and the other one somewhat off it will strongly deviate. This all shows that mixing between the stable manifold (black) and its complement (blue) is strong.

The unstable manifold has the same properties for the time-reversed particle motion. Thus, to a given point we can find another one so that they stay close to each-other over their entire past

only if the pair falls on the same line of the unstable manifold. But a random choice of two nearby points of the flow will provide us with probability 1 points whose past was drastically different.

Measuring the residence time, i.e. how long it takes for particles (initially homogeneously distributed in a chosen box) to leave the box results in Fig. 48. Short residence times (black and

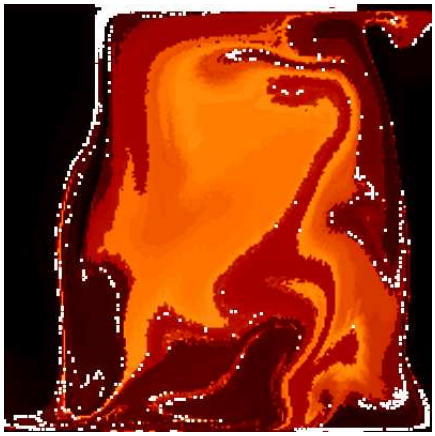

FIG. 48: Color-coding of the residence time of particles of the box shown in Fig. 46. Dependant on the time how long it takes for the particles to leave the box it has been started in (how long it takes it mixes with the surroundings), its starting position will be colored differently: black colors denote starting positions where from particles escape very rapidly, light red towards white denote places where particles started tend to stay a long time within the box.

dark red) stand for locations where particles escape rapidly out of the box. Positions with large residence times (light red and white) correspond to an approach towards one of the never escaping orbits. Points with large residence times must therefore be close to the converging foliation, i.e.,to the stable manifold. Light regions mark regions wherefrom particles become mixed very slowly with their surroundings. They mey purely survive for a longer (but limited) time as heterogenous structures as found in field-observations.

4. Discussion

In order to understand mixing properties in the Earth mantle more properly, we applied the leaking method to visualize transport routes of the convection. The leaking method is based on following tracer trajectories. By selecting a region of observation smaller than the full region accessible by the tracers, and keeping only those trajectories which stay within this region over

a long period, a filamentation appears by plotting the initial and the final positions of the not yet escaped tracers.

We applied this method to a simulation of a very viscous convecting flow. Using passive tracers, we identified basic transport directions of the flow by showing the unstable manifolds.

We confirmed earlier investigations that mixing within convection-cells operates on smaller time-scales than mixing across convecting cells.

Also, we characterized mixing of smaller regions with their surroundings. We found that the mixing strength is spatially inhomogenous. In other words, within the well convecting and mixing regions some smaller domains can exist which survive over a longer time-span without beeing properly mixed with its surroundings. This could be seen in the figures where some of the filaments are thicker (more blob-like).

This result suggests that although we model the Earth mantle as a vigorously convecting high Rayleigh number fluid, some heterogenities may survive for a longer time-period.

In conclusion, by leaking, i.e., by cutting out a finite region of a closed chaotic flow, and thus making an escape of particles possible, we can visualize filamental patterns out of a formerly homogenous tracer distribution and quantify mixing properties between certain regions of the flow.

V. SUMMARY

We introduced a computationally cheap and efficient numerical method with which it is possible to obtain the underlying dynamical structures of a chaotic system.

This method, the leaking method, has it's advantage that it visualizes subsets of the underlying full chaotic set of the system and not only the manifolds belonging to a few detected fixed points. The technique of this method is based on selecting a sub-region of the flow (a region smaller than the whole accessible region of the system) and examining motion of particles as long as they do not leave the given spatial region. The initial- and endpositions of particles which do not leave the sub-region for a given time can be identified, denoting the stable and unstable manifold of the system's chaotic saddle. Alternatively, exchange basins between two sub-regions can also be identified.

Furthermore, the obtained structures are of fractal type, in contrary to structures obtained with dye spreading experiments. Since the measure of the fractal dimension is related to the system's chaoticity describing Lyapunov exponent, the determination of the fractal dimension of the visualized structures gives information about the chaoticity of system (Kantz-Grassberger relation). Therefore, by applying the leaking method, we have a powerful tool to visualize the basic dynamical structures of a chaotic system -e.g. the routes of transport- and to quantify chaoticity and mixing strength of the system.

In this thesis, we first investigated the effect of leaking in a closed chaotic Hamiltonian toy-model (sine-map). We found that even if the system is considered to be fully chaotic, there is a sensitive dependence of the escape rate (of passive particles through the leak) not only on the size of the leak, but also on it's shape and orientation. The origin of this dependence was discovered to be due to the existence of main directions of the stable and unstable manifolds of the system's chaotic saddle: defining the leak to be in the direction of either along the stable or the unstable manifold, the escape rate through the leak will have a maximum value.

This finding will be important e.g. for designeing mesoscopic devices where the strength of conductance is determined by the position of the leads.

Also, we showed that the with the leaking method obtained structures of the unstable manifold correspond to concentration distributions of chemical or biological reactions superimposed on the same flow. Therefore, we are able to mimick or even to forecast distributions or structures generated by chemical or biological reactants on flows without the need of knowing the basic

reactions.

The applicability of the leaking method in higher dimensional systems was shown in the example of leaking a time-periodic three-dimensional conservative non-hamiltonian chaotic system (ABC map).

In two-dimensional conservative systems the preservation of volume implies that the two Lyapunov exponents must be equal in magnitude and opposite in sign. Consistently with this, the invariant manifolds of the leaked system present some sort of statistical time-reversal symmetry. For example, the fractal dimension of the stable and of the unstable manifolds are the same. New to 3D systems is the fact that generically, these systems present either two positive and one negative expansion rates or viceversa. Consequently, the 3D system becomes non-hamiltonian if all three Lypaunov exponents are non-zero.

We gave first (numerical) evidence that the manifolds of the chaotic saddle in three-dimensional systems are of different topological character when having three non-zero Lyapunov exponents: the manifold related to the Lyapunov exponents with the same sign has the larger dimension. Consequently, the geometrical structures of the manifold with the larger dimension are curtain like and the structures of the other one filamental like (or, taking a look on the structures on two-dimensional slices, first one is more filamental like while the other one will be a cloud of points).

After these theoretical considerations, we looked for some applicational possibilities of our method.

As a first simple example we considered a two-dimensional kinematic model of the Gulf Stream and a dynamically consistent one with barriers. We showed that the leaking method can be used in order to post-process drifter data: the monitored trajectories of floaters or drifters are usually highly intertwined and it is therefore difficult to extract information about the basic dynamics of the ocean/sea out of these so-called spaghetti diagrams. But when considering a region smaller than accessible by the drifters (thus applying the leaking method), then the spaghetti diagrams clean out and a filamentation appears when plotting only the final positions of those drifters which did not leave the sub-region.

These filamentations mark the unstable manifold which shows the basic dynamical properties of the flow.

A more realistic application was performed when applying the leaking method to a model of the Mediterranean Sea. The model considered was a three-dimensional primitive equation baroclinic ocean model (DieCast), applied to the Mediterranean Sea. The model had realistic coastlines, topography and single year forcings (wind stres, sea-surface temperature, salinity).

Restricting our calculations to a single layer of the Mediterranean Sea in 16meters deepness (using only the horizontal velocity component and neglecting the vertical components is a good approximation since the vertical components are three orders of magnitude smaller), we investigated the seasonal variability of exchange rates between two sub-basins.

We chose two neighboring sub-basins in the western Mediterranean, calculating the South-North and North-South exchange rates of older / saltier water from the North with less saltier water from the Atlantic Ocean coming through the Strait of Gibraltar from the South.

The leaking method was slightly modified for this purpose to the exchange method by defining a starting (North) and a target (South) region for examining the North-South exchange (and vice versa) in the western basin of the Mediterranean.

We visualized the exchange basins of the northern and southern regions, showing their filamental structures. The seasonal variability could be seen in the filamental structures of the basins of attraction which varied accordingly. Also, the calculated exchange rates showed the seasonal variability. Furthermore, we found that the South to North transport is larger (202 days in average) than the transport from North to South (378 days in average). The explanation for this strong difference lies in the fact that we restricted our simulations to a layer in 16 meters deepness. Since during the cyclonic circulation in the Mediterranean water masses become saltier and sink down to deeper layers, the main transport flux of water masses from North to South is expected to be in a deeper layer than 16 meters.

Furthermore, we investigated the change in the dynamics when adding Lagrangian diffusion. We found that the transport rates become, as expected, higher (169 days in average for the South-North, 352 days in average for the North-South transport, respectively).

As a last example, we applied the leaking method to a highly viscous Rayleigh-Bénard convection, modelling the convection in the Earth's mantle. Using passive tracers, we confirmed earlier investigations that mixing within convection-cells operates on smaller time-scales than mixing across convecting cells.

Also, we could characterize mixing of smaller regions with their surroundings. We found that the mixing strength is spatially inhomogenous. In other words, within the well convecting and mixing regions some smaller domains can exist which survive over a longer time-span without beeing properly mixed with its surroundings. This result suggests that although we model the Earth mantle as a vigorously convecting high Rayleigh number fluid, some heterogenities may survive for a long time-period.

In conclusion, by leaking, i.e., by cutting out a finite region of a closed chaotic flow, and thus making an escape of particles possible, we can visualize filamental patterns out of a formerly homogenous tracer distribution and quantify mixing properties between certain regions of the flow. The knowledge of these structures is crucial for forecasting purposes: active or passive tracers released on places belonging to the exchange basins, such as for example an oil spill, will spread towards the target region.

VI. BIBLIOGRAPHY

[1] M.J. Alperin, I.B. Suayah, L.K. Benninger, C.S. Martens, 'Modern organic carbon burial fluxes, recent sedimentation rates, and particle mixing rates from the upper continental slope near Cape Hatteras, North Carolina (USA)', Deep-Sea Research II **49**, 4645-4665 (2002)

[2] M.M.Alvarez MM, Muzzio FJ, Cerbelli S, Adrover A, Giona M (1998) Self-Similar Spatiotemporal Structure of Intermaterial Boundaries in Chaotic Flows. Phys. Rev. Lett. 81: 3395-3398

[3] M. Astraldi, S. Balopoulos, J. Candela, J. Font., M. Gacic, G.P. Gasparini, B. Manca, A. Theocharis, J. Tintoré, 'The role of straits and channels in understanding the characteristics of Mediterranean circulation', Progr. Oceanogr. **44**, 65-108 (1999)

[4] D. Beigie, A. Leonard, S. Wiggins, 'Invariant manifold templates for chaotic advection', Chaos, Sol. Fractals **4**, 749-868 (1990)

[5] S. Bleher, C. Grebogi, E. Ott, R. Brown, Phys. Rev. A **38**, 930 (1988)

[6] A. Bower, 'A Simple Kinematic Mechanism for Mixing Fluid Parcels across a Meandering Jet', J. of Phys. Ocean. **21**, 173-180 (1991)

[7] G. Buffoni, P. Falco, A. Griffa, E. Zambianchi, 'Dispersion processes and residence times ina a semi-enclosed basin with recirculatino gyres: An application to the Tyrhenian Sea', JGR **102**, C8, 18,699-18,713 (1997)

[8] J.H.E. Cartwright, M. Feingold, O. Piro, Physica D **76**, 22 (1994) J.H.E. Cartwright, M. Feingold, O. Piro, Phys. Rev. Lett. **75**, 3669 (1995) J.H.E. Cartwright, M. Feingold, O. Piro, J. Fluid Mech. **316**, 259 (1996)

[9] M. Cencini, G. Lacorata, A. Vulpiani, E. Zambianchi 'Mixing in a Meandering Jet: A Markovian Approximation' J. of Phy. Ocean. **29**, 2578-2594 (1999)

[10] U. Christensen, 'Mixing by time-dependent convection', Earth and Planetary Scie. Let. **95**, 382-394 (1989)

[11] F. Christiansen and P. Grassberger, Phys. Lett. **181 A**, 47 (1993)

[12] D. del-Castillo-Negrete, P.J. Morrison 'Chaotic transport by Rossby waves in shear flow', Phys. Fluids A **5**, 948-965 (1993)

[13] D.E. Dietrich, 'Application of a modified 'a' grid ocean model having reduced numerical dispersion

to the gulf of mexico circulation', Dyn. of Atm. and Oceans **27**, 201-217 (1997)

[14] S. Dutkiewicz, N. Paldor 'On the Mixing Enhancement in the Meandering Jet Due to the Intercation with an Eddy', J. of Phys. Ocean. **24**, 2418-243 (1994)

[15] D. Farmer, R. Pawlowicz, R. Jiang, 'Tilting separation flows: a mechanism for intense vertical mixing in the coastal ocean', Dynamics of Atmospheres and Oceans **36**, 43-58 (2002)

[16] M. de Fatima, I.T. Gabardo, M.E.R. Carneiro, S.M. Barbanti, G.C. da Silva, C.G. Massone 'Brazilian Oil Spills Chemical Characterization - Case Studies', Environmental Forensics **3**, 303-321 (2002)

[17] V. Fernandez, D.E. Dietrich, R.L. Haney, J. Tintoré, 'Mesoscale, seasonal and interannual variability in the Mediterranean Sea using a numerical ocean model', Progress in Oceanography *in press* (2004)

[18] C.N. Flagg, L.J. Pietrafesa, G.L. Weatherly, 'Springtime hydrography of the southern Midlle Atlantic Bight and the onset of seasonal stratification', Deep-Sea Research II **49**, 4297-4329 (2002)

[19] S. Galluccio, A. Vulpiani, Physica A **212**, 75 (1994)

[20] M. Giona, A. Adrover, F. Muzzio, S. Cerbelli, 'The geometry of mixing in time-periodic chaotic flows. Asymptotic directionality in physically realizable flows and global invariant properties', Physica D **132**, 298-324 (1999)

[21] G. Haller, 'Characterization of finite-time Lyapunov exponents and vectors in two-dimensional flows' Chaos **10**, 99 (2000)

[22] G. Haller, A.C. Poje, 'Finite time transport in aperiodic flows', Physica D **119**, 352-380 (1998)

[23] G. Haller, G. Yuan, 'Lagrangian coherent structures and mixing in two-dimensional turbulence', Physica D **147**, 352-370 (2002)

[24] S.R. Hart, 'A large-scale isotope anomaly in the Southern Hemisphere mantle', Nature **309**, 753-757 (1984)

[25] E. Hernández-Garcia, C. López, Z. Neufeld, 'Small-scale structure of nonlinearly interacting species advected by chaotic flows', Chaos **12**, 470-478 (2002)

[26] Robert C. Hilborn, 'Chaos and Nonlinear Dynamics', Oxford University Press, 2nd edition (2000)

[27] N.R.A. Hoffman, D.P. McKenzie, 'The destruction of geochemical heterogenities by differential fluid motion during mantle convection', Geophys. J. R. Astron. Soc. **82**, 163-206 (1985)

[28] A. Huppert, L. Stone, 'Chaos in the Pacifict's Coral Reef Bleaching Cycle', The American Naturalist **152**, 447-459 (1998)

[29] E. Atlee Jackson, 'Perspectives of nonlinear dynamics' Vol.I,II Cambridge University Press (1991)

[30] J. Jacobs, E. Ott, T. Antonsen, and J. Yorke, Physica **D110**, 1 (1997); Z. Neufeld and T. Tél, Phys.

Rev. **E 57**, 2832 (1998)

[31] C.K.R.T. Jones, S. Winkler, 'Do invariant manifolds hold water?', In: Fiedler B, Iooss G, Koppell N (eds) 'Handbook of Dynamical Systems III: Towards Applications' World Scientific (2002)

[32] B. Joseph, B. Legras, 'Relation between kinematic boundaries, stirring, and barriers for the Antarctic Polar vortex', J. Atm. Sci. **59**, 1198-1212 (2002)

[33] C. Jung, T. Tél, E. Ziemniak, Chaos **3**, 555 (1993)

[34] H. Kantz, P. Grassberger, Physica D **17**, 75 (1985)

[35] G. Károlyi, A. Péntek, Z. Toroczkai, T. Tél, C. Grebogi, 'Chemical or biological activity in open chaotic flows', PRE **59**, 5468 (1999)

[36] E. Knobloch, J.B. Weiss, 'Chaotic Advection by modulated traveling waves', Phys. Rev. A **36**, 1522-1524 (1987)

[37] L. Kuznetsov, M. Toner, Kirwan Jr. Ad, C.K.R.T. Jones, L.H. Kantha, J. Choi, 'The loop current and adjecent rings delineated by Lagrangian analysis of the new-surface flow', J. Marine Res. **60**, 405-429 (2002)

[38] G. Lacorata, E. Aurell, A. Vulpiani, 'Drifter dispersion in the adriatic sea: Lagrangean data and chaotic model', Annales Geophysicae 19, 121-129 (2001)

[39] Y.-C. Lai, T. Tél, C. Grebogi, Phys. Rev. E **48**, 709 (1993)

[40] G. Lapeyre, 'Finding finite-time invariant manifolds in two-dimensional velocity fields' Chaos **12**, 888 (2002)

[41] O. Legrand and D. Sornette, Europhys. Lett. **11**, 538 (1990)

[42] A. Lopes and R. Markarian, SIAM J. Appl. Math. **56**, 651 (1996)
N. Chernov and R. Markarian, Bol. Soc. Bras. Math. **28**, 271 (1997)
N. Chernov, R. Markarian and Troubetzkoy, Ergod. Theory Dyn. Syst. **18**, 1049 (1998)

[43] C. López, Z. Neufeld, E. Hernández-Garcia, P.H. Haynes, 'Chaotic Advection of Reacting Substances: Plankton Dynamics on a Meandering Jet', Physics and Chemistry of the Earth B **26**, 313-317 (2001)

[44] A.J. Mariano, A. Griffa, T.M. Özgökmen, E. Zambianchi, 'Lagrangean analyses and predictability of coastal and ocean dynamics 2000', J. Atm. Ocean. Tech. **19**, 1114-1125 (2002)

[45] M.R. Maxey, J.J. Riley, 'Equation of motion for a small rigis sphere in a nonuniform flow', Phys. Fluids **26**, 883 (1983)
A. Babiano, J.H.E. Cartwright, O. Piro, A. Provenzale, 'Dynamics of a small neutrally buoyant sphere in a fluid and targeting in Hamiltonian systems', PRL **84**, 5764 (2000)

I.J. Benczik, Z. Toroczkai, T. Tél, 'Advection of finite-size particles in open flows', PRE **67**, 036303 (2003)

[46] D.P. McKenzie, J.M. Roberts, N.O. Weiss, 'Convection in the Earth's mantle: towards a numerical simulation', J. Fluid Mech. **62**, 465-538 (1974)

[47] P.D. Miller, C.K.R.T. Jones, A.M. Rogerson, L.J. Pratt, ' Quantifiying transport in numerically generated velocity fields', Physica D **110**, 105-122 (1997)

[48] A. E. Motter and P. S. Letelier, Phys. Lett. A **285**, 127 (2001)

[49] Z. Neufeld, P. Haynes, and G. Picard, Phys. Fluids **12**, 2506 (2000)

[50] Z. Neufeld, C. López, and P. Haynes, Phys. Rev. Lett **82**, 2606 (1999); Z. Neufeld et al., Phys. Rev. **E 61**, 3857 (2001); C. López et al., Phys. Chem. Earth **B 26**, 313 (2001)

[51] Z. Neufeld, T. Tél, J.P.A. **30**, 2262 (1997)

[52] Z. Neufeld, T. Tél, 'Advection in chaotically time-dependent open flows', Phys. Rev. E **57**, 2832-2842 (1998)

[53] H.E. Nusse, J.A. Yorke, Physica D **36**, 137 (1989)

[54] A. Okubo, 'Oceanic diffusion diagrams', Deep-Sea Research **18**, 789-802 (1971)

[55] E. Ott, C. Grebogi, J. A. Yorke, Phys. Rev. Lett. **64**, 1196 (1990)

[56] E. Ott, *Chaos in Dynamical Systems* (Cambridge University Press, Cambridge, England, 1993)

[57] J.M. Ottino, 'The kinematics of mixing: stretching, chaos and transport', Cambridge University Press (UK) (1989)

[58] V. Paar and N. Pavin, Phys. Rev. E **55**, 4112 (1997)
V. Paar and H. Buljan, Phys. Rev. E **62**, 4869 (2000)
H. Buljan and V. Paar, Phys. Rev. E **63**, 066205 (2001)

[59] R.C. Pacanowski, S.G.H. Philander, 'Parameterization of vertical mixing in numerical models of tropical oceans', J. Phys. Oceanogr. **11**, 1443-1451 (1981)

[60] Á. Péntek, G. Károlyi, I. Scheuring, T. Tél, Z. Toroczkai, J. Kadtke, C. Grebogi, 'Fractality, chaos, and reactions in imperfectly mixed open hydrodynamical flows' Physica A **274**, 120 (1999)

[61] D. Perugini, G. Poli, G.D. Gatta, Lithos **65**, 313 (2002)

[62] G. Pianigiani, J.A.Yorke, Trans. Am. Math. Soc. **252**, 351 (1979)

[63] R.T. Pierrehumbert, 'Tracer microstructure in the large-eddy dominated regime', Chaos, Solitons and Fractals **4**, 1091 (1994)

[64] J.M. Pinot, J.L. López-Jurado, M. Riera, 'The CANALES experiment (1996-1998). Interannual, sea-

sonal, and mesoscale variability of the circulation in the Balearic channels', Progr. Oceanogr. **55**, 335-370 (2002)

[65] A.C. Poje, M. Toner, A.D. Kirwan,Jr., C.K.R.T. Jones, 'Drifter launch strategies based on Lagrangian templates', J. Phys. Ocean. **32**, 1855-1869 (2002)

[66] G. Puentes, A. Aiello, J.P. Woerdman, 'Ray splitting in paraxial optical cavities', Phys. Rev. E **69**, 036209 (2004)

[67] F.M. Richter, 'Convection and the large scale circulation of the mantle', J. Geophys. Res. **78**, 8735-8745 (1973)

[68] A.M. Rogerson, P.D. Miller, L.J. Pratt, C.K.R.T. Jones, 'Lagrangian Motion and Fluid Exchange in a Barotropic Meandering Jet', Journal of Physical Oceanography **29**, 2635-2655 (1999)

A. Alvarez, C. López, M. Riera, E. Hernández-García, J. Tintoré, 'Forecasting the SST space-time variability of the Alboran Sea with genetic algorithms', Geophysical Research Letters **27**, 2709-2712 (2000)

[69] E. Romeiras, C. Grebogi, E. Ott, 'Multifractal properties of snapshot attractors of random maps', Phys. Rev. A **41**, 784-799 (1990)

[70] V. Rom-Kedar, A. Leonard, S. Wiggins, 'An analytical study of transport, mixing and chaos in an unsteady vortical flow', J. Fluid. Mech. **214**, 347-394 (1990)

[71] D. Rothstein, E. Henry, J.P. Gollub, 'Persistent patterns in transient chaotic fluid mixing' Nature **401**, 770 (1999)

[72] R.M. Samelson, 'Fluid Exchange across a Meandering Jet', J. of Phys. Ocean. **22**, 431-440 (1992)

[73] B. Sandstede, S. Balasuriya, C.K.R.T. Jones, P. Miller, 'Melnikov theory for finite-time vector fields', Nonlinearity **13**, 1357-1377 (2000)

[74] J. Schmalzl, 'Mixing properties of thermal convection in the Earth's mantle', PhD thesis (1996)

[75] J. Schmalzl, G.A. Houseman, U. Hansen, 'Mixing properties of three-dimensional stationary convection', Phys. Fluids **7**, 1027-1033 (1995)

[76] J. Schneider, T.Tél 'Extracting flow structures out of tracer data', Ocean Dynamics **53**, 64 (2003)

[77] J. Schneider, T. Tél, Z. Neufeld, 'Dynamics of leaking Hamiltonian systems', PRE **66**, 066218 (2002)

[78] M. L. Roukes, O. L. Alerhand, Phys. Rev. Lett. **65**, 1651 (1990); S. Ree, L.E. Reichl, Phys. Rev. E **65**, 055205 (2002); H.-S. Sim, H. Schomerus, e-print cond-mat/0203091.

[79] H.S. Sim, H. Schomerus, Phys. Rev. Lett. **89**, 066801 (2002)

[80] J.C. Sommerer, H.-C. Ku, H.E.Gilreath, 'Experimental Evidence for Chaotic Scattering in a Fluid

Wake', Phys. Rev. Lett. **77**, 5055 (1996)

[81] J.C. Sommerer, E. Ott, 'Particles floating on a moving fluid: A dynamically comprehensive physical fractal', Science **259**, 335-339 (1993)

[82] T. Tél, 'Transient Chaos: a type of metastable state', in: Statphys 19, 346, edited by Hao Bailin, World Scientific (1996)

[83] T. Tél, G. Márton, 'Kaotikus Dinamika', Nemzeti Tankönyvkiadó, Budapest (2002)

[84] I. Tuval, J. Schneider, O. Piro, T. Tél, 'Opening up fractal structures of three dimensional flows via leaking', Europhysics Letters **65**, 633-639 (2004)

[85] Z. Toroczkai, G. Károlyi, A. Péntek, T. Tél, C. Grebogi, 'Advection of Active Particles in open Chaotic Flows', Phys. Rev. Lett. **80**, 500-503 (1998)

[86] Focus Issue on Active Chaotic Flow (2002), eds.: Toroczkai Z, and Tél, T, Chaos 12: 372-530

[87] G.A. Voth, G. Haller, J.P. Gollub, 'Experimental measurements of stretching fields in fluid mixing' PRL **88**, 254501 (2002)

[88] S. Wiggins, 'Chaotic Transport in Dynamical Systems', Springer Verlag, New York (1992)

[89] L. Yu, E. Ott, Q. Chen, 'Fractal distribution of floaters on a fluid surface and the transition to chaos for random maps', Physica D **53**, 102-124 (1991)

[90] G.-C. Yuan, L.J. Pratt, C.K.R.T. Jones, 'Barrier destruction and Lagrangian predictability at depth in a meandering jet', Dynamics of Atmospheres and Oceans **35**, 41-61 (2002)

[91] J.T.F. Zimmerman 'The tidal whirlpool: a review of horizontal dispersion by tidal and residual currents', Netherlands Journal of Sea Research **20**, 133 (1986)

E. Knobloch, J.B. Weiss, 'Chaotic advection by modulated traveling waves' PRA **36**, 1522 (1987)

M. Feingold, L.P. Kadanoff, O. Piro, 'Transport of passive scalars: KAM surfaces and diffusion in three-dimensional Liouvillian maps', in: 'Instabilities and Nonequilibrium Structures II', Eds.: P.Collet, E. Tirapegui, D. Villarroel; Reidel, Dordrect (1989)

Acknowledgments

I want to thank Prof. Jürgen Kurths for giving me the possibility of writing my thesis in his institute and for opening me the possibility of taking part in many conferences and summer schools. Im thankful to Prof. Tamás Tél who gave me the first contact to chaos theory and accompanied my learning and understanding in this field. Thanks to Prof. Emilio Hernández-García for giving me the possibility of working on a model of the Mediterranean and for his seemingly endless patience during the long bug-hunting periodes.

Also, I want to thank the International Max Planck Research School on Biomimetic Systems (IMPRS) for the financial support.

Furthermore thanks to my father and my friends for encouraging me during my work on this thesis.